A STUDY OF ELECTROMAGNETIC WAVE INTERACTIONS WITH AIR PLASMAS

William H. Rudderow

Advanced Technology Center,
Incorporated

Prepared for:

Air Force Cambridge Research Laboratories

July 1975

AFCRL-TR-75-0418

A STUDY OF ELECTROMAGNETIC WAVE INTERACTIONS WITH AIR PLASMAS

William H. Rudderow

ADVANCED TECHNOLOGY CENTER, INC.
P. O. Box 6144
Dallas, Texas 75222

July 1975

Final Report: 15 December 1972 to 30 June 1975

AIR FORCE CAMBRIDGE RESEARCH LABORATORIES
AIR FORCE SYSTEMS COMMAND
UNITED STATES AIR FORCE
HANSCOM AFB, MASSACHUSETTS 01731

Unclassified

SECURITY CLASSIFICATION OF THIS PAGE (When Data Entered)

REPORT DOCUMENTATION PAGE		READ INSTRUCTIONS BEFORE COMPLETING FORM
1. REPORT NUMBER AFCRL-TR-75-0418	2. GOVT ACCESSION NO.	3. RECIPIENT'S CATALOG NUMBER
4. TITLE (and Subtitle) A STUDY OF ELECTROMAGNETIC WAVE INTERACTIONS WITH AIR PLASMAS		5. TYPE OF REPORT & PERIOD COVERED Final Report Dec. 15, 1972-June 30, 1975 6. PERFORMING ORG. REPORT NUMBER ATC Rept. No. B-94300/5CR-28
7. AUTHOR(s) William H. Rudderow		8. CONTRACT OR GRANT NUMBER(s) F19628-73-C-0140
9. PERFORMING ORGANIZATION NAME AND ADDRESS Advanced Technology Center, Inc. P. O. Box 6144 Dallas, Texas 75222		10. PROGRAM ELEMENT, PROJECT, TASK AREA & WORK UNIT NUMBERS 4642-03-01 62101F
11. CONTROLLING OFFICE NAME AND ADDRESS Air Force Cambridge Research Laboratories Hanscom AFB, Massachusetts 01731 Contract Monitor: Walter Rotman/LZP		12. REPORT DATE July 1975 13. NUMBER OF PAGES ~~100~~ 103
14. MONITORING AGENCY NAME & ADDRESS (if different from Controlling Office)		15. SECURITY CLASS. (of this report) Unclassified 15a. DECLASSIFICATION/ DOWNGRADING SCHEDULE

16. DISTRIBUTION STATEMENT (of this Report)

Approved for public release; distribution unlimited

17. DISTRIBUTION STATEMENT (of the abstract entered in Block 20, if different from Report)

18. SUPPLEMENTARY NOTES

TECH, OTHER

19. KEY WORDS (Continue on reverse side if necessary and identify by block number)

Plasmas, Reentry, Microwaves, Ionization, Electrophilics, Shock Tube

20. ABSTRACT (Continue on reverse side if necessary and identify by block number)

A high performance shock tube has been used to study the effect of thin plasma layers upon the transmission characteristics of low and high power microwave transmission. Flush mounted X band waveguide aperture antennas or special H-plane horn antennas were used to launch and detect the microwave signals. Thin plasma layers were cut from the shock-generated air plasma using sharp-edged ground planes mounted inside the shock tube. Initial shock tube pressures were established at 5.0 torr or 10.0 torr

(continued)

DD FORM 1 JAN 73 1473 EDITION OF 1 NOV 65 IS OBSOLETE
S/N 0102-014-6601

Unclassified

SECURITY CLASSIFICATION OF THIS PAGE (When Data Entered)

20. ABSTRACT (continued)

while the shock velocities were varied to produce electron densities of 10^{11} - 10^{14} cm^{-3}. Diagnostic measurements were performed with various flush mounted electrostatic probes, stagnation point electrostatic probe, and supporting static pressure gages. Results of the electrostatic probes were compared with simple theories and reasonable agreement was obtained. Low power cw transmission measurements at 10 GHz were performed for a range of plasma thicknesses varying from 3.18 to 12.7 mm. High power pulse measurements were performed for a 3.18 mm thick plasma layer ranging from 18 W to 7.0 kW. Strong field induced ionization effects were observed at incident peak powers above 600 W for the experimental conditions. The addition of a 1% mole fraction of the electrophilic agent Freon 114B2 vapor to dry air provided a reduction in attenuation losses up to 7 dB at 5.0 kW peak incident power. The reduction of the electron density over the entire incident power range was measured by flush mounted electrostatic probes located immediately downstream of the transmitting antenna.

SUMMARY

An experimental study has been performed to study the effect of thin plasma layers upon the transmission characteristics of low and high power microwave transmission. A high performance shock tube using dry air as the test gas was used to generate the plasma. Plasma conditions were established to simulate the reentry environment encountered during the terminal phases of a slender reentry vehicle. Flush mounted X band waveguide aperture antennas or special H-plane horn antennas were used to launch and detect the microwave signals. Thin plasma layers were cut from the shock-generated plasma using sharp-edged ground planes mounted inside the shock tube. Initial shock tube pressures were established at 5.0 torr or 10.0 torr while the shock velocities were varied to produce electron densities of 10^{11} - 10^{14} cm^{-3}. Diagnostic measurements were performed with various flush mounted electrostatic probes, stagnation point electrostatic probe, and supporting static pressure gages. Results of the electrostatic probes were compared with simple theories and reasonable agreement was obtained. Low power cw transmission measurements at 10 GHz were performed for a range of plasma thicknesses varying from 3.18 to 12.7 mm. High power pulse measurements were performed for a 3.18 mm thick plasma layer ranging from 18 W to 7.0 kW. Measurements of the transmission coefficient and reflection coefficient were made for all power levels. Additional measurements of the reflected phase were made for the high power levels. Strong field induced ionization effects were observed at incident peak powers above 600 W for the experimental conditions. The effect of the electrophilic additive Freon 114B2 upon the transmission properties of high power pulse transmission was also studied. The addition of a 1% mole fraction of Freon 114B2 vapor to dry air provided a reduction in attenuation losses up to 7 dB at 5.0 kW peak incident power. The reduction of the electron density was also measured by flush mounted electrostatic probes located immediately downstream of the transmitting antenna.

ACKNOWLEDGEMENTS

It is a pleasure to acknowledge the stimulating discussions with Walter Rotman of the Air Force Cambridge Research Laboratories. The advice and suggestions of Dallas Hayes, Robert Papa, and other members of the Microwave Physics Group at AFCRL is also gratefully acknowledged. The shock tube measurements were capably carried out by J. D. Ward.

TABLE OF CONTENTS

	Page
SUMMARY	1
LIST OF FIGURES	4
INTRODUCTION	7
PLASMA DIAGNOSTIC EXPERIMENTS	9
Shock Tube Facility	9
Flow Verification	9
Wall Mounted Electrostatic Probe Measurements	19
Flat Plate Electrostatic Probe Measurements	24
Stagnation Point Electrostatic Probe Measurements	28
Conductivity Probe	34
FLUSH MOUNTED APERTURE ANTENNA EXPERIMENTS	34
Low Power Microwave System	39
High Power Microwave System	43
Horn Antennas	44
Experimental Results	48
Low Power Experiments	48
High Power Experiments	53
Horn Antenna Measurements	66
ELECTROPHILIC MEASUREMENTS	71
CONCLUSIONS	96

LIST OF FIGURES

Figure		Page
1	Shock Tube Schematic	10
2	Flush Electrostatic Probe	12
3	Flush Electrostatic Probe Response	13
4a	Ground Plane Electrostatic Probes	15
4b	Plate Mounted Electrostatic Probe	15
5	Plate Mounted Electrostatic Probe Response	16
6	Run Time, P = 10 torr	17
7	Run Time, P = 5 torr	18
8	Electron Density Measurement	22
9	Electron Density Based on Ion Current, P = 10 torr	25
10	Electron Density Based on Electron Current, P = 10 torr	26
11	Electron Density Based on Ion Current, P = 5 torr	27
12	Ion Current Density	29
13a	Stagnation Point Electrostatic Probe	31
13b	Stagnation Point Electrostatic Probe Response	31
14	Electron Density Based on Stagnation Point Electrostatic Probe	33
15	Conductivity Probe	35
16	Photograph of Shock Tube	38
17	Test Section Schematic	40
18	Photograph of Test Section	41
19	Schematic of Low Power Microwave Circuit	42
20	Schematic of High Power Microwave Circuit	45
21	Horn Antenna Design	46

LIST OF FIGURES (continued)

Figure		Page
22	Photograph of Horn Antenna and Test Section	47
23	Low Power Transient Response	50
24	Transmission Coefficient 3.18 mm Layer	51
25	Reflection Coefficient 3.18 mm Layer	52
26	Transmission Coefficient 6.35 mm Layer	54
27	Reflection Coefficient 6.35 mm Layer	55
28	Transmission Coefficient 12.7 mm Layer	56
29	Reflection Coefficient 12.7 mm Layer	57
30	Flush Probe Transient Response	58
31	High Power Transient Response 539 W	60
32	Transmission Coefficient 600 W	61
33	Reflection Coefficient 600 W	62
34	Transient Response 1.74 kW	63
35	Transmission Coefficient 1.75 kW	64
36	Transient Response 6.04 kW	65
37	Transmission Coefficient 7 kW	67
38	Reflection Coefficient 7 kW	68
39	Incident Power Effects	69
40	Horn Antenna Transient Response 1.77 kW	70
41	Horn Antenna Transmission Coefficient 1.77 kW	74
42	Horn Antenna Reflection Coefficient 1.77 kW	75
43	Horn Antenna Reflected Phase 1.77 kW	76
44	Horn Antenna Transient Response 7.0 kW	77
45	Horn Antenna Transmission Coefficient 7.0 kW	78

LIST OF FIGURES (continued)

Figure		Page
46	Horn Antenna Reflection Coefficient 7.0 kW	79
47	Horn Antenna Reflected Phase 7.0 kW	80
48	Transient Response Comparison	84
49	Power Transmission Coefficient, Seeded Flow, 18 W	85
50	Power Reflection Coefficient, Seeded Flow, 18 W	86
51	Probe Current, 18 W	87
52	Power Transmission Coefficient, Seeded Flow, 1.5 kW	89
53	Power Reflection Coefficient, Seeded Flow, 1.5 kW	90
54	Probe Current, 1.5 kW	91
55	Power Transmission Coefficient, Seeded Flow, 5.0 kW	92
56	Power Reflection Coefficient, Seeded Flow, 5.0 kW	93
57	Probe Current, 5.0 kW	94

INTRODUCTION

During the flight of a high speed reentry vehicle, sufficient ionization occurs during the termiral phase of the flight to cause a significant reduction in the microwave power transmitted by a surface mounted antenna. The reentry plasma for a slender reentry vehicle is confined to the thin boundary layer surrounding the vehicle which, although inhomogeneous, is usually in thermodynamic equilibrium at altitudes below 100,000 feet. At this period in the reentry trajectory communication requirements must be met where the plasma is overdense for the applied signal frequency. In addition, the electron-neutral collision frequency is usually of the same order of magnitude as the signal frequency. Efforts to increase the amount of transmitted power by simply increasing the incident power are hampered by the coupling of the incident electric field to the plasma causing an increase in the total amount of attenuation caused by the plasma. In order to obtain more basic data for low altitude, high speed reentry conditions, an experimental program was conducted to simulate typical low altitude reentry environments and perform controlled laboratory measurements to determine the effect of an overdense plasma upon high power microwave transmission. Based upon trajectories of high ballistic coefficient reentry vehicles, typical plasma conditions were established. Simple X band waveguide antennas loaded with dielectric antenna windows were selected for the radiating and receiving antennas.

The effect of the addition of an electrophilic agent into a dense plasma was also investigated in order to study the effect upon microwave transmission. Previous laboratory and flight test measurements have indicated the effectiveness of certain electrophilic compounds upon the microwave performance of a reentry antenna at relatively high altitudes. The effectiveness of the fluorocarbon Freon 114B2 as a plasma quenchant was studied during this program over a range of input power and plasma conditions simulating low altitude reentry.

A high performance shock tube was used to generate the air plasma. Plasma conditions were controlled by adjusting the shock tube initial conditions. A diagnostic study of the shock generated air plasma was performed

and a calibration of all instrumentation was accomplished. Microwave experiments were performed at low and high incident power levels using conventional microwave hardware. Details of the experimental techniques and results are described in detail in subsequent sections.

PLASMA DIAGNOSTIC EXPERIMENTS

Shock Tube Facility

The shock tube used for the experimental measurements utilizes a converging conical driver section to heat the driver gas. Electromagnetic forces supplied by the discharge of a 20 kV, 392 μF capacitor bank were used to compress and heat the driver gas and provide increased performance over more conventional driver techniques. After bursting a thin diaphragm, the flow expands and forms a new moving shock wave system in the driven section. A schematic of the shock tube is shown in Figure 1. The details of the driver technique and shock tube performance have been published previously[1,2]. The driver section consists of a 3.81 x 1.27 cm rectangular tube with a length of 111.5 cm. The tube was machined from aluminum and several observation ports were located along the axis of the tube. The driver section was terminated with a cylindrical dump tank which was connected to the vacuum system. The driver and driver sections were separated with a diaphragm of Saran and room air was used as the driver and driven gas. A liquid nitrogen cold trap was used to remove water vapor from the test gas. The pressure in the driver section was maintained at 0.5 torr while the pressure in the driver section was either 5.0 torr or 10.0 torr. A precision capacitance manometer was used to measure all static gas pressures. The shock velocity was varied by adjusting the capacitor bank voltage to the desired level. Capacitor bank voltages from 7-9 kV provided shock velocities of 2.8-4 mm/μsec for the prescribed initial conditions. The rectangular test section had provisions for observation ports at 10 cm intervals along the length of the tube. Provisions for special dielectric test sections were available at a distance of 80 cm from the diaphragm.

Flow Verification

The shock velocity is the most important parameter in the determination of test gas conditions. Once the shock velocity is known, the thermodynamic

---

[1] Rudderow, W. H., J. Appl. Phys. 43, 373 (1972).

[2] Rudderow, W. H., J. Appl. Phys. 43, 380 (1972).

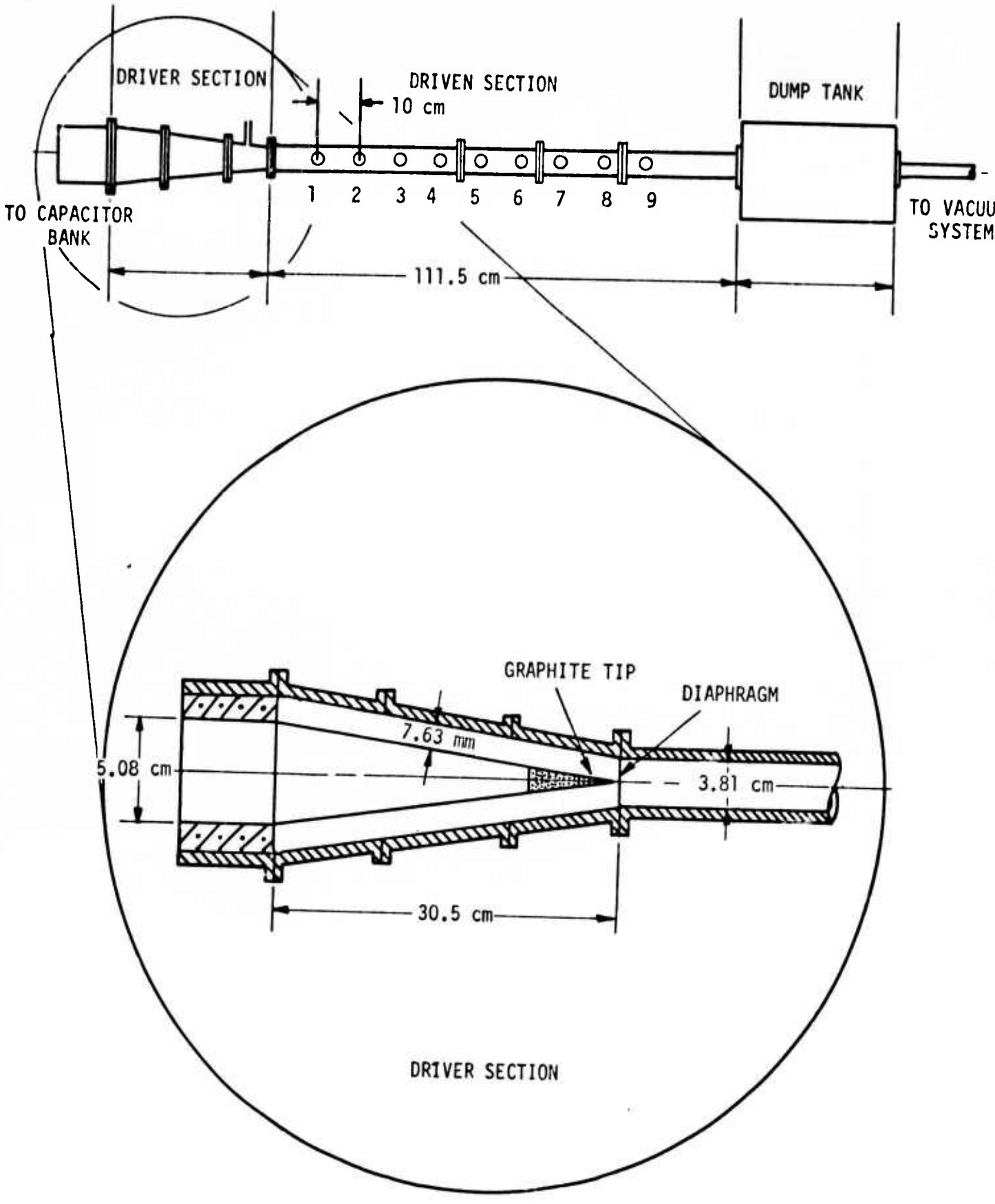

FIGURE 1 SHOCK TUBE SCHEMATIC

state of the gas flowing behind the shock wave can be determined from well-known shock tube theory. The equilibrium thermodynamic properties of air in the temperature range of interest have been calculated and are available[3]. The shock velocity can be accurately determined by the measurement of the passage of the shock wave at several locations along the axis of the tube. Piezoelectric static pressure gages were installed along the axis of the tube to indicate the passage of the shock wave. The pressure gages were developed previously by this laboratory and have a nominal rise time of 0.1 microseconds[4]. The piezoelectric probe outputs were then input into dual beam oscilloscopes to determine the time interval of the passage of the shock wave between several locations and permit the calculation of the average shock velocity.

The useful test time and flow uniformity can be determined from the response of a flush mounted electrostatic probe. Experiments were conducted to evaluate the test time and flow uniformity using a number of wall mounted electrostatic probes and plate mounted probes. The output of an electrostatic probe was used to determine the useful test time. Simple flush mounted electrostatic probes for wall measurements were constructed as shown in Figure 2. The collecting electrode was fabricated from copper and insulated from the shock tube wall with a Teflon spacer. The shock tube wall was used as the reference electrode, and the entire probe was mounted in a coaxial arrangement. The center electrode was biased relative to the wall with a battery, and the collected current was measured by observing the voltage drop across a load resistor placed in the circuit. The load resistor was selected according to the expected probe current. A typical response of a wall electrostatic probe and a pair of static pressure probes is shown in Figure 3. The output of two identical static pressure probes were input into a differential amplifier and the signals were subtracted to permit the time interval for shock passage to be displayed on the same trace.

The flow uniformity was also investigated in two perpendicular directions at a fixed axial location. Several small diameter electrostatic probes

---

[3]Menard, W. A. and Horton, T. E., NASA CR 10660 (1969).

[4]Rudderow, W. H., J. Appl. Phys. 39, 1 (1968).

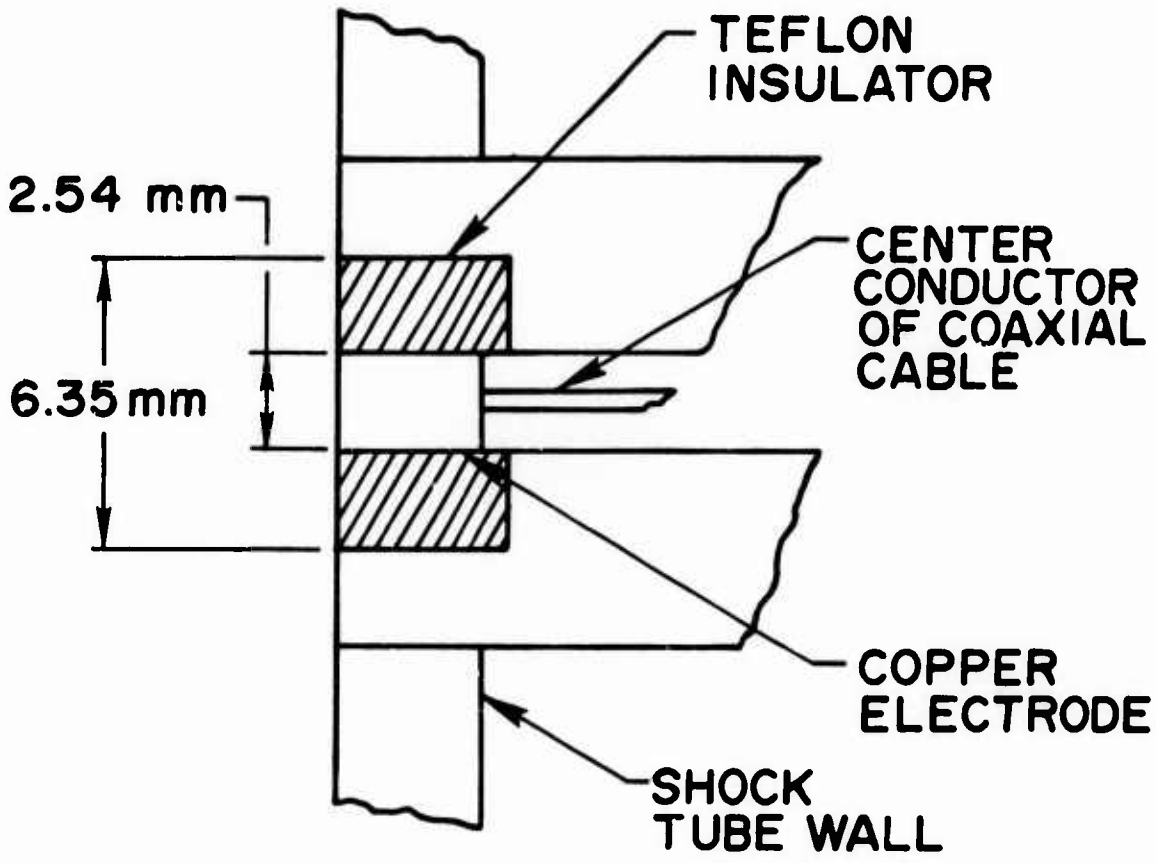

FIGURE 2. FLUSH ELECTROSTATIC PROBE

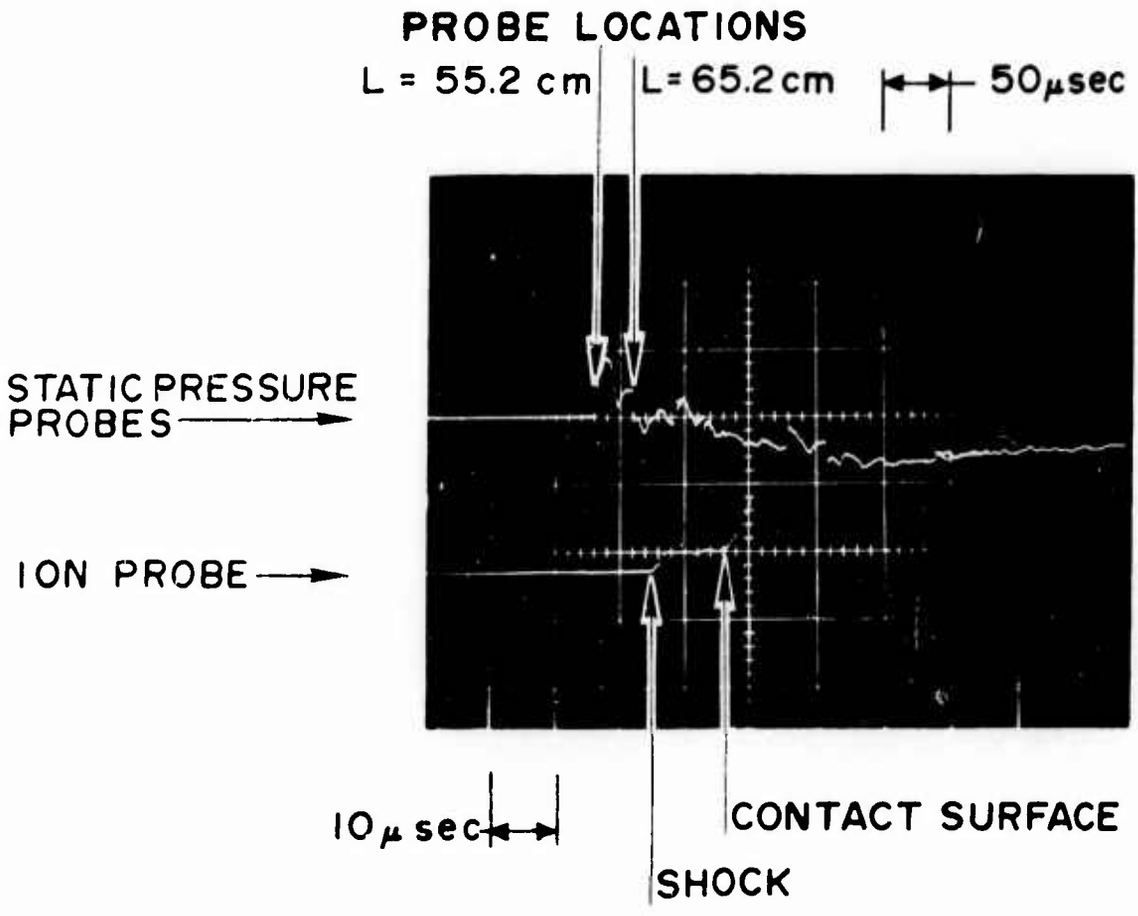

FIGURE 3. FLUSH ELECTROSTATIC PROBE RESPONSE

were located in a brass sharp edged ground plane to measure the planarity of the shock wave and the flow uniformity across the maximum dimension of the rectangular shock tube. A photograph of the ground plane with several electrostatic probes installed is shown in Figure 4a. The results indicated good uniformity and negligible curvature to the shock front. The uniformity across the minimum dimension of the shock tube was measured with three probes mounted in a sharp edged plate as shown in Figure 4b. Typical response of the electrostatic probes is shown in Figure 5 which indicates the flow uniformity in the transverse direction. Measurements over a wide range of shock velocities indicated similar results.

The useful test time is defined as the time between the passage of the shock wave and the arrival of the contact surface. The gas contained between the region of the shock wave and the contact surface has been heated by the shock wave and is generally free from contaminants. However, viscous effects cause a loss of mass flow in the test gas with a net result in the loss of available test time as compared to inviscid shock tube theory[5]. For the pressures and velocities encountered over the range of selected experimental conditions, losses due to an equilibrium turbulent boundary layer are expected. Wall mounted electrostatic probes are quite useful in the determination of useful test time since the arrival of the shock wave and the contact surface are easily and accurately determined from output oscilloscope traces indicating the collected probe current. The results of the measured test time for an initial shock tube pressure of 10 torr are shown in Figure 6 and compared with the theoretical prediction of available test time including losses due to a turbulent wall boundary layer[5]. The effect of varying probe bias was also investigated but no significant effect upon run time measurement was observed. The scatter in the run time measurements is probably caused by diaphragm opening effects, and this effect is seen in many high performance shock tubes. The available test time is shown in Figure 7 for an initial shock tube pressure of 5 torr for a fixed probe bias of -12 volts. Similar scatter in run time is observed, but sufficient run time is available for all planned experiments.

---

[5]Mirels, H., AIAA J. 2, 84 (1964).

[6]Bredfeldt, H. R., Scharfman, W. E., Guthart, A., and Morita, T., AIAA J. 5, 91 (1967).

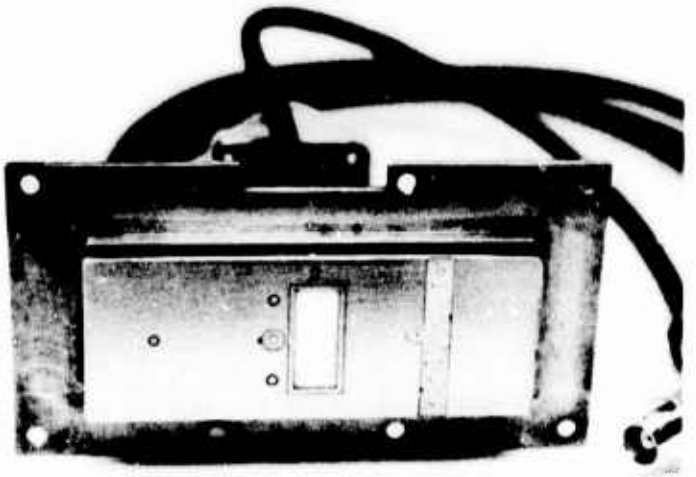

FIGURE 4A. GROUND PLANE ELECTROSTATIC PROBES

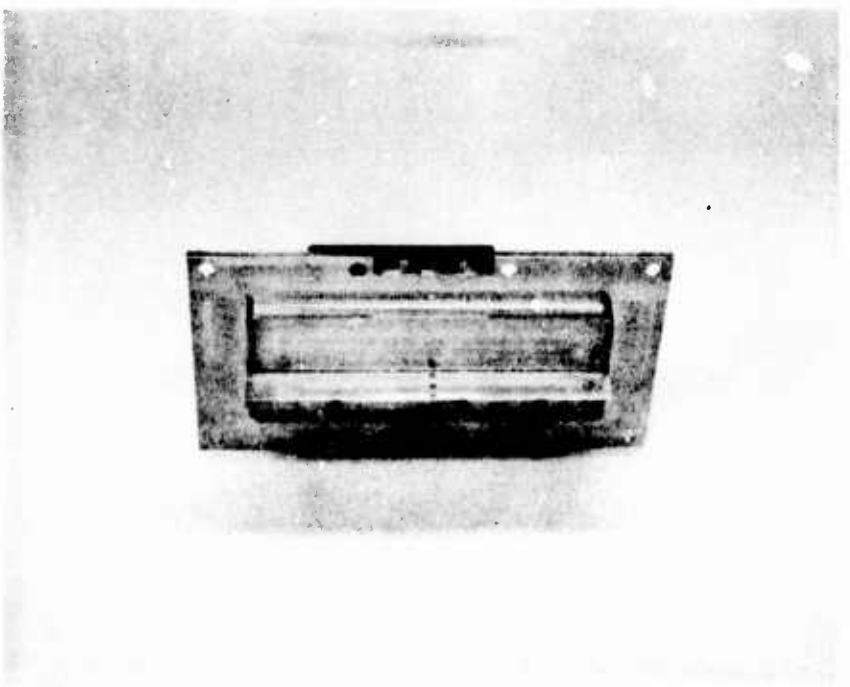

FIGURE 4B. PLATE MOUNTED ELECTROSTATIC PROBE

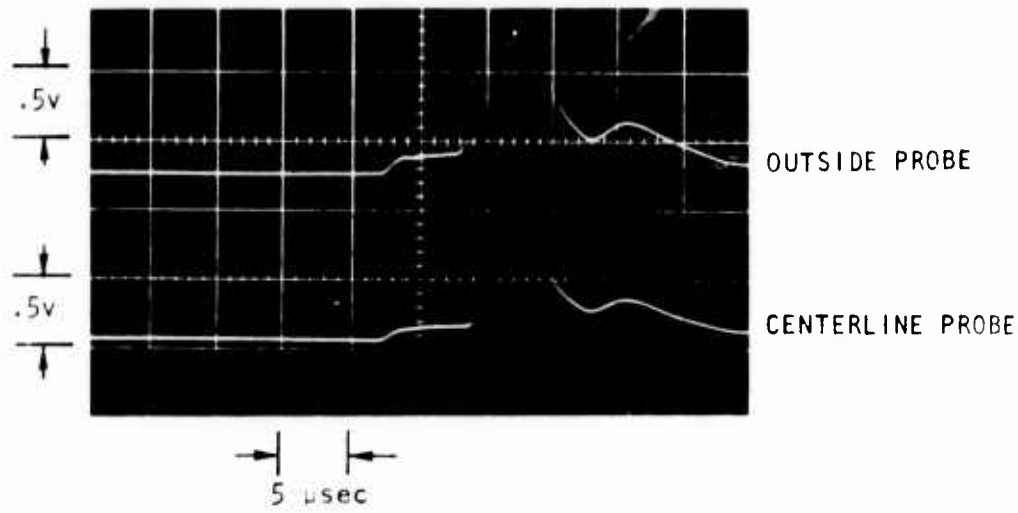

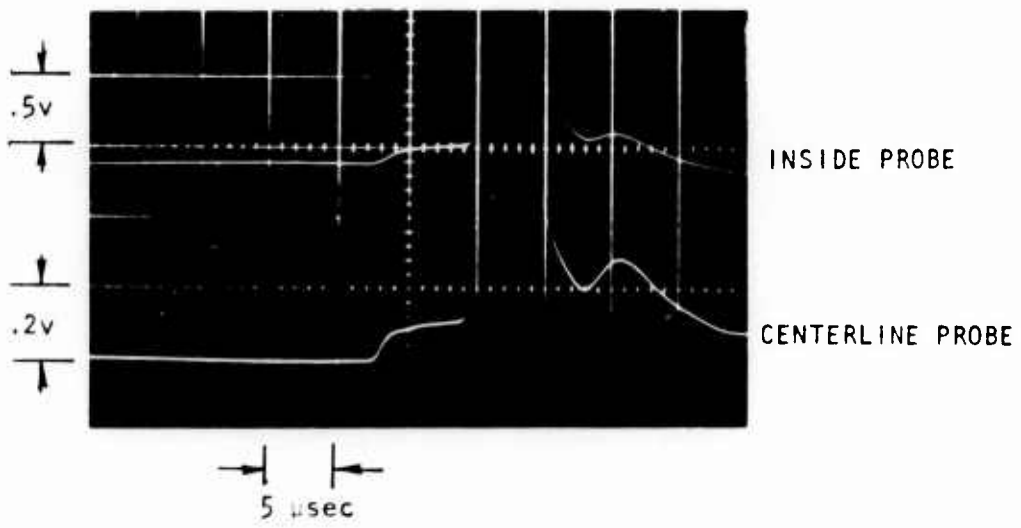

FIGURE 5. PLATE MOUNTED ELECTROSTATIC PROBE RESPONSE

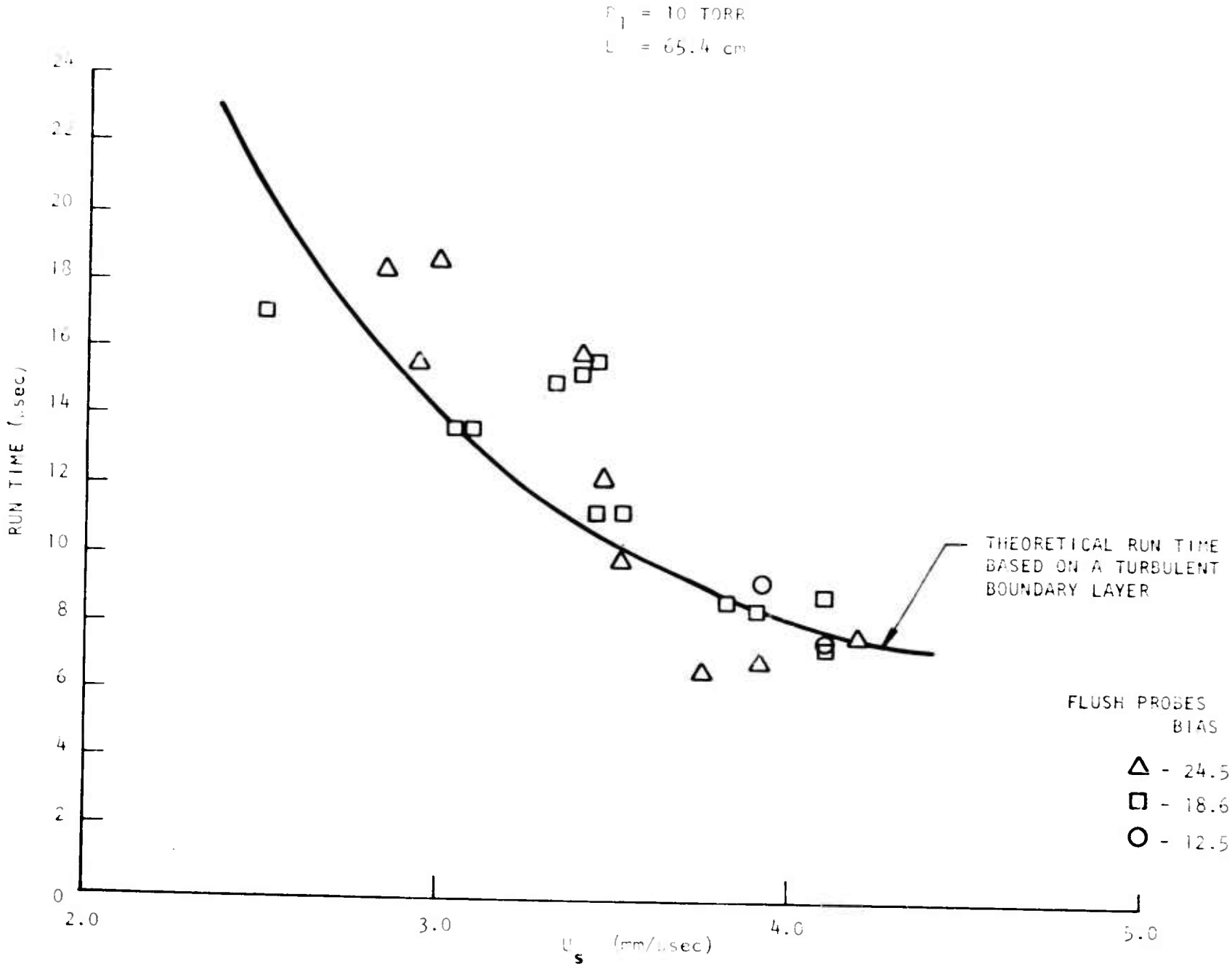

FIGURE 6. RUN TIME P = 10 TORR.

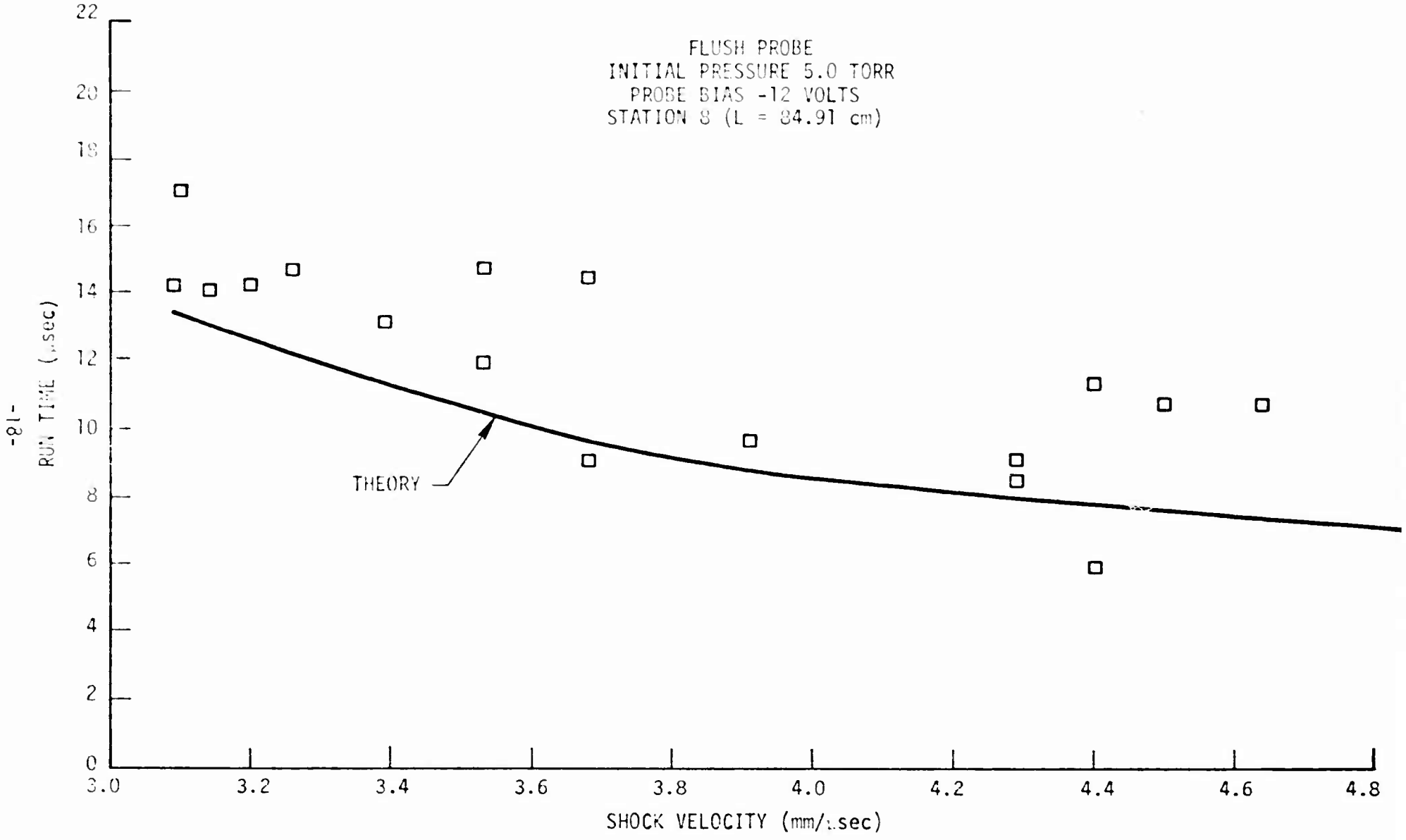

FIGURE 7. RUN TIME P = 5 TORR

Wall Mounted Electrostatic Probe Measurements

The usefulness of the flush mounted electrostatic probe in the determination of local electron concentrations in high speed flows has been demonstrated in laboratory[6-11] and full scale flight experiments[12,13]. Most of the experiments have been performed at relatively low density levels where the assumption of frozen flow is a good approximation. At higher pressure levels equilibrium flow is expected, and a series of diagnostic experiments were performed to measure local electron concentration levels using an extension of simple probe theories to deduce the local electron density.

A simple theoretical approach to flush probe operation is the theory presented by Bredfeldt et al[6]. The basic assumption considers the sheath dimension smaller than the boundary layer thickness such that convective effects can be neglected and the full random flux is collected by the probe. The sheath edge is then determined from the planar, space-limited, mobility controlled diode equation. Fringing field effects are also neglected, therefore the collected current depends only on probe geometric area. The theory also indicates a weak dependence upon temperature and mobility, therefore only an estimate of these quantities is required to analyze the results of the measurements. The theory of Bredfeldt et al does not predict a relationship between the free stream electron density and the density at the sheath edge located within the boundary layer. In order to check the validity of the theory an estimate of the electron density at the sheath edge must be made from boundary layer theory based upon measured edge conditions.

---

[7]Lederman, S., and Avidor, J., Israel J. of Tech. 9, 19 (1971).

[8]Burke, A. F., AIAA Paper No. 68-166, 1968.

[9]Chung, P. M., and Blankenship, V. D., AIAA J. 4, 442 (1966).

[10]Boyer, D. W., and Touryan, AIAA J. 10, 1667 (1972).

[11]Russo, A. J., and Touryan, K. J., AIAA J. 10, 1675 (1972).

[12]Hayes, D. T., and Rotman, W., AIAA J. 2, 675 (1973).

[13]Hayes, D. T., AIAA Paper No. 72-694, 1972.

Following Bredfeldt et al, the full random current at the sheath edge is assumed to be collected by the probe,

$$j = 1/4\ neV_{th} ,$$

where the charged particle thermal speed is[13]

$$V_{th} = \left(\frac{3kT_e}{m}\right)^{1/2} .$$

For the data analysis the geometric area of the probe was used as the collecting area, and the electron temperature was assumed to be equal to the equilibrium gas temperature. The location of the sheath edge was determined from the planar, space-limited, mobility controlled diode equation

$$j = 9/8\ \epsilon_o \mu_i \left(\frac{V^2}{y_s^3}\right)$$

where ϵ_o is the permitivity of free space, μ_i is the charged particle mobility, V is the probe voltage, and y_s is the normal distance from the probe surface to the sheath edge. Based on an estimate of the charged particle mobility, the distance to the sheath edge can be determined from the measured experimental parameters. The ion mobility was calculated from the Langevin equation[14] using thermodynamic properties defined at the edge of the boundary layer. Since the mobility is not a strong function of temperature, the temperature at the boundary layer edge value was used for the data reduction. When the probe was biased to collect ions, the ion current was assumed to consist of NO^+ ions for the entire range of shock velocity. This assumption is based upon calculations of equilibrium air specie concentrations in the temperature range of 3000-6000°K[3].

In order to relate the measured current density to the free stream electron density, an estimate of the electron density profile is required. Bredfeldt et al, have derived a zero order laminar boundary layer theory based upon frozen flow and unity values of Prandtl, Schmidt, and Lewis numbers.

---

[14] Cobine, J. D., Gaseous Conductors, p. 36, Dover, New York, 1958.

Since equilibrium, turbulent boundary layer flow is expected over the range of initial shock tube conditions for the experiments described here, a new estimate of the electron density profile must be made.

The shock tube wall boundary layer appears unsteady to an observer fixed in the laboratory frame of reference according to well-known shock tube theory. Immediately behind the moving shock the boundary layer forms and grows rapidly according to the initial shock tube conditions. Transition from a laminar to a turbulent boundary layer will occur above a certain Reynolds number based upon the shocked gas flow conditions and any disturbances induced in the flow during the diaphragm opening process. For the experimental conditions described here a fully turbulent boundary layer is expected. This has been substantiated with the measurements of the available test time based on losses due to a turbulent boundary layer; however, a complete experimental verification of the existence of a wall turbulent boundary layer was not made.

Preliminary measurements of the ion current collected by an electrostatic probe biased over a wide range of bias voltages indicated a steady time response during the useful test time period. This result indicates that the probe sheath edge was either located outside the boundary layer edge or that the unsteady effects for the shock tube conditions and probe location were of secondary importance. In order to examine this question, a comparison was made of the measured electron density with the free stream electron density based upon calculations of equilibrium air[3] using measured shock velocity. The results of these measurements are shown in Figure 8. The agreement is quite poor with the electron density well below the predicted free stream value which suggests that the sheath edge was located within a wall boundary layer. Based upon these observations, a simple engineering model of a steady, ionized, turbulent boundary layer was selected as a crude approximation to the observed flow and the electron density profile calculated and compared to measured results.

The flow conditions behind the shock were defined as the edge conditions of the boundary layer and were determined from calculated real air equilibrium

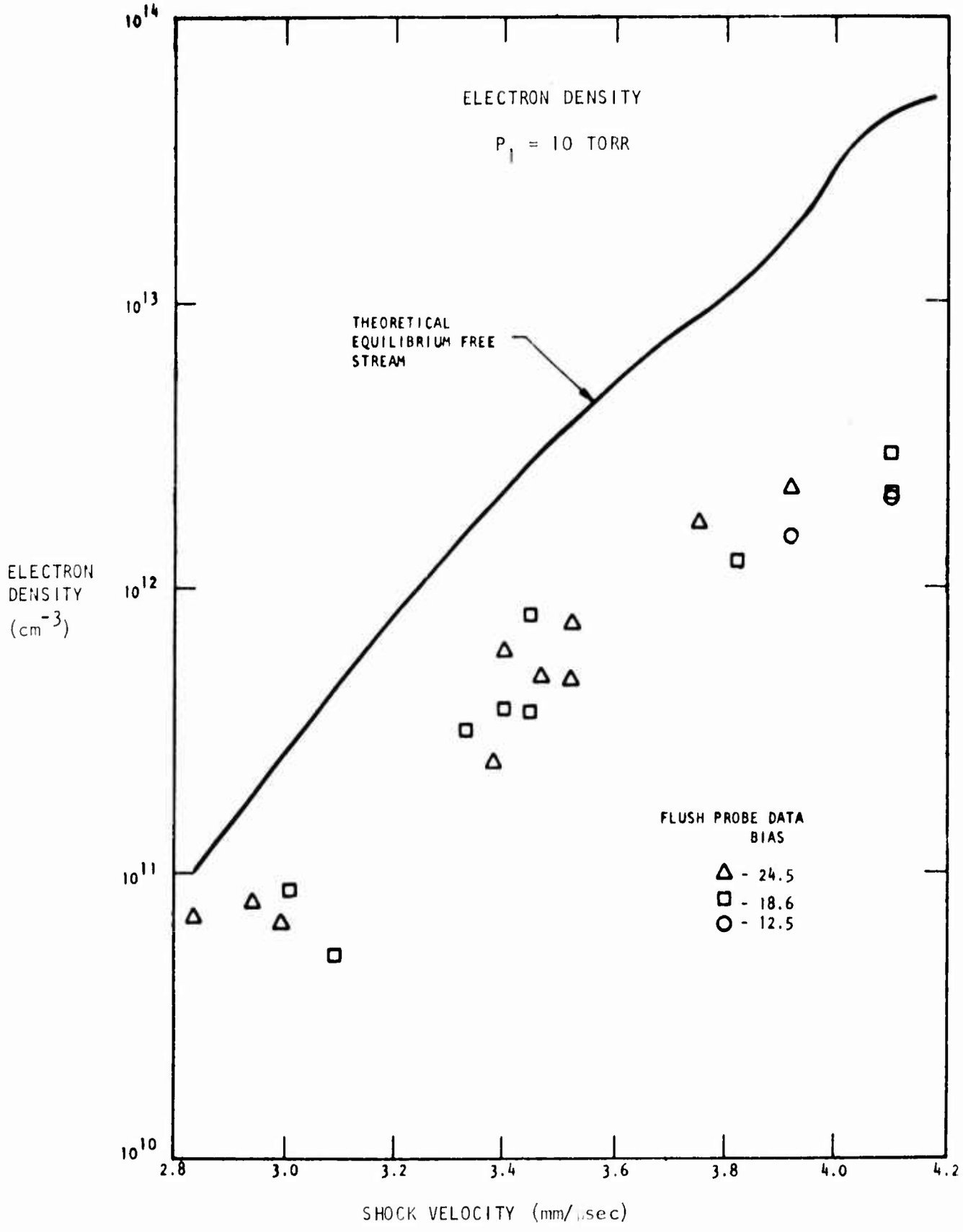

FIGURE 8 ELECTRON DENSITY MEASUREMENT

thermodynamic properties[3]. The turbulent boundary layer profiles were calculated from the method presented by Jacobs[15]. Following Jacobs the velocity profile is assumed to follow a 1/7 power law relationship

$$\frac{U(y)}{U_e} = \left(\frac{y}{\delta}\right)^{1/7}$$

where U_e is the edge velocity, y is the normal distance in the boundary layer profile, and δ is the velocity thickness. The relation between the velocity thickness and the momentum thickness is obtained from the power law relationship

$$\frac{\delta}{\theta} = (n+1) + \left[\left(\frac{n+2}{n}\right)\frac{h_w}{h_r}\right]\left[1 + .845r\,\frac{U_e^2}{h_e}\right]$$

where n is the integer (=7) in the velocity power law relationship, θ is the momentum thickness, h_r is the recovery enthalpy, h_w is the wall enthalpy, h_e is the enthalpy at the boundary layer edge, and r is the recovery factor. The momentum thickness is obtained from the Blasius relation

$$\frac{\theta}{x} = .0194\,\varepsilon$$

where x is the wetted distance and

$$\varepsilon = \left(\frac{\rho^* \mu^*}{\rho_e \mu_e}\right)^{.2} \left(\frac{\rho^*}{\rho_e}\right)^{.6} \Big/ \left(\frac{\rho_e U_e x}{\mu_e}\right)^{.2}$$

where the starred quantities are evaluated at the reference enthalpy. The enthalpy profile in the boundary layer is predicted by the Crocco integral

$$h(y) = h_w + \frac{U(y)}{U_e}(H_t - h_w) - \left[\frac{U(y)}{U_e}\right]^2 \frac{U_e}{2}$$

where h_w is the wall enthalpy and H_t is the total enthalpy. Since the pressure is assumed to be constant across the boundary layer, the remaining thermodynamic

---

[15] Jacobs, H. R., "Engineering Approximations of the Effects of Blunting on Cones in Laminar and Turbulent Flow," Aerospace Report No. TR-0158 (S3816-41)-1, 1967.

properties and specie concentrations can be determined from real air thermodynamic tables[16,17] after the local enthalpy has been determined.

Measurements of the ion current collected by a negatively biased and positively biased wall mounted probe were made for an initial shock tube pressure of 10 torr. The probe was located 65.2 cm from the diaphragm and biased at ±18.6 volts relative to the shock tube wall. The sheath edge location was calculated from the diode equation using the measured current density and calculated charged particle mobilities. The boundary layer thickness was also calculated for the range of expected conditions using the distance from the diaphragm as the wetted distance. This approximation treats the side wall as a flat plate in a uniform stream. The boundary layer thickness was calculated to be greater than the measured sheath distance over the entire range of flow conditions. The results of the measurements are compared to the theoretical predictions in Figure 9 for a probe biased to collect ions and in Figure 10 for a probe biased to collect electrons. The agreement with the theoretical predictions appear to be reasonable in both cases. An evaluation of the theoretical model at a different value of probe bias, probe location and initial pressure was also performed. The results of these measurements are shown in Figure 11 where similar agreement with theory is also observed.

Flat Plate Electrostatic Probe Measurements

Owing to the theoretical difficulties in the analysis of wall mounted electrostatic probes, a series of measurements were performed using probes mounted in a sharp edged flat plate mounted inside the shock tube test section. For these measurements the flow over the plate will appear steady to an observer in the laboratory frame of reference after a short transition time to initiate the flow.

---

[16] "Thermodynamic Properties of High Temperature Air," Chance Vought Research Center Report RE-1R-14, 1961.

[17] Logan, J. G. and Treanor, C. E., Tables of Thermodynamic Properties of Air from 300°K to 10,000°K at Intervals of 100°K, Cornell Aero. Lab. Report BE-1007-A-3, 1957.

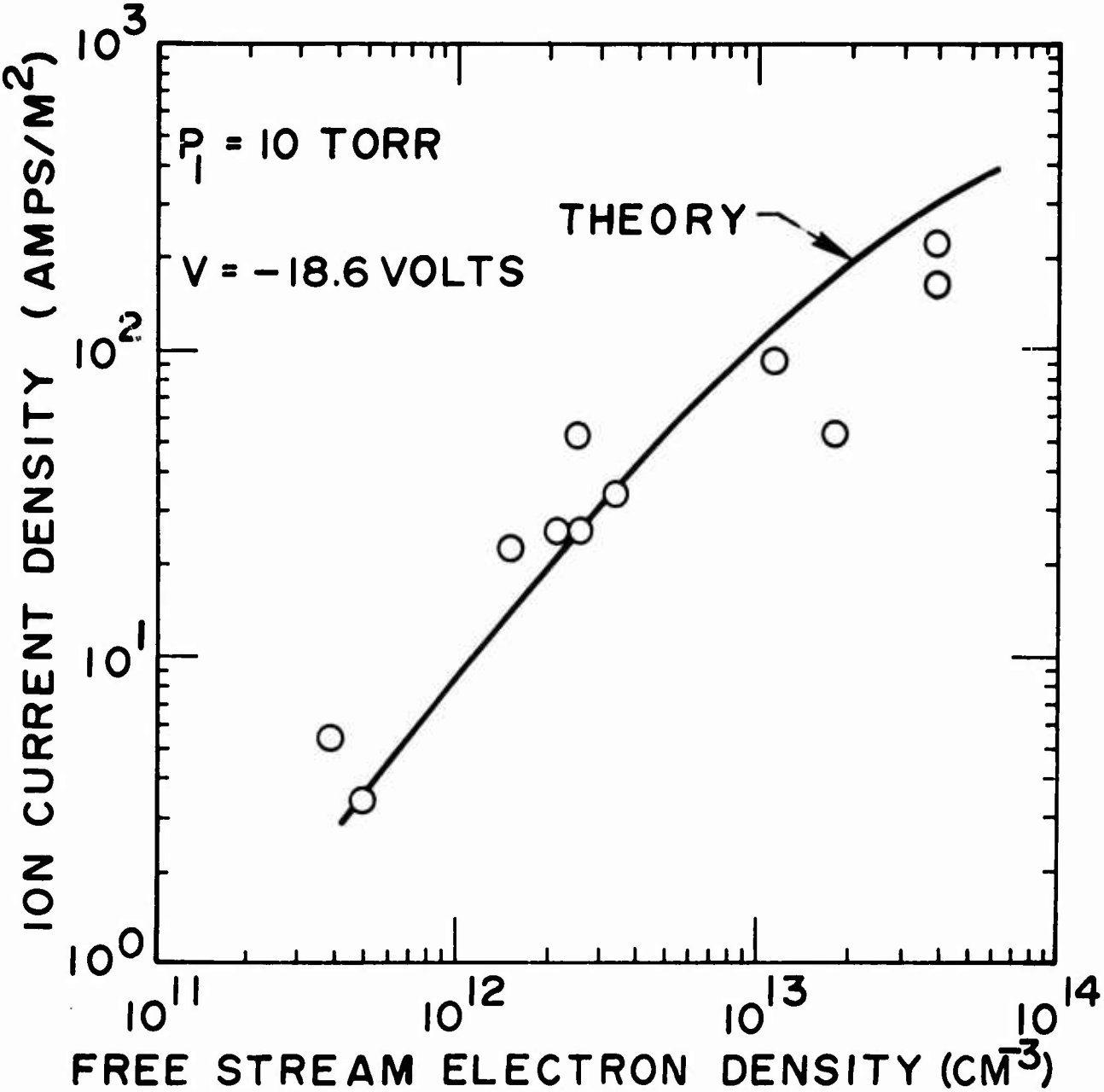

FIGURE 9. ELECTRON DENSITY BASED ON ION CURRENT

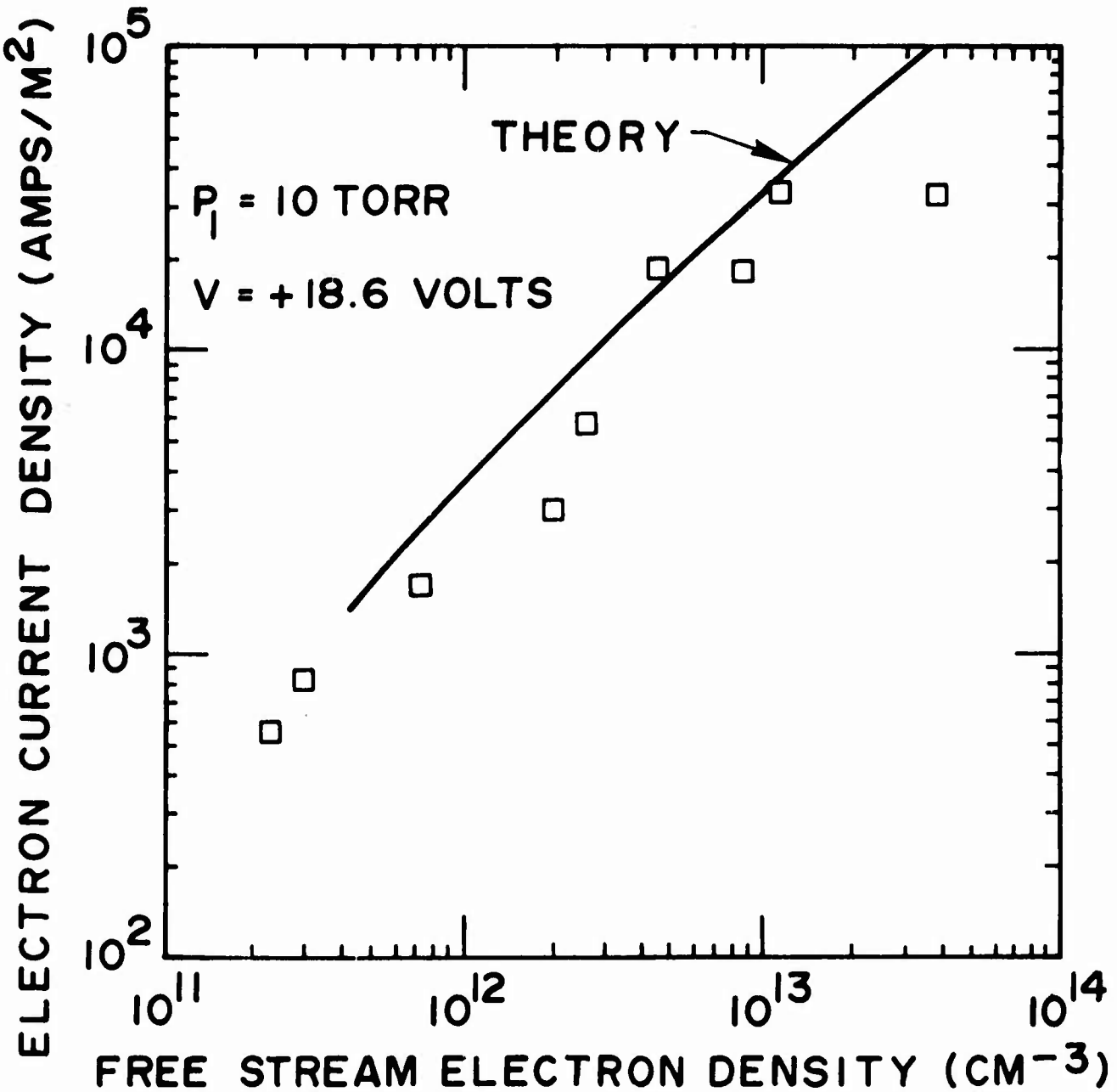

FIGURE 10. ELECTRON DENSITY BASED ON ELECTRON CURRENT

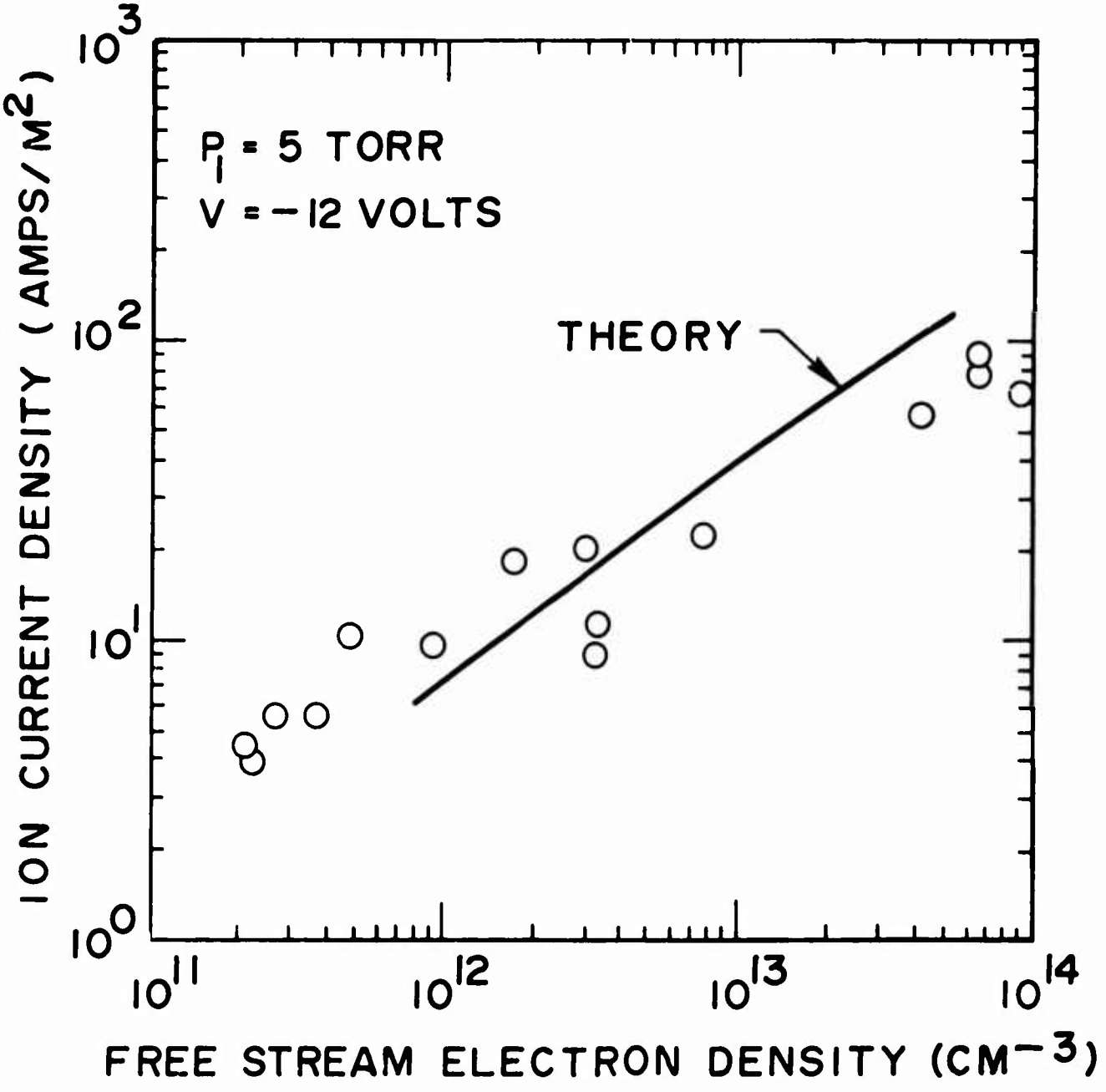

FIGURE 11. ELECTRON DENSITY BASED ON ION CURRENT

The probe theory of Chung et al[18] offers the advantage of an explicit relationship between measured current density and free stream electron density. For conditions on a flat plate located in the center of the shock tube the Chung theory becomes appropriate for low levels of probe bias. The effect of probe bias has been investigated by Scharfman and Bredfeldt[19] who found that reasonable agreement with Chung theory was possible for probes biased at -3 volts. Since the purpose of the measurements was to determine the free stream electron density at various positions in the shock tube test section, all probes were biased in a -3 volts relative to the plate and the theory of Chung et al[18] was used to deduce the electron density. A series of measurements of the collected ion current over a range of free stream electron densities was performed for a fixed initial pressure of 5 torr. The results are shown in Figure 12 and compared with the prediction of Chung. The agreement with theory appears good; however, a reduction in slope with increasing electron density is apparent. This observation is in agreement with previous measurements.[19]

Stagnation Point Electrostatic Probe Measurements

The stagnation point electrostatic probe has been suggested as a useful means of measuring the electron density in ionized flows[20,21]. The operation of the stagnation point probe is similar to the flush mounted probe for the collection of probe current; however, the advantage of the stagnation point probe is the fact that the flow field surrounding the probe is usually known with a greater amount of confidence than flow conditions far downstream of the stagnation point. For shock tube applications a shock wave will form in front of a blunt protruding probe requiring additional flow field calculations to determine boundary layer edge conditions. The non viscous flow around the probe will consist of a region between the stand-off shock and the boundary of the viscous layer. The probe sheath will extend into this region

---

[18] Chung, P. M., Talbot, L. and Touryan, AIAA J. 12, 144 (1974).

[19] W. E. Scharfman, and H. R. Bredfeldt, SRI Final Report Subcontract 601603 under Contract DA 30-069 AMC-333(Y), 1967 (unpublished).

[20] Talbot, L., Phys. Fluids 3, 289 (1960).

[21] Pollin, I., Phys. Fluids 7, 1433 (1964).

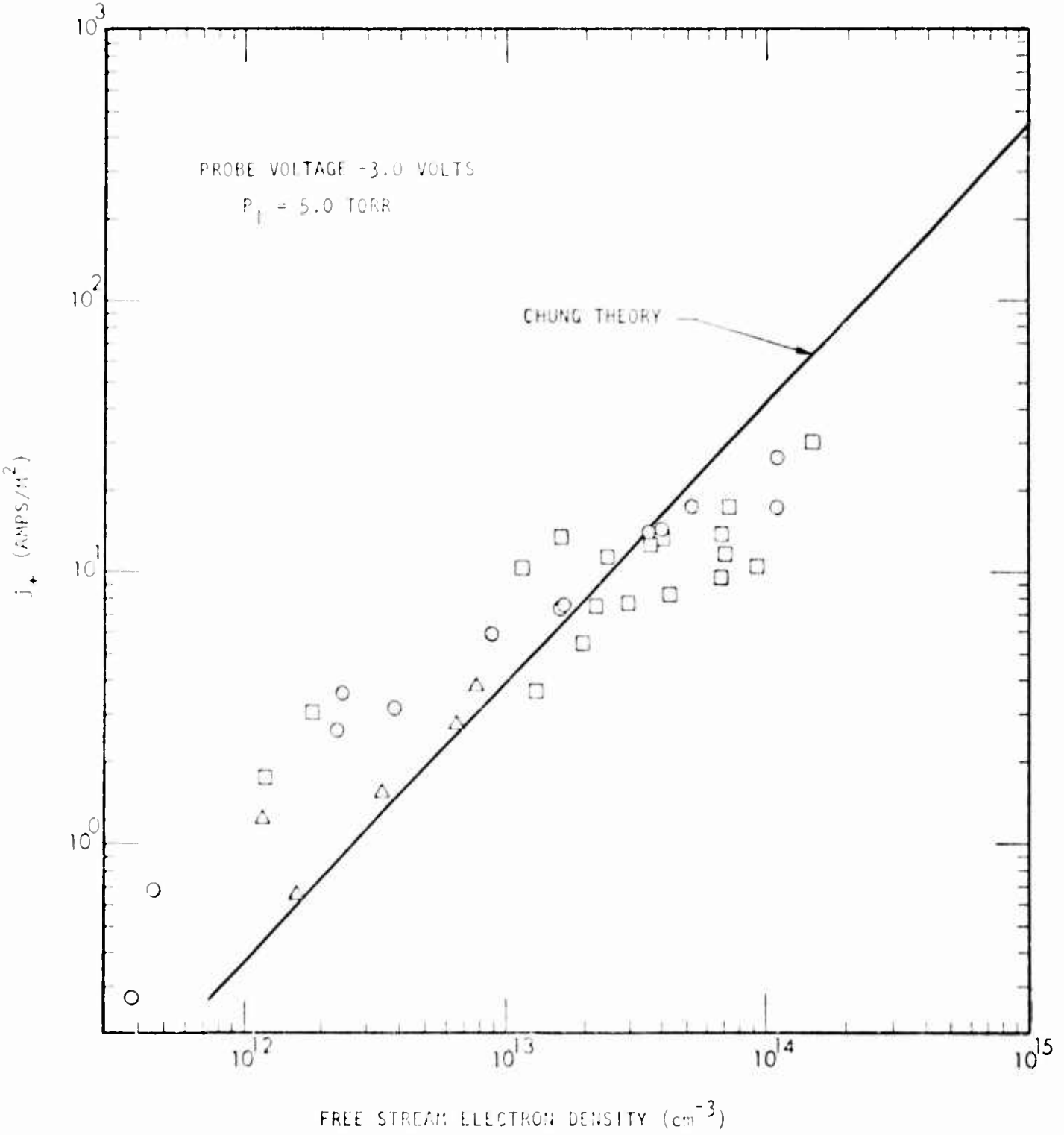

FIGURE 12. ION CURRENT DENSITY

depending on the probe bias. For the experiments performed here the probe sheath thickness is less than the boundary layer thickness and the electron density will be measured within the laminar boundary layer.

The construction of the stagnation point probe is similar to the flush mounted probe with the copper center electrode biased relative to the shock tube wall. A sketch of the probe which illustrates the coaxial configuration is shown in Figure 13a. The probe was biased with a battery and the probe current was determined from the voltage drop across a load resistor inserted in the circuit. A typical response of the probe is shown in Figure 13b where the velocity at the same axial location of the probe was also measured from the output of piezoelectric static pressure probes. The shock wave ahead of the stagnation point probe forms rapidly, and the flow relaxes to an equilibrium flow in a few microseconds.

The Bredfeldt probe theory was also used to define the stagnation point probe operation. The sheath edge was calculated with the same diode equation used to define the flush probe sheath edge. The full random flux was assumed to be collected by the probe at the sheath edge, and stagnation properties were determined from conditions at the edge of the viscous layer.

The flow surrounding the probe is the classical hypersonic stagnation point flow field. The most universally accepted solutions to the stagnation point problem are the solutions of Fay and Riddell[22] where the heat transfer through the boundary layer has been shown to be adequately predicted by a simple correlation formula. For an equilibrium boundary layer the Fay-Riddell formula presents a simple relation for Nusselt number. The Stanton number can then be calculated from the definition of Nusselt, Prandtl, and Reynolds numbers. With the aid of the modified Reynolds analogy between heat transfer and skin friction, a relation for the boundary layer momentum thickness can be obtained. The momentum thickness for a flow in which the Lewis number is unity is

---

[22]Fay, J. A. and Riddell, F. R., AIAA J. 25, 73 (1958).

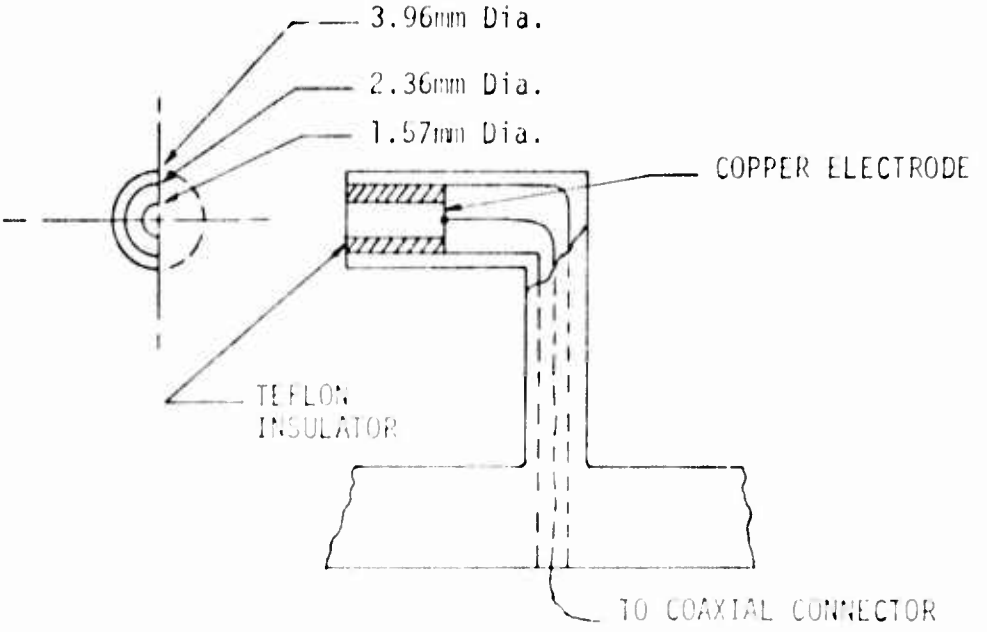

FIGURE 13A. STAGNATION POINT ELECTROSTATIC PROBE

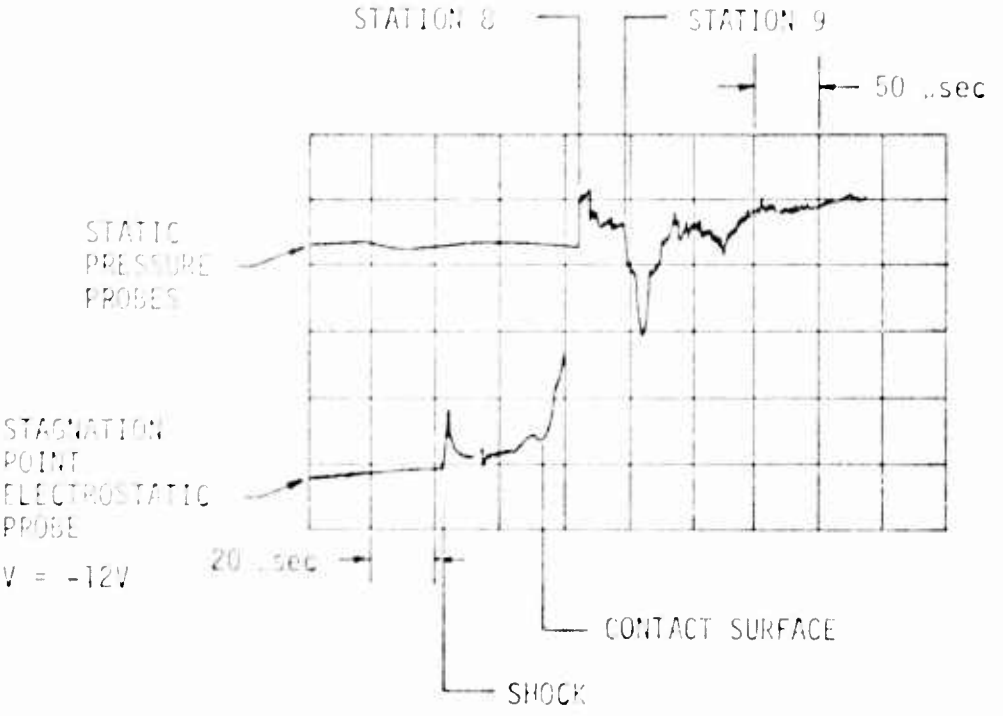

FIGURE 13B STAGNATION POINT ELECTROSTATIC PROBE RESPONSE

$$\frac{\theta}{x} = 1.34\left(\frac{\rho_s \mu_s}{\rho_w \mu_w}\right)^{.4} (R_e)^{-1/2} (P_r)^{-1/3}$$

where θ = momentum thickness

x = probe radius

ρ = density

μ = viscosity

R_e = Reynolds number

P_r = Prandtl number

and the subscript s refers to conditions at the edge of the boundary layer and the subscript w refers to conditions at the wall. With the assumption of a power law velocity profile a relation between the momentum thickness and boundary layer thickness can be established from their respective definitions[23]. An approximation to the velocity profile may be made from the similar solutions of Fay and Riddell. A power law variation of velocity profile with an exponent of 1/4 is an approximation which holds for 80% of the total profile. The enthalpy profile can now be calculated for the assumed velocity profile using the Crocco integral method. The electron density at the sheath location can be determined with the aid of real gas tables[16,17] after the enthalpy and pressure have been determined.

Measurements of the probe current collected by a stagnation point probe located on the centerline of the rectangular test section were made for a range of incident shock velocity. For these measurements the shock tube initial pressure was maintained at 5 torr and the probe bias was fixed at -12 volts. The electron density and the sheath distance were calculated in the same manner as the wall mounted flush probes. The electron density as deduced from the probe current measurements is shown in Figure 14 where the results are compared with the theoretical predictions. The stagnation point probe electron density measurements appear to agree within a factor of three with the predicted values.

---

[23]Schlichting, H., Boundary Layer Theory, McGraw-Hill, 1960.

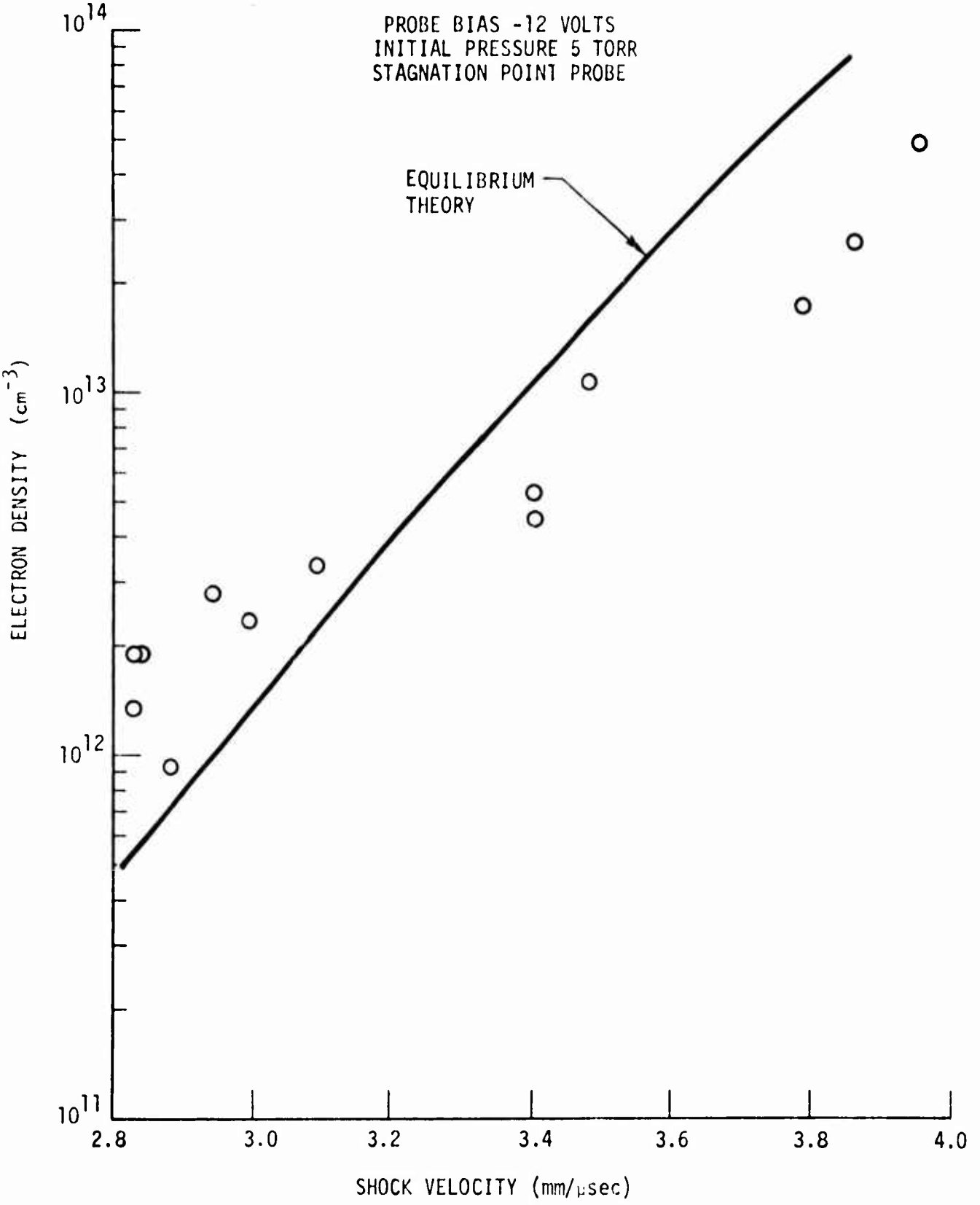

FIGURE 14. ELECTRON DENSITY BASED ON STAGNATION POINT PROBE MEASUREMENTS

Conductivity Probe

Another method of measuring the electron density in ionized gas flows is the conductivity probe proposed by Aisenberg and Chang[24]. The technique uses a sensitive marginal oscillator whose oscillation amplitude is a function of the Q of a tank circuit. A coil of the resonant circuit is placed adjacent to the plasma where RF eddy currents are induced according to the plasma conductivity. The RF coupling causes a reduction of the Q of the resonant circuit which results in a reduction in the amplitude of the oscillation. Using the design of Aisenberg and Chang, a coil probe and marginal oscillator circuit was constructed and is shown in Figure 15. The coil probe was fabricated to enable the face of the probe to the flush mounted to the shock tube wall as suggested by Aisenberg and Hu[25]. Using the suggested probe geometry and circuit component values, a compact circuit suitable for shock tube use was built. The oscillator circuit was adjusted and a suitable output signal was observed from the circuit when the probe was placed in close contact with a metallic conductor. Difficulty, however, was encountered when the probe was placed in close contact with salt solutions which gave conductivities in the range of the expected air plasma conductivity. The lack of sensitivity proved to be a severe problem which indicated that the conductivity probe was unsuitable for the present application. Other laboratory plasma experiments using the conductivity probe yield similar difficulties with sensitivity[26].

FLUSH MOUNTED APERTURE ANTENNA EXPERIMENTS

The effect of a high power microwave pulse incident upon a layer of partially ionized air can cause additional electron production due to electric field induced ionization. The result of the additional ionization produced

---

[24]Aisenberg, S., and Chang, K. W., "An RF Coil System for the Measurement of Plasma Electrical Conductivity," AFCRL-70-0033, October 1969.

[25]Aisenberg, S., and Hu, P. N., "A Theoretical and Experimental Study of Plasmas," AFCRL-71-0018, November 1970.

[26]Churchill, R. J., Chan, P. W., and Wilhelm, H. E., "Environmental Effects on Aerospace Sensor Systems," AFCRL-TR-74-0535, October 1974.

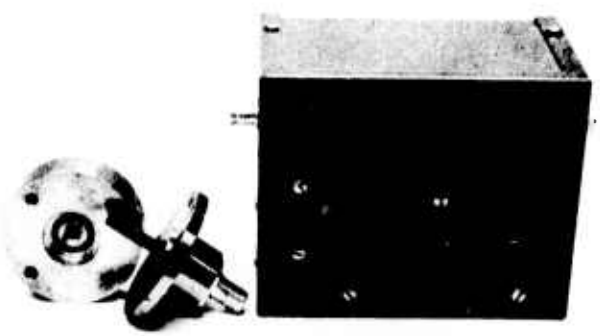

FIGURE 15. CONDUCTIVITY PROBE

by the intense electric fields in the near zone of a reentry antenna is a further degradation of the transmitted signal. Flight test measurements of an S band antenna located in the stagnation region of a blunt reentry vehicle indicate the strong effect of incident power level upon antenna performance[27]. The increased electron concentration also causes an increase in the reflected power level which places an additional constraint upon the designer of a reentry communication system. Mutual coupling and other near field effects also become important at high power levels.

The breakdown of air at microwave frequencies has been studied for standard temperatures and low pressures[28]. The effect of elevated temperatures upon the ionization frequency has also been carefully studied for low pressure air[29-32]. Theoretical and experimental studies of antenna system performance including the non-linear interaction of the incident wave and plasma medium have been made for a number of cases of interest[33-38]. Shock tube experiments

---

[27]Rotman, W. and Maloney, L. R., Air Force Cambridge Research Laboratories Report No. AFCRL-TR-73-0072, 1973.

[28]Gould, L. and Roberts, L., J. Appl. Phys. 27, 1162 (1956).

[29]Taylor, W. C., Chown, J. B., and Morita, T., J. Appl. Phys. 39, 191 (1968).

[30]Epstein, M., Phys. Fluids, 11, 896 (1968).

[31]Light, G. C. and Taylor, E. C., J. Appl. Phys. 39, 1591 (1968).

[32]Light, G. C., J. Appl. Phys. 40, 1715 (1969).

[33]Fante, R., J. Appl. Phys. 42, 4202 (1971).

[34]Mayhan, J. T., Fante, R., O'Keefe, R., Elkin, R., Klugerman, J., and Yos, J., J. Appl. Phys. 42, 5362 (1971).

[35]Mayhan, J., IEEE Trans. Antennas Prop., 251 March (1969).

[36]Mayhan, J. and Fante, R., J. Appl. Phys., 40, 449 (1969).

[37]Mayhan, J. and DeVore, R. V., J. Appl. Phys. 39, 5746 (1968).

[38]Mayhan, J. and Fante, R., J. Appl. Phys. 40, 5207 (1969).

have also been performed examining the interaction[39-40] of intense electric fields interacting with a plasma contained in a waveguide. Recent theoretical and experimental results have also been published which include the effect of chemical alleviants upon the non-linear interaction phenomena[41-43]. The microwave results all indicate a rapid attenuation of the incident pulse followed by a relaxation to an equilibrium value. A perhaps more significant result is the observation that there is a critical input power level above which there is no increase in transmitted power[33,34]. The critical input power level will be a function of the plasma conditions and the aperture electric field.

Owing to the many complexities of wave-plasma interaction phenomena, an experimental program was undertaken to extend the range of high power transmission measurements to include high plasma frequencies and high electron-neutral collision frequencies. Supporting plasma diagnostic data were also obtained to determine local electron density and local flow velocity. For the high power measurements a single pulse located near the center of the uniform test gas slug length was selected.

The shock tube rectangular driven section had provisions for observation ports at 10 cm intervals along the length of the tube, and a special dielectric test section was installed at an axial location of 80 cm from the diaphragm. The shock velocity was measured with several piezoelectric static pressure gages installed along the shock tube wall while the electron density was measured with flush mounted electrostatic probes mounted in the antenna sharp-edged ground plane. A photograph of the shock tube facility is shown in Figure 16. The initial pressure in the driven section was maintained at 5.0 torr for all measurements using dry, room air as the test gas.

---

[39] Mayhan, J. T., Air Force Avionics Laboratory Technical Report 2151-6, December 1967.

[40] Mayhan, J. T., Stockum, L., and DeVore, Air Force Avionics Laboratory Technical Report 2151-5, August 1967.

[41] Papa, R. J. and Taylor, R. L., J. Appl. Phys. 45, 684 (1974).

[42] Papa, R. J. and Taylor, R. L., Air Force Cambridge Research Laboratories Report No. AFCRL-TR-73-0754, 1973.

[43] Papa, R. J. and Taylor, R. L., Air Force Cambridge Research Laboratories Report No. AFCRL-TR-73-0362, 1973.

FIGURE 16. PHOTO OF SHOCK TUBE

Low Power Microwave System

The initial microwave experiments were performed for a low power (15 mW) cw signal. A simple waveguide aperture antenna was installed in a brass ground plane and installed inside the dielectric test section as the transmitting antenna. A small horn antenna or a waveguide antenna was installed outside the test section as the receiving antenna for the initial experiments. A half wavelength Teflon plug was inserted in the transmitting antenna as an antenna window. A sharp edged ground plane was positioned inside the test section and was shaped to minimize the flow disturbances over the antenna aperture. The test gas consists of a portion of the shock generated plasma which flowed between the ground plane and the dielectric wall of the test section. The plasma layer thickness covering the antenna could be varied from 3.18 mm to 12.7 mm by adjusting the location of the transmitting antenna ground plane relative to the dielectric wall. A schematic of the test section is shown in Figure 17. Reflections from the dielectric wall of the test section were minimized by cutting a series of horizontal and vertical grooves in the inside wall of the test section. The location and depth of the grooves was conducted on a trial and error basis until the reflections were minimized. The outside of the test section was covered with a microwave absorbing material to further reduce scattering. A photograph of the test section is shown in Figure 18. Provision for the installation of a piezoelectric static pressure probe was provided in the top of the test section. Several flush mounted electrostatic probes were mounted in the antenna ground plane to monitor the local electron density. The collecting electrodes were fabricated from 1.59 mm diameter copper with a Teflon spacer to insulate the electrode from the ground plane. One probe was located on the aperture centerline at the edge of the ground plane while the remaining probes were located downstream of the aperture centerline.

The low power microwave signals were generated by an x-band test set and were launched and detected using conventional x-band waveguide hardware. A schematic of the low power microwave circuit is shown in Figure 19.

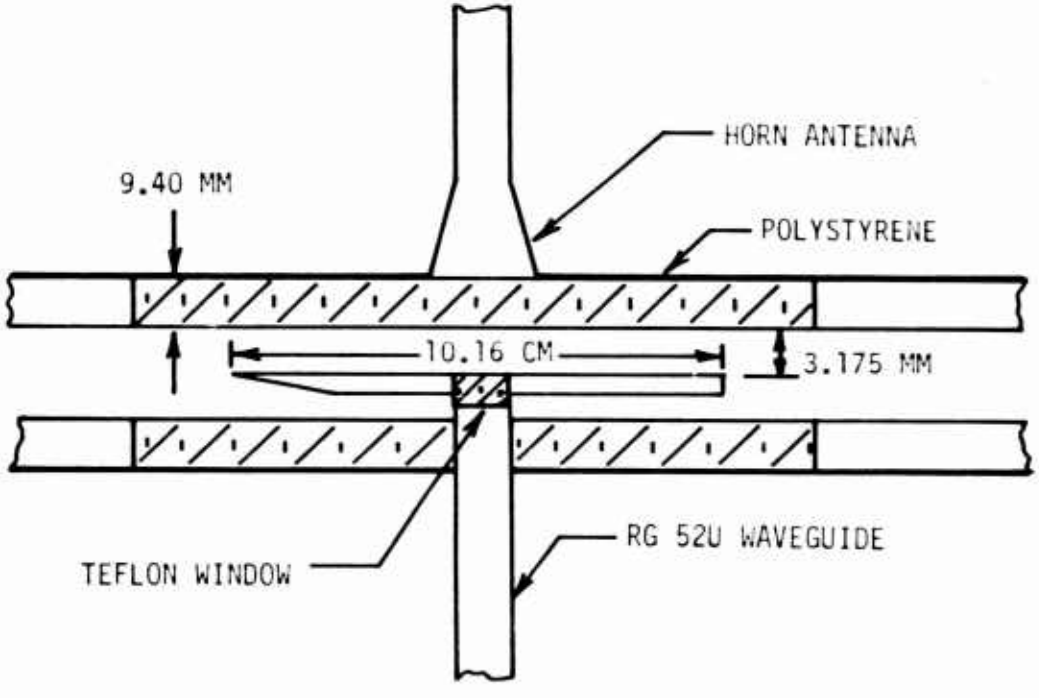

FIGURE 17. TEST SECTION SCHEMATIC

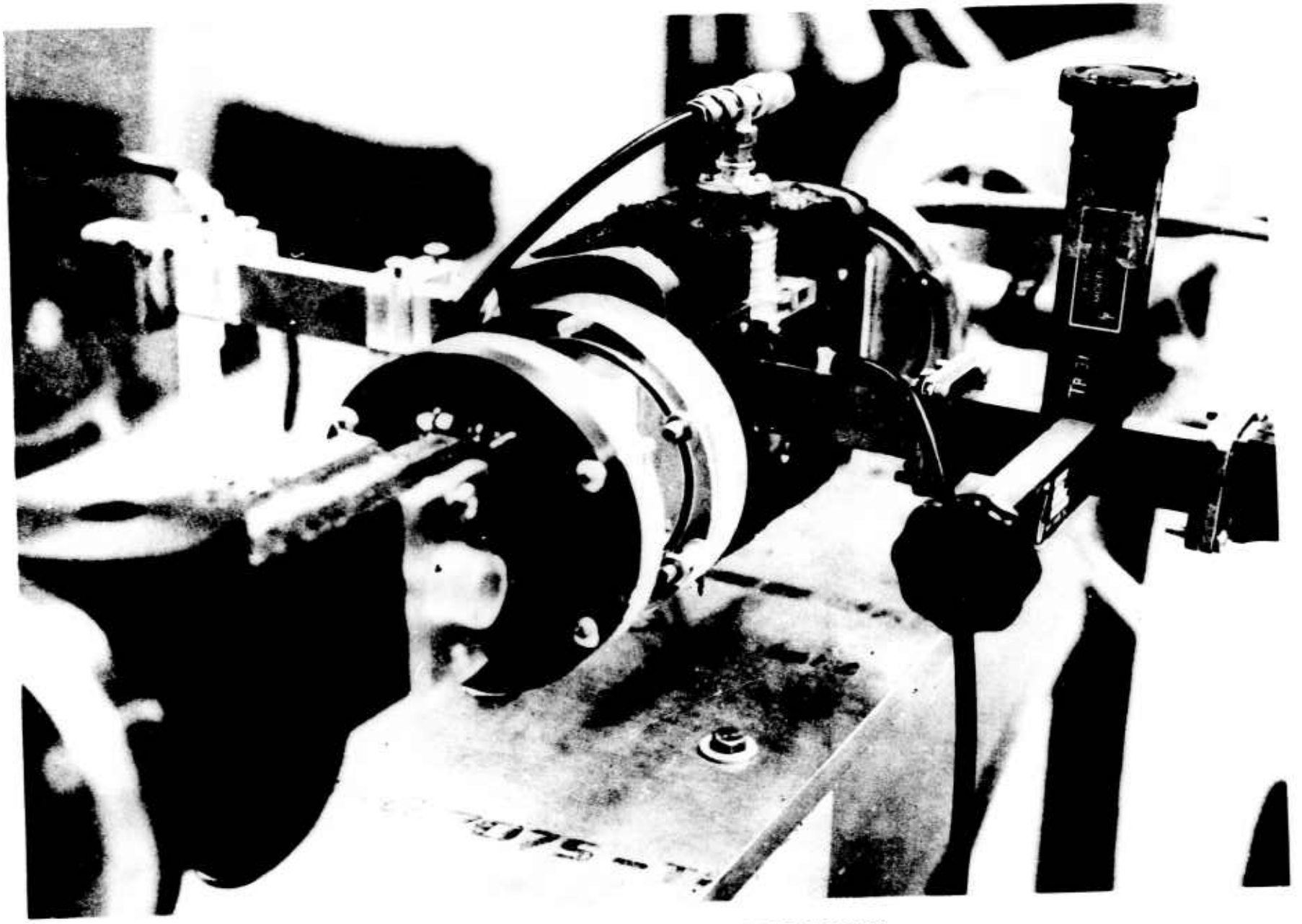

FIGURE 18. PHOTOGRAPH OF TEST SECTION

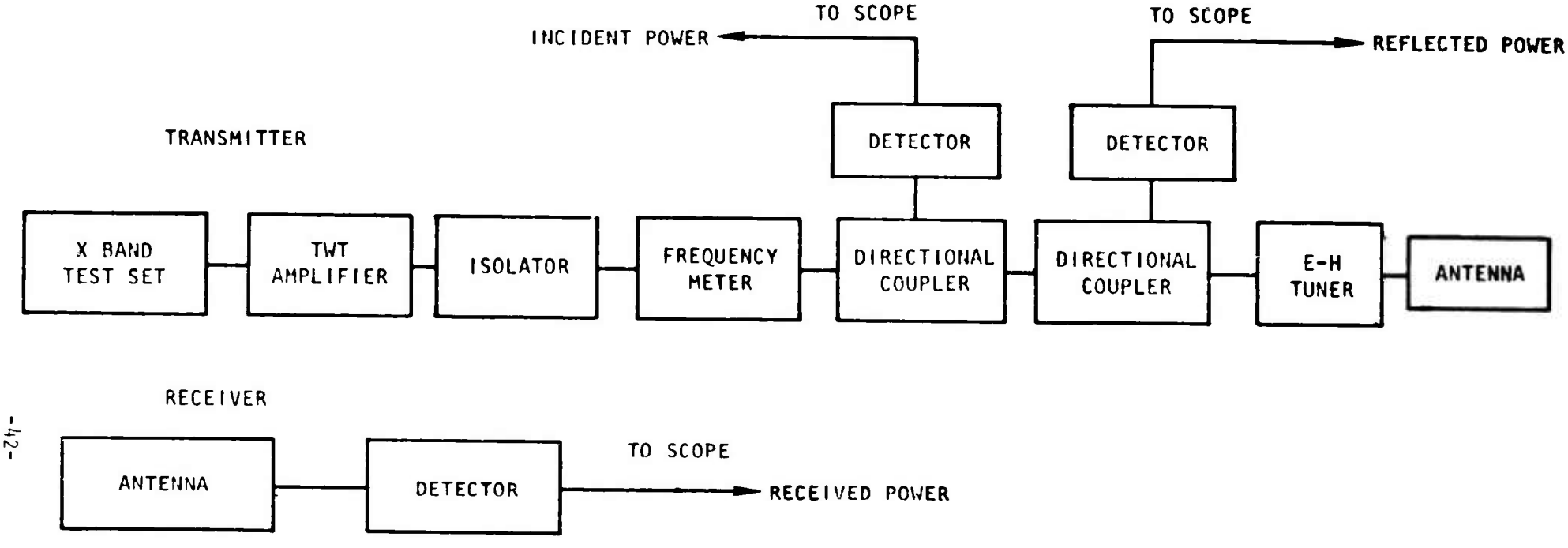

FIGURE 19. SCHEMATIC OF LOW POWER MICROWAVE CIRCUIT

High Power Microwave System

Conventional magnetrons were used to generate the high power signals. A QK790 and a RKJ42 magnetron were used to generate signals with peak pulse power varying from 600 W to 7.0 kW. The QK790 frequency was fixed at 9.02 GHz. The RK2J42 had a fixed frequency of 9.382 GHz. Power could be varied using suitable power dividers and attenuators. The pulse modulation was supplied by a Velonex Model 350 high power pulse generator using a Model 1123 pulse transformer module. The 20 kW pulse generator supplied sufficient power to drive either magnetron to maximum capability. The pulse generator also provided a variable pulse length and pulse repetition frequency. For all experiments a pulse length of 2.0 microseconds and a single pulse mode was selected. Since the pulse modulator did not have a provision for supplying power for the magnetron heater filaments, an ordinary 6 volt storage battery was used as a floating power supply. This simple system provided system flexibility and reliable operation.

In order to trigger the magnetron at the proper time, a trigger circuit consisting of a fast rise piezoelectric static pressure probe and a variable delay pulse generator were used to trigger the pulse modulator. The static pressure gage was located in the top of the test section at the centerline of the aperture antenna. The pressure gage was developed previously by this laboratory and has a nominal rise time of 0.1 microseconds. The trigger pulse was delayed to insure a uniform flow existed over the aperture before triggering the pulse modulator. Typical delays of 2.0 to 4.0 microseconds were employed for the range of shock velocities.

Diode detectors were used to measure the incident, reflected, and received power using suitable attenuators to maintain peak power levels within the detector operating range. All detectors and attenuators were carefully calibrated at the magnetron operating frequency at low power levels. The detectors were also checked at high power levels by measuring the average detected power with a bolometer power meter while pulsing the magnetron at a known duty cycle. Detector calibrations included all connecting cables and terminations used for the shock tube measurements. In order to obtain maximum reflected power levels, a brass plate or a graphite slab was clamped to the transmitting antenna ground plane and the peak incident and reflected power

were recorded for a range of incident power levels. The reference received power was measured with the shock tube at atmospheric pressure. A schematic of the high power microwave system is shown in Figure 20. Various tuners were used to remove residual discontinuities in the line and to minimize reflections due to mismatch.

The high power measurements were conducted at a fixed plasma layer-thickness of 3.18 mm. The waveguide antennas used for the low power measurements were also used for the high power experiments.

Horn Antennas

In order to more closely simulate plane wave transmission of the microwave signals, a pair of H-plane horn antennas were fabricated. Each antenna was mounted in a brass ground plane and located inside a dielectric test section. The ground planes were shaped to minimize any disturbances to the flow and to permit a fixed thickness of shock generated plasma to fill the space between the antennas and completely cover the antenna apertures. Owing to the limited length of shock processed test gas in the shock tube, an H-plane horn design was selected. Two horns were fabricated from brass using the dimensions shown in Figure 21. Four flush mounted electrostatic probes were installed in the transmitting antenna ground plane to monitor local electron density. The two antennas were mounted inside the dielectric test section with a spacing of 3.18 mm between the antenna ground planes. The ground planes sliced a portion of the shock generated plasma from the center of flow to minimize shock tube wall boundary layer effects upon the electron density profile over the antenna apertures. A photograph of the antennas installed in the test section is shown in Figure 22. Extensive bench testing of the antennas was performed in order to minimize reflections and scattering from the antennas. A slotted line and a low power signal source were used to measure the VSWR of the antennas. The thickness of a resonant antenna window was determined experimentally for the fixed magnetron frequency of 9.382 GHz. Improvement of the VSWR was obtained by machining a radius of curvature on one surface of the Teflon window to form a cylindrical microwave lens. The final antenna configuration installed in the test section had a measured VSWR of 1.74. The insertion loss measured with a power meter was found to be 3.0 dB for the 3.18 mm spacing. A slotted line and a voltage

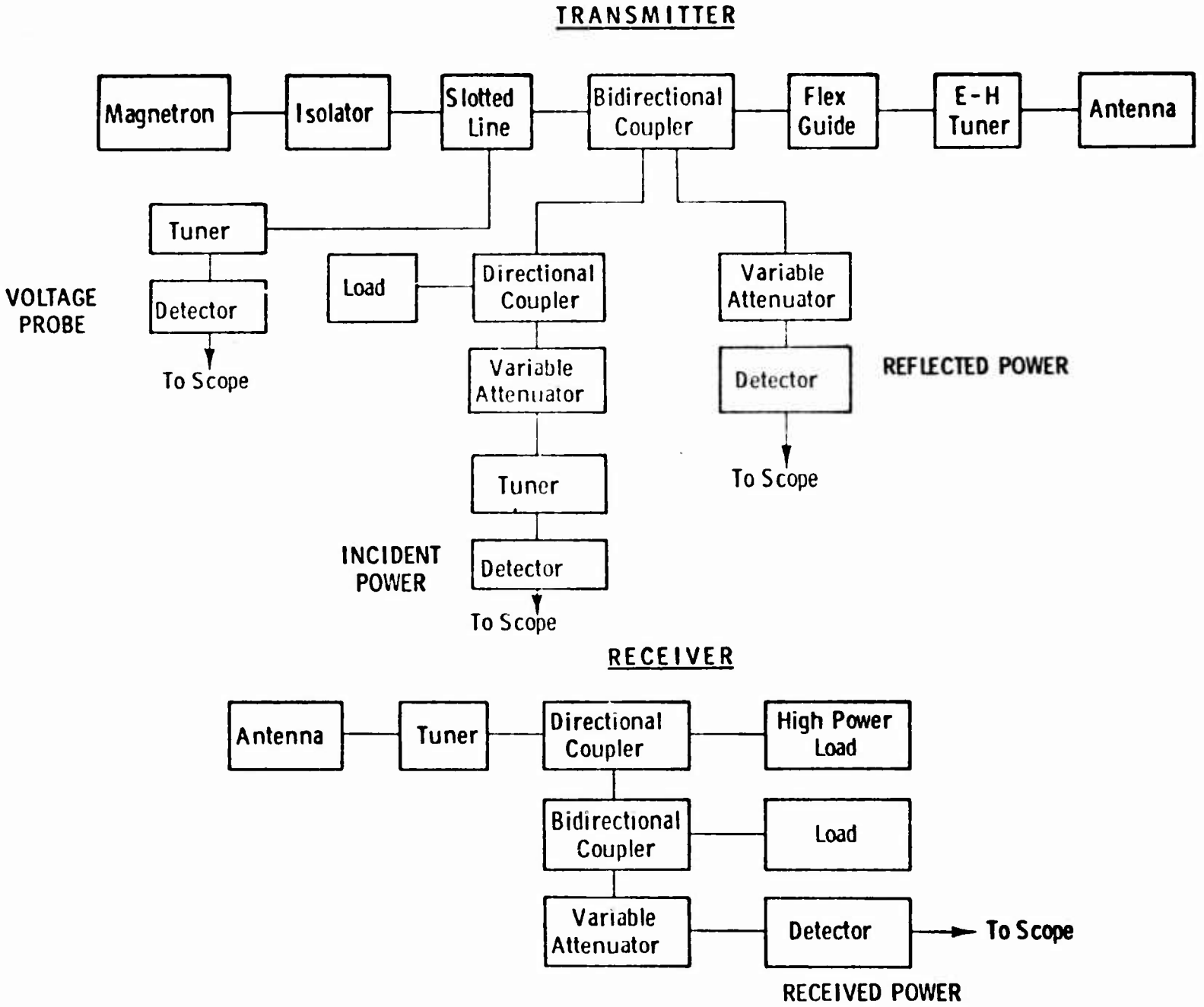

FIGURE 20. SCHEMATIC OF HIGH POWER MICROWAVE CIRCUIT

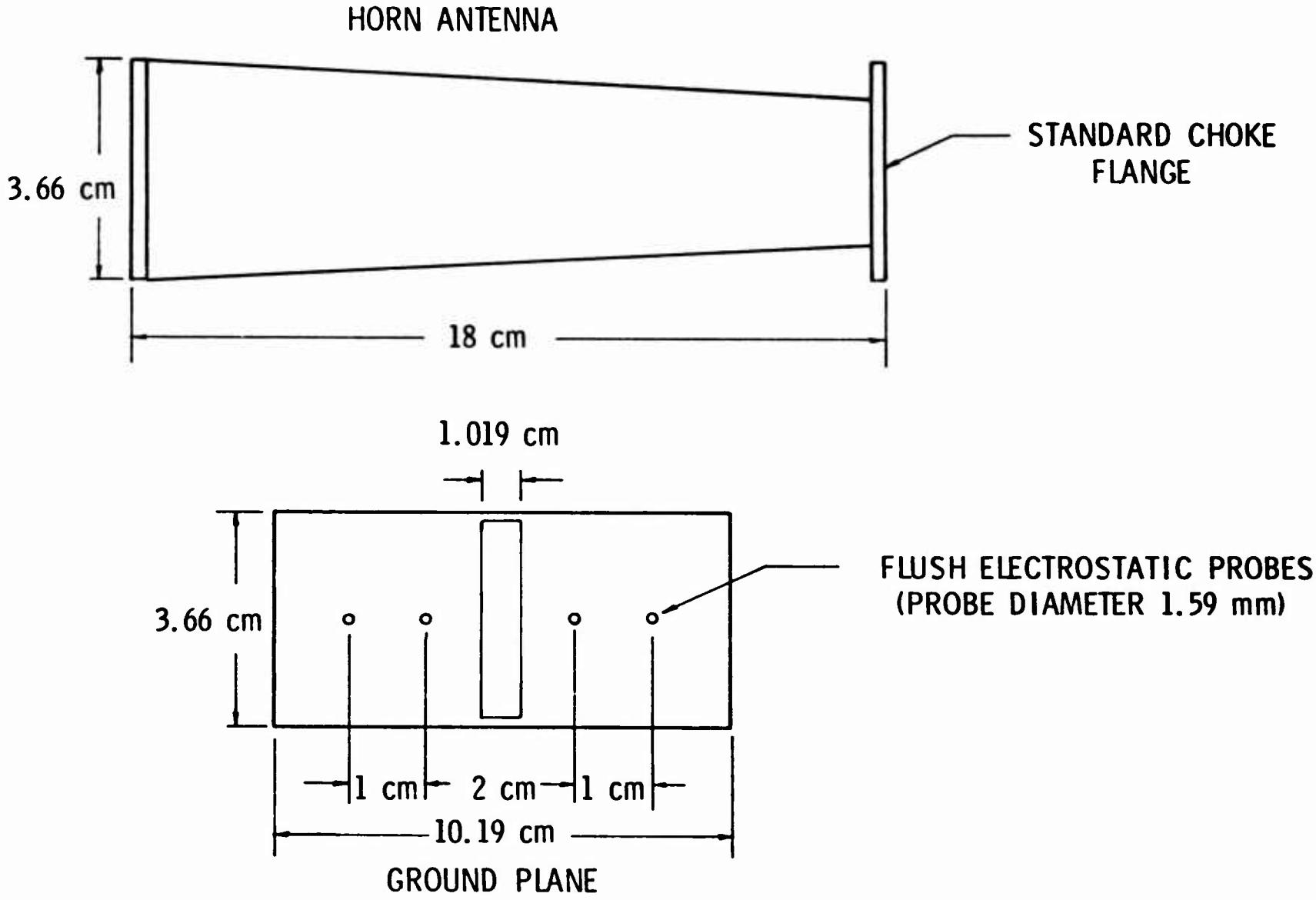

FIGURE 21. HORN ANTENNA DESIGN

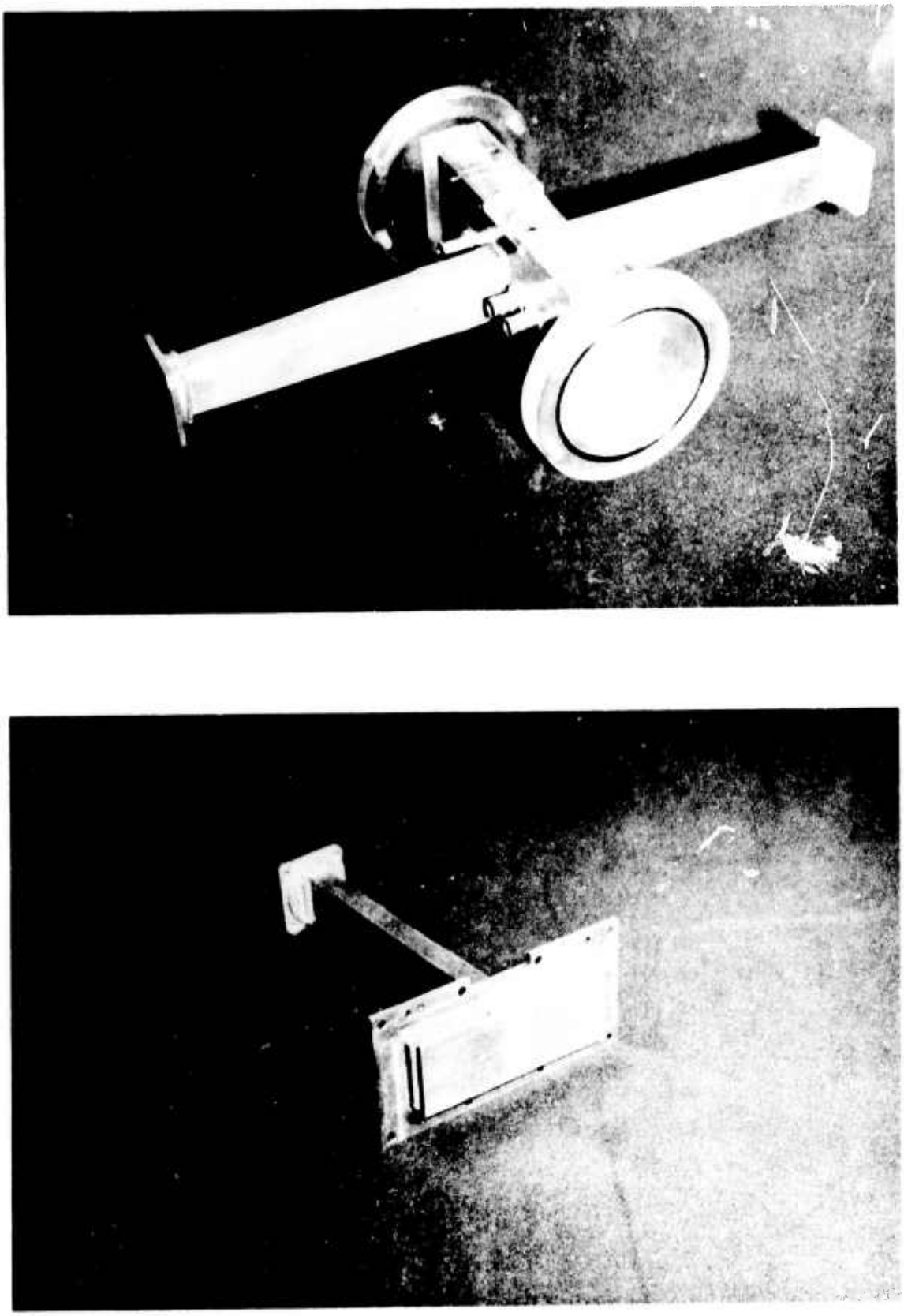

FIGURE 22. PHOTOGRAPH OF HORN ANTENNA AND TEST SECTION

probe were also added to the microwave circuit to permit the measurement of the phase of the reflected wave when the plasma covered the antenna.

The four flush mounted electrostatic probes were constructed from 1.59 mm copper electrodes insulated from the ground plane with Teflon spacers. The probes were biased to -3.0 volts relative to the antenna ground plane which served as a common electrode for all four probes. The probes were biased with a battery, and the collected ion current was determined by measuring the voltage across a precision resistor in the probe circuit.

Experimental Results

Low Power Experiments - The initial microwave experiments were performed to study the transmission characteristics of the plasma at low power levels where incident wave electric field induced ionization was not expected. Incident power levels of the order of 15 mW were used at a fixed frequency of 10.0 GHz. A low power klystron contained in a Hewlett Packard Model 624 X-band test set generated the cw signal. Measurements of the incident, reflected, and received power were made for a range of shock velocities at a fixed initial shock tube pressure of 5.0 torr. A calibration of the microwave system was performed to determine the reference incident and maximum reflected power levels prior to the initiation of the shock tube runs.

In addition to the microwave measurements, the incident shock velocity and the local electron density were measured. The shock velocity was measured with the use of piezoelectric static pressure probes. One probe was located in the shock tube sidewall and another probe was located downstream at the centerline of the transmitting antenna. The current collected by a flush mounted electrostatic probe was also measured for each run. A probe located on the antenna ground plane at the centerline of the transmitting antenna was used to determine shock front passage and uniform test time. For these measurements the local free stream electron density was determined from the measured shock velocity using equilibrium real air thermodynamic tables[3]. The plasma frequency was determined by the relationship

$$\frac{\omega_p}{2\pi} = 8.98 \times 10^3 \sqrt{n_e} \text{ Hz}$$

where n_e is the electron density (cm^{-3}).

The transient response of the detected reflected power and collected ion current is shown in Figure 23 for two values of plasma thickness. The static pressure response and the received power are also shown in the figure. Evidence of scattering of the incident wave is indicated by the small oscillation of the reflected and received signals.

The measured transmission coefficient for a 3.18 mm plasma layer is shown for a range of free stream plasma frequency in Figure 24. The measured results are compared to Fante's impedance sheet theory[44] which includes the admittance contributions of a TE_{10} waveguide mode and the aperture admittance of an unloaded rectangular aperture in a conducting ground plane. The plasma admittance was based upon calculations of the wall boundary layer profile assuming a steady turbulent boundary layer[15]. The assumption of a steady wall boundary layer is a questionable assumption, but previous wall electron current measurements indicated that unsteady effects are not significant for the present operating conditions. The electron-neutral collision frequency was calculated using the relationship

$$\nu = 5.3 \times 10^9 \, p^* \ (sec^{-1})$$

$$p^* = \rho/\rho_o \ (760).$$

The density ratio in the test gas was determined from shock tube tables[3]. The plasma admittance profile was then numerically integrated to determine the average plasma admittance. The experimental results indicate a reasonable agreement with Fante's theory with most of the scatter attributed to experimental inaccuracies. The data does indicate the correct trend with increasing electron density as predicted by theory. The measured reflection coefficient is shown in Figure 25 and compared to Fante's theory. The agreement is similar to the transmission coefficient data, and the correct trend with plasma frequency is predicted.

---

[44] Fante, R. L., Radio Sci. 2, 87 (1967).

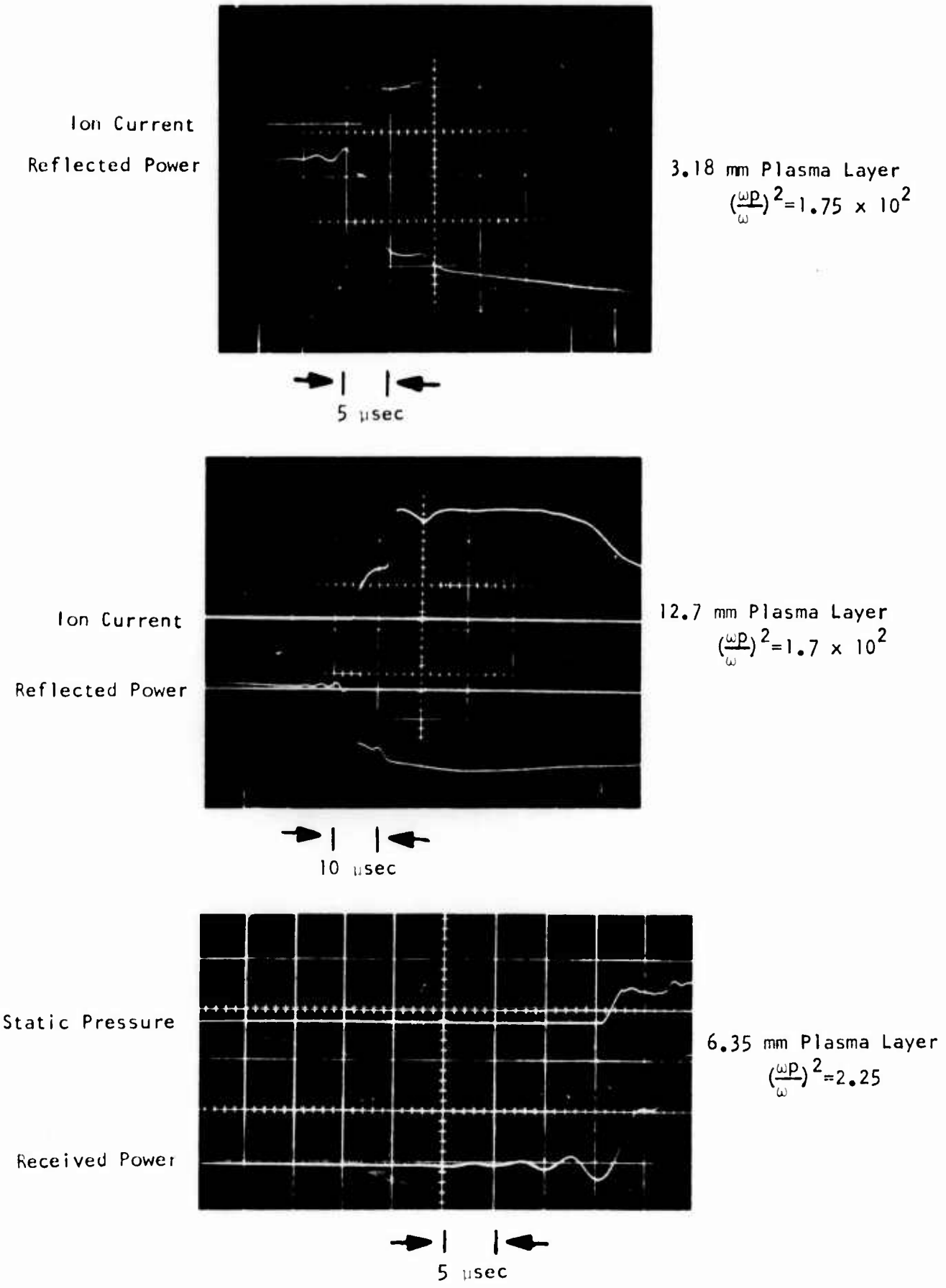

FIGURE 23. LOW POWER TRANSIENT RESPONSE

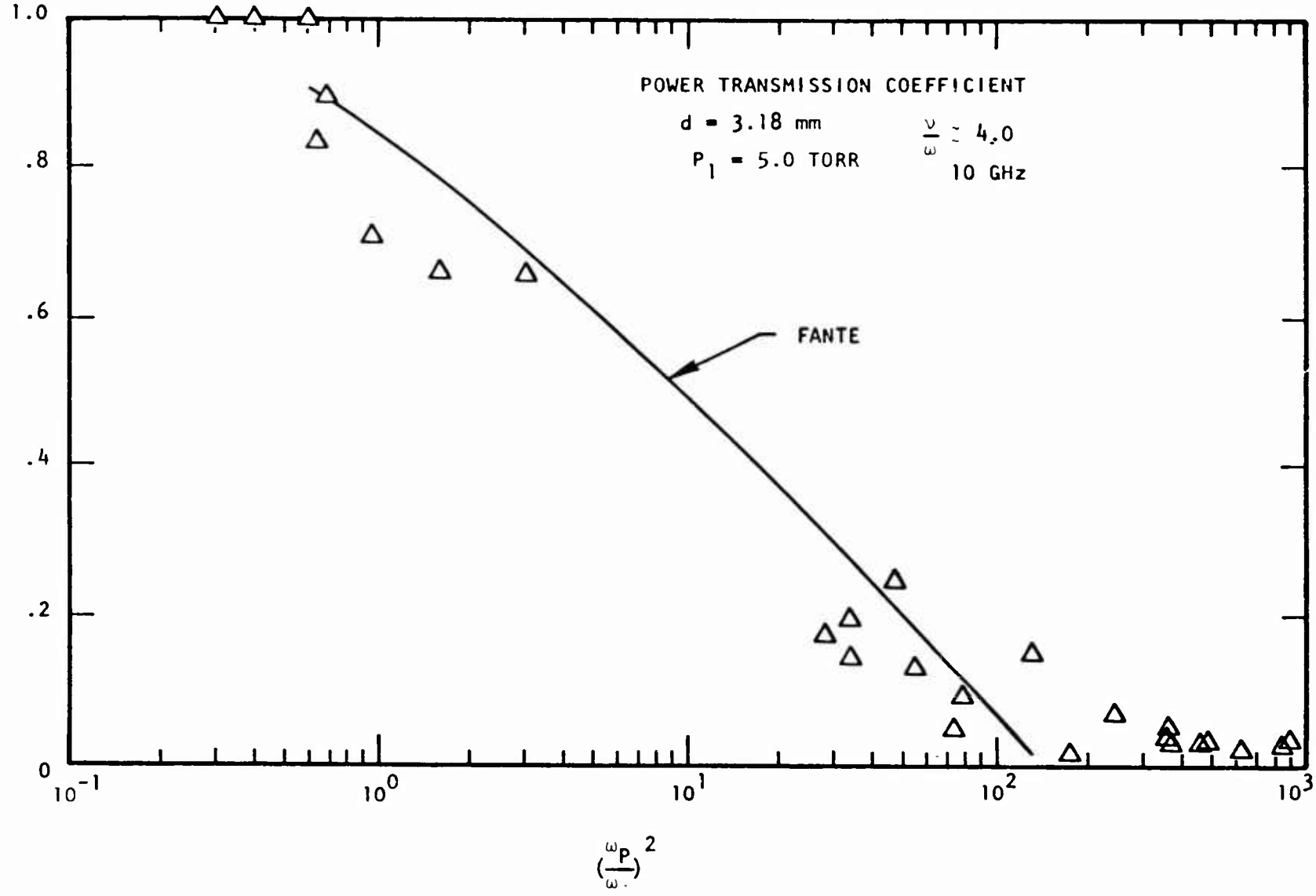

FIGURE 24. TRANSMISSION COEFFICIENT 3.18 mm LAYER

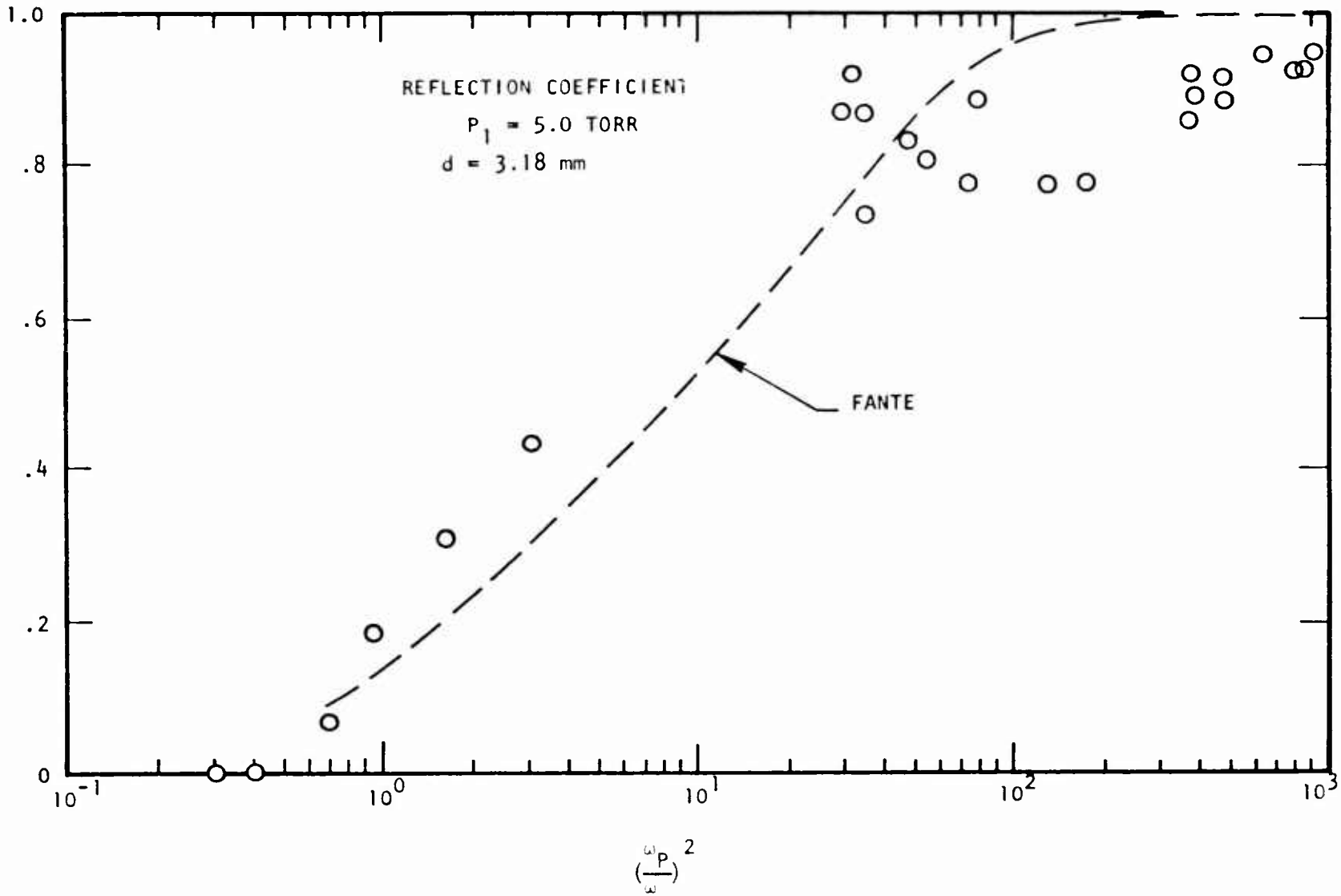

FIGURE 25. REFLECTION COEFFICIENT 3.18 mm LAYER

The measured transmission coefficient for a 6.35 mm plasma layer thickness is shown in Figure 26. The results are compared to the plane wave solutions of Poverlein[45] since the restrictions on the applicability of Fante's theory are not met for the increased plasma layer thickness. The results again indicate the correct trend with increasing plasma frequency. The power reflection coefficient is shown in Figure 27 and compared with Poverlein's theory. The theory of Baños and Golden[46] is also shown for comparison. The data appears to be bracketed by the two theories at the higher values of electron density.

The transmission coefficient for a 12.7 mm plasma layer is shown in Figure 28 and compared with Poverlein's theory. The reflection coefficient is shown in Figure 29. Included in the cw reflection coefficient data are a few measurements where the incident wave was pulse modulated. No significant change in the transmission characteristics was observed for the cw or pulsed mode as shown in the figure.

High Power Measurements - A series of high power measurements were performed for a wide range of free stream electron density and incident power level. The shock tube initial pressure was fixed at 5.0 torr and the transmitting antenna was located 3.18 mm from the dielectric wall of the test section. For these experiments an additional flush mounted electrostatic probe was mounted on the antenna ground plane 9.5 mm downstream of the antenna centerline. The probe was biased at -3 volts for these measurements. The ion probe was used to monitor the increased ionization due to the incident microwave pulse interacting with the plasma. A check of the ion probe response over a range of free stream electron density was undertaken to evaluate the performance of the probe. Typical transient response of the ion current is shown in Figure 30 for three values of incident power level. The increased ion current due to the incident pulse is evident for the highest power levels.

The peak pulse power was established at nominal levels of 600 W, 1.7 kW, and 7.0 kW. Slight variations of peak power were encountered, but the actual

---

[45] Poverlein, H., J. Atmospheric and Terres, Phys. 12, 126 (1958).

[46] Baños, A. and Golden, K. E., Aerospace Report No. TR-1001 (2220-10)-2, February (1967).

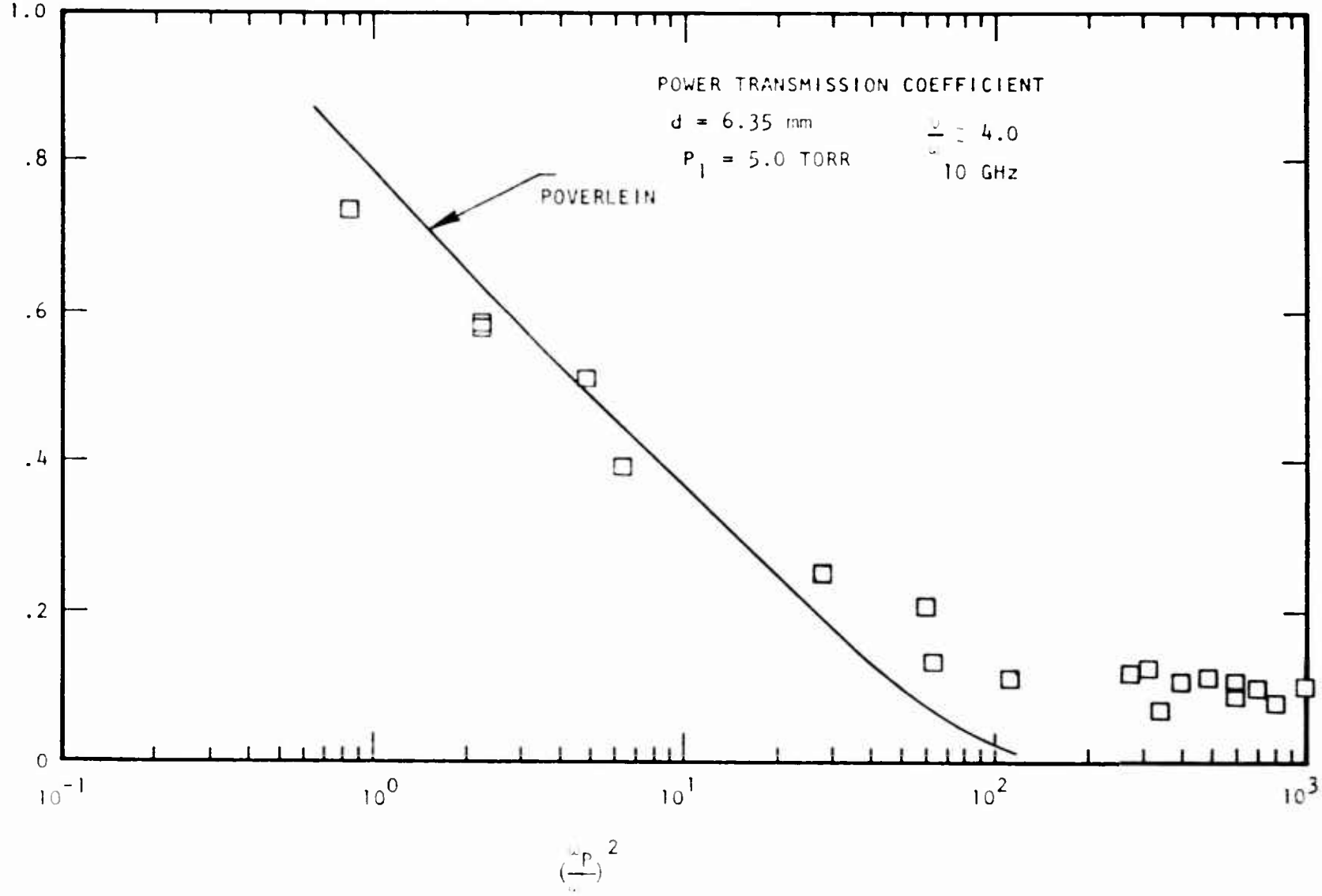

FIGURE 26. TRANSMISSION COEFFICIENT 6.35 mm LAYER

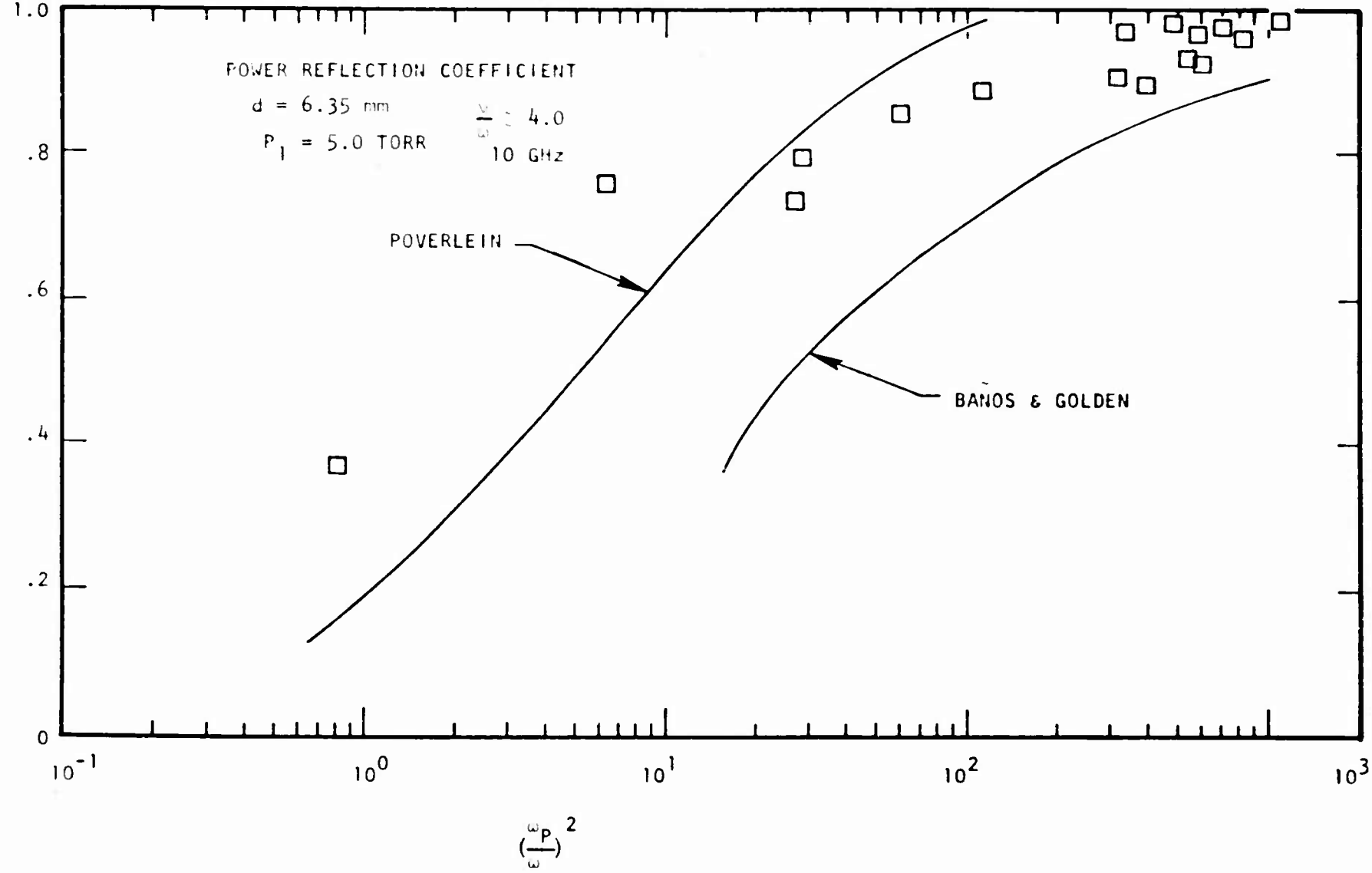

FIGURE 27. REFLECTION COEFFICIENT 6.35 mm LAYER

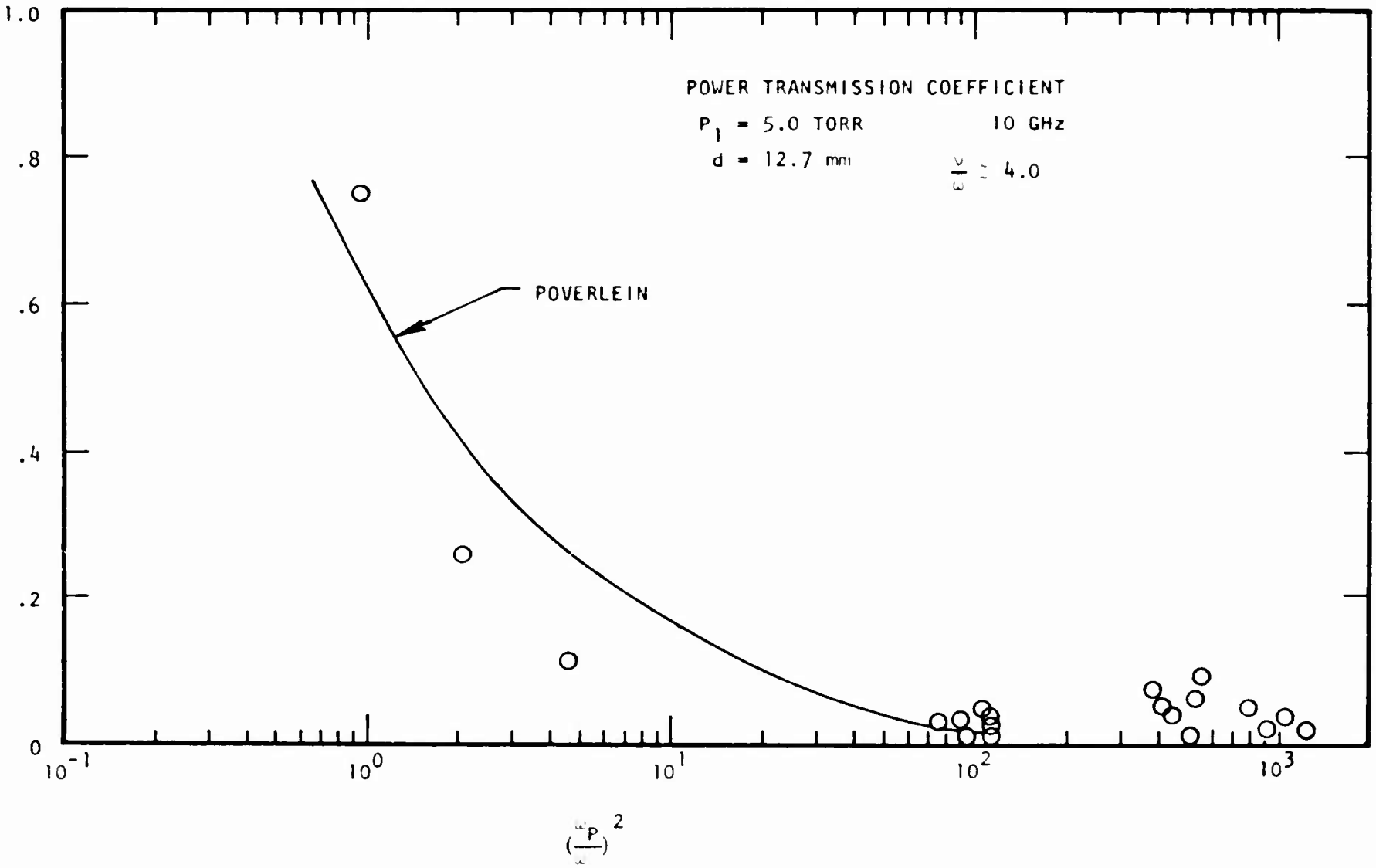

FIGURE 28. TRANSMISSION COEFFICIENT 12.7 mm LAYER

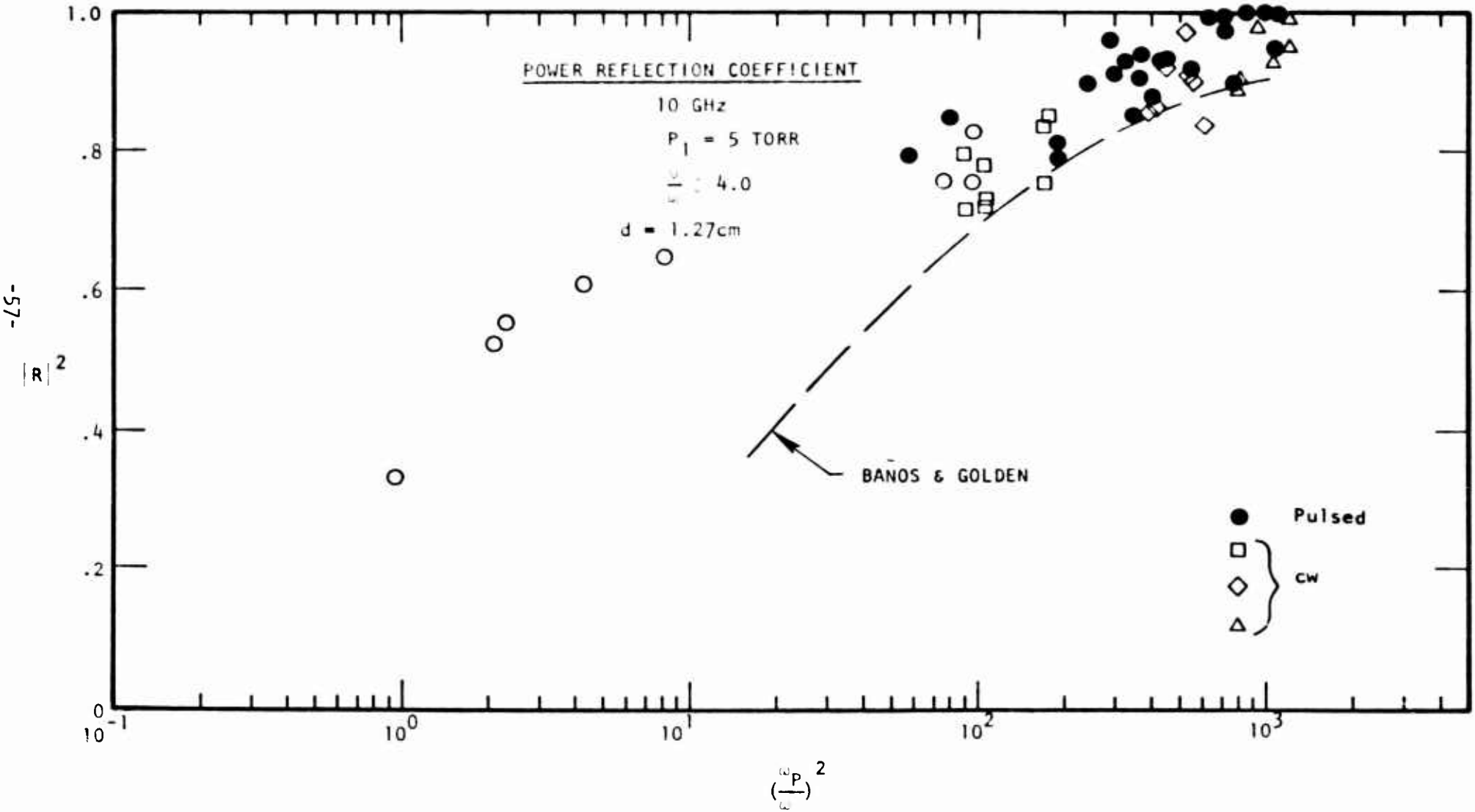

FIGURE 29. REFLECTION COEFFICIENT 12.7 mm LAYER

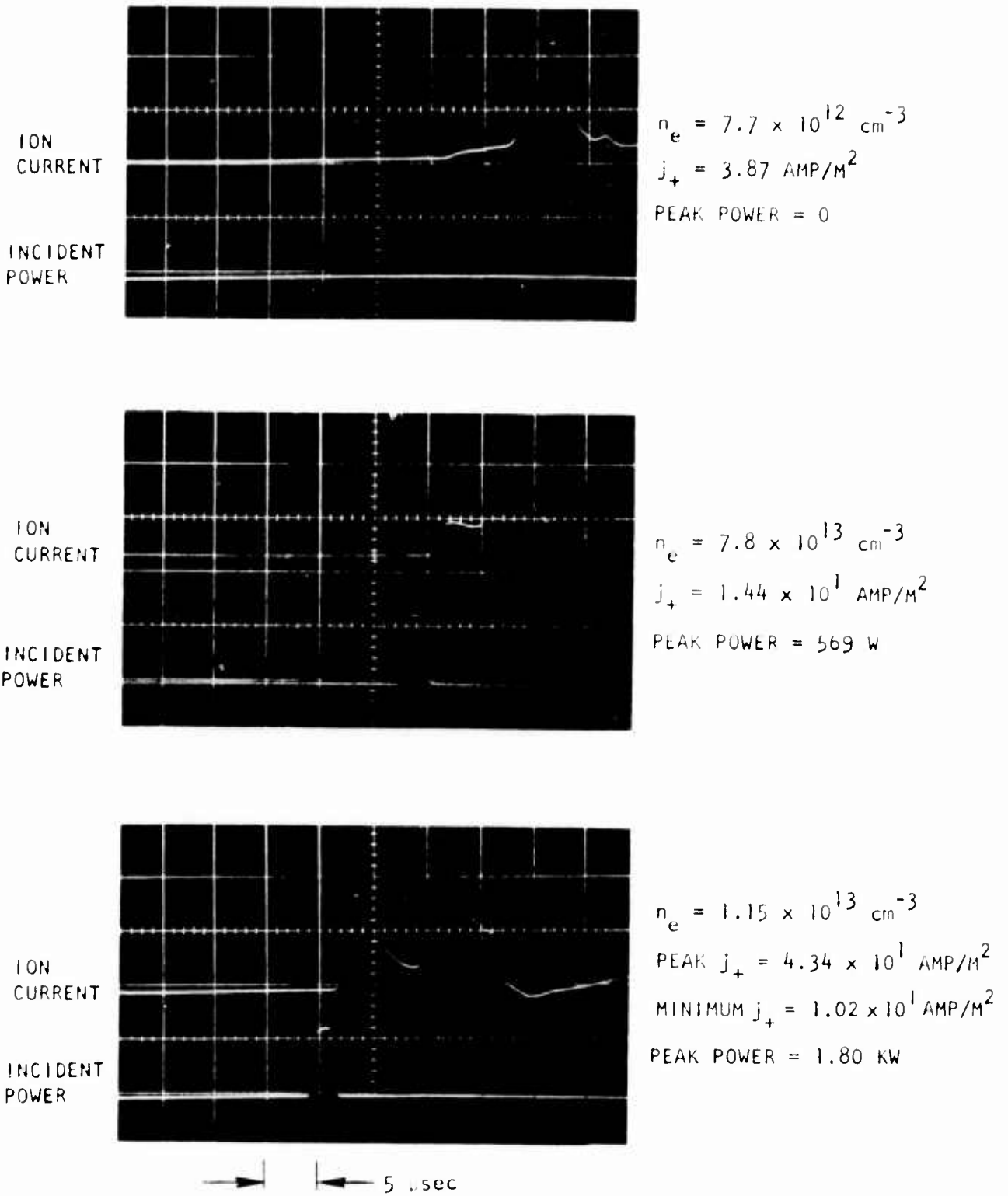

FIGURE 30. FLUSH PROBE TRANSIENT RESPONSE

measured power levels were used in the data reduction. The transient response of the incident, reflected and received power in addition to the ion current is shown in Figure 31 for a peak power of 539 W. The ion probe shows only a slight increase in collected current, however, the reflected and received pulse show increased distortion with time over the pulse interval indicating a time-dependent interaction with the plasma. Measurements of the attenuation of the incident pulse were made over a range of plasma frequencies and the power transmission coefficient and the results are shown in Figure 32. The results are compared with Fante's impedance sheet theory simply as a reference. All data indicate conditions at the end of the 2 microsecond pulse. The attenuation is shown to be greater at the low levels of plasma frequency and merging with the linear theory at the higher levels. The power reflection coefficient is shown in Figure 33 in addition to previous measurements at 15 mW. The results appear to be scattered about the linear theory prediction for this power level.

The transient response of the microwave pulse at a nominal peak power of 1.74 kW is shown in Figure 34. The received and reflected pulse show noticeable distortion with a -4.4 dB change in the received pulse in less than 1 microsecond. The ion probe shows a large peak in collected current as the electrons produced by the incident electric field are swept over the probe collecting area followed by a relaxation to ambient conditions prior to the arrival of the contact surface. The attenuation over a range of plasma frequencies is shown in Figure 35. The attenuation is greater than the value predicted by linear theory until $(\omega_p/\omega)^2 = 30$ after which increased attenuation is not observed.

Figure 36 presents the microwave pulse transient response for a peak power of 6.04 kW. The breakdown phenomena is very rapid at this power level with most of the power being reflected. The slight peak in the ion current at the time of the incident microwave pulse is caused by electric field ionization of the precursor electrons which exist in front of the moving shock wave. Later results which delayed the microwave pulse until the shocked

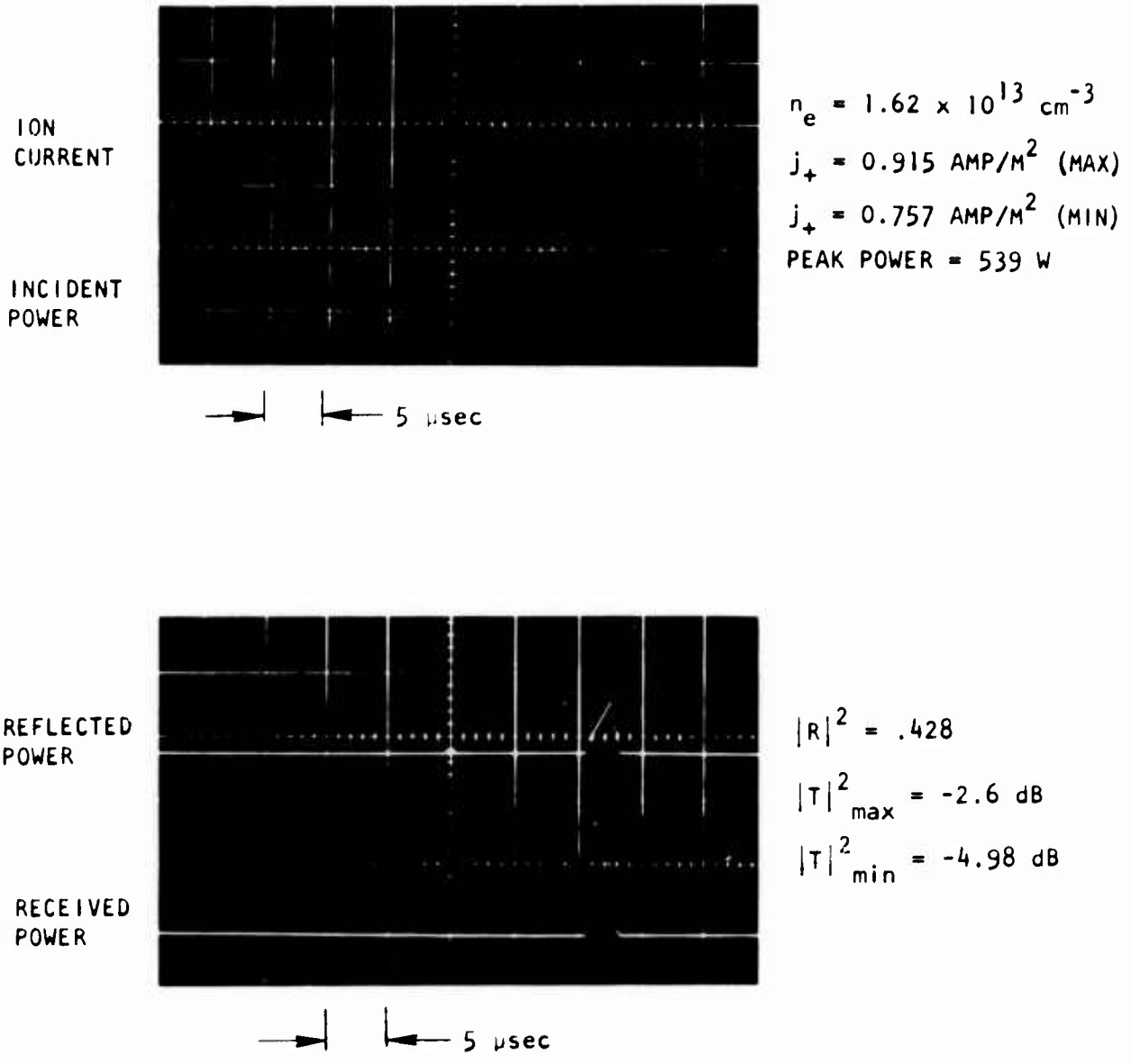

FIGURE 31. HIGH POWER TRANSIENT RESPONSE 539 W

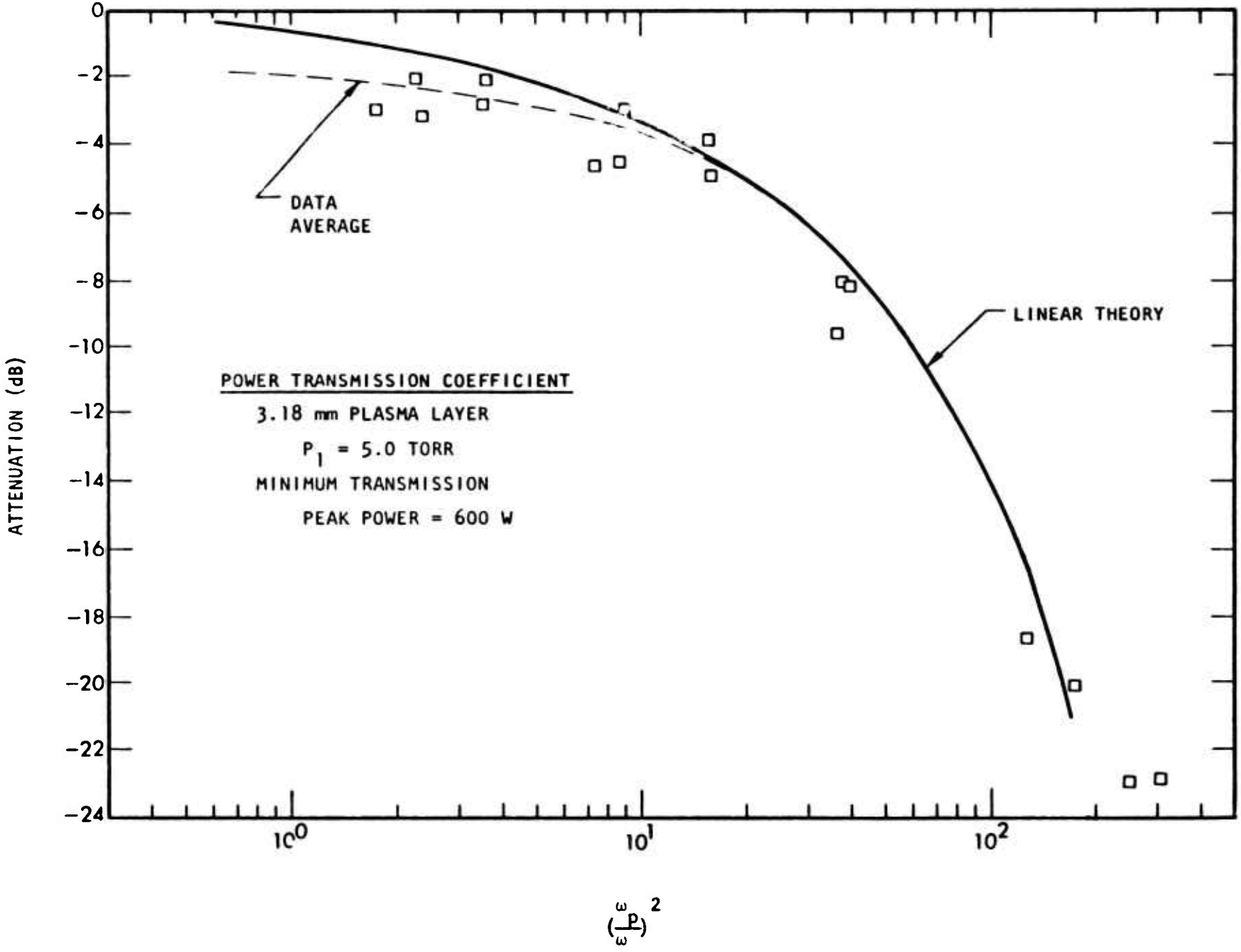

FIGURE 32. POWER TRANSMISSION COEFFICIENT 600 W

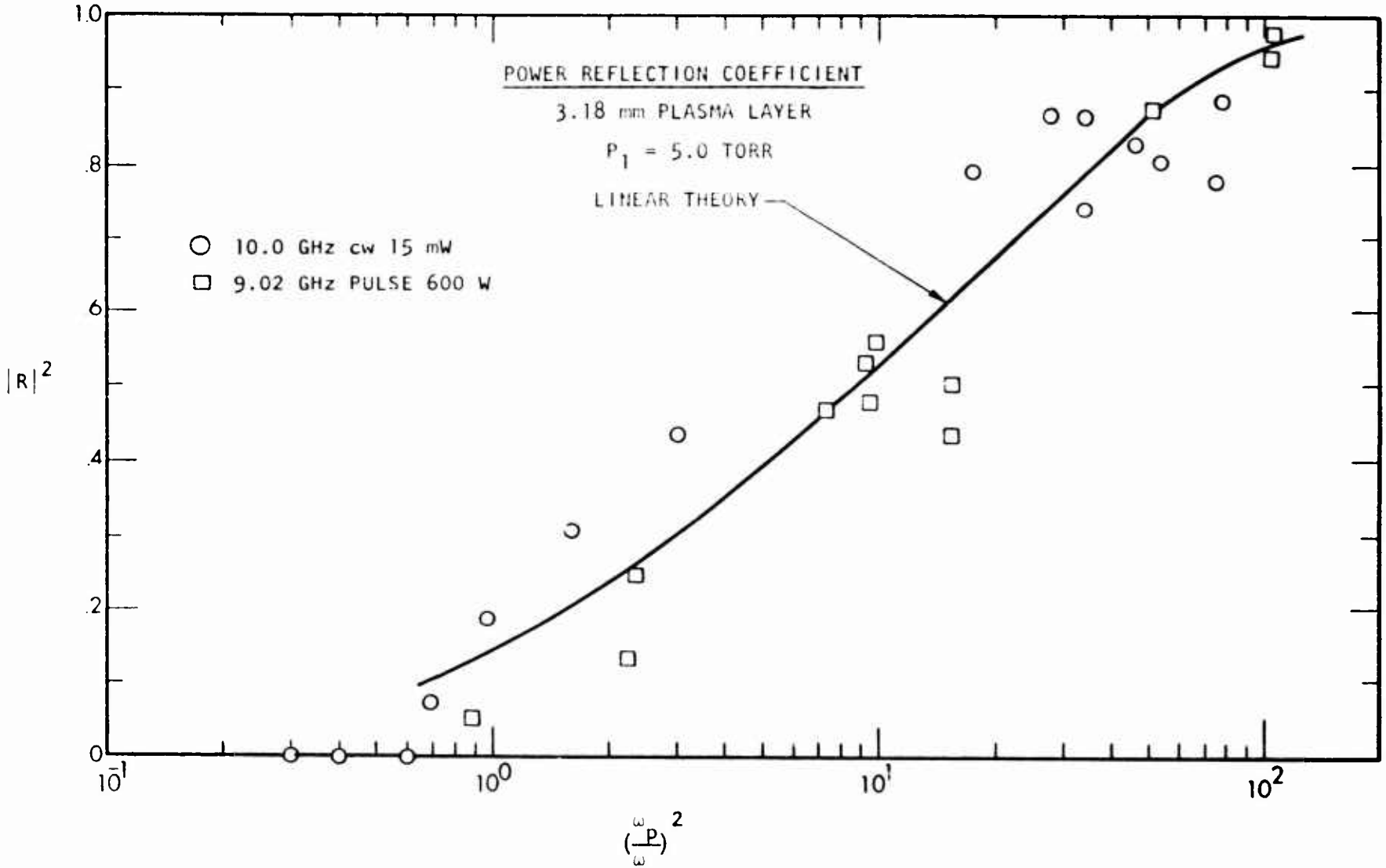

FIGURE 33. POWER REFLECTION COEFFICIENT 600 W

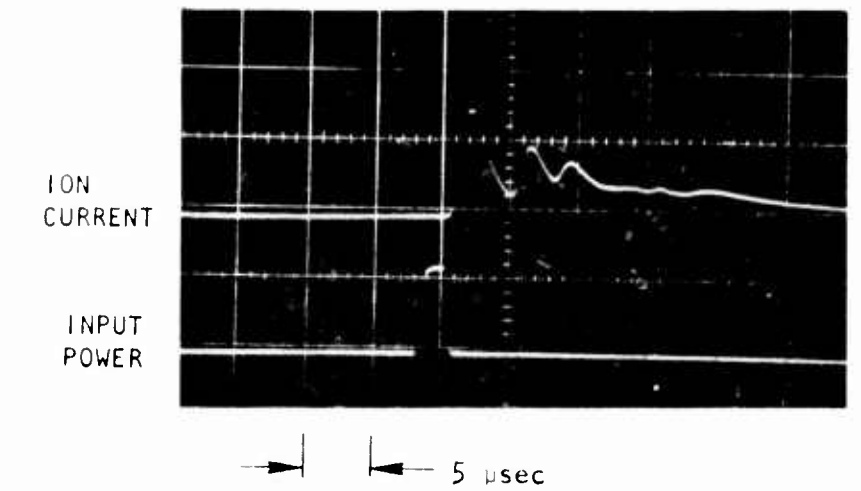

$n_e = 4.3 \times 10^{13}\ cm^{-3}$

$j_+ = 3.81 \times 10^{1}\ AMP/M^2$ (MAX)

$j_+ = 8.01\ AMP/M^2$ (MIN)

PEAK POWER = 1.74 KW

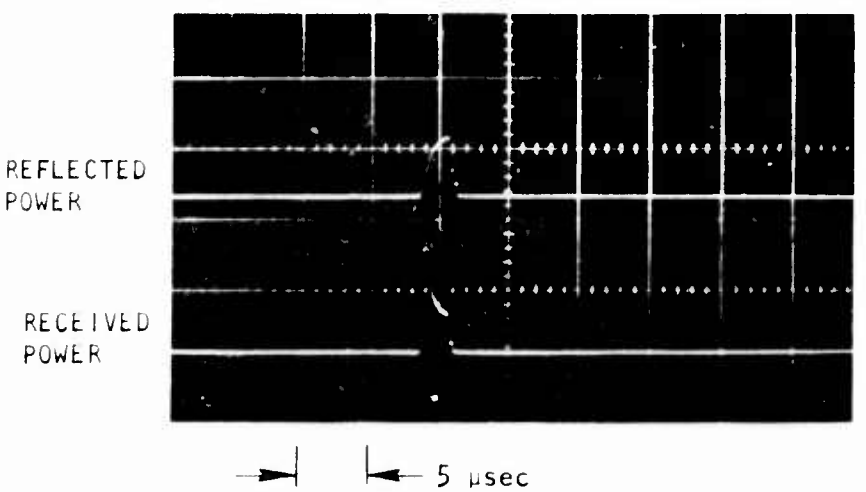

$|R|^2 = .435$

$|T|^2_{max} = -4.08$ dB

$|T|^2_{min} = -8.45$ dB

FIGURE 34. TRANSIENT RESPONSE 1.74 kW

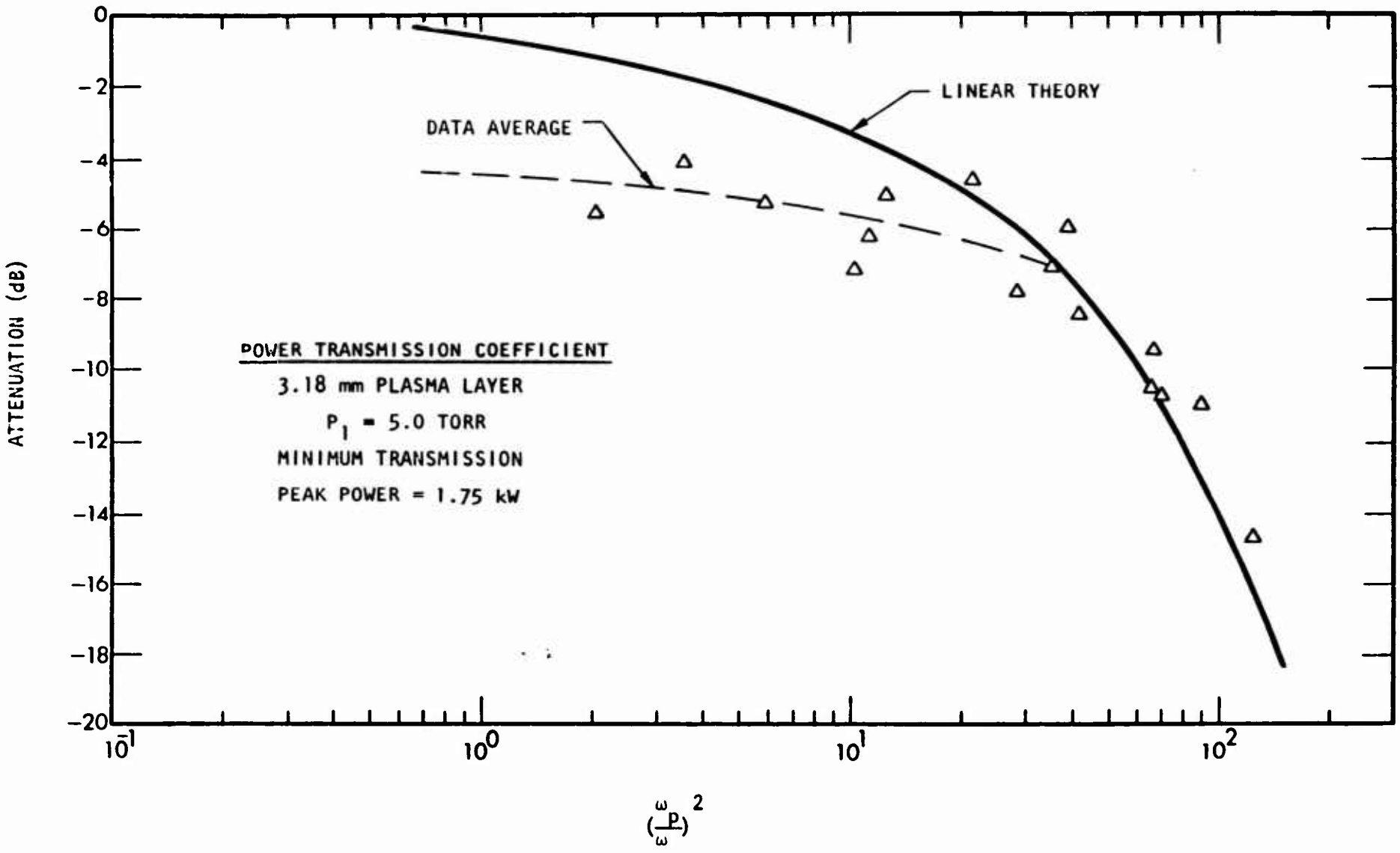

FIGURE 35. POWER TRANSMISSION COEFFICIENT 1.75kW

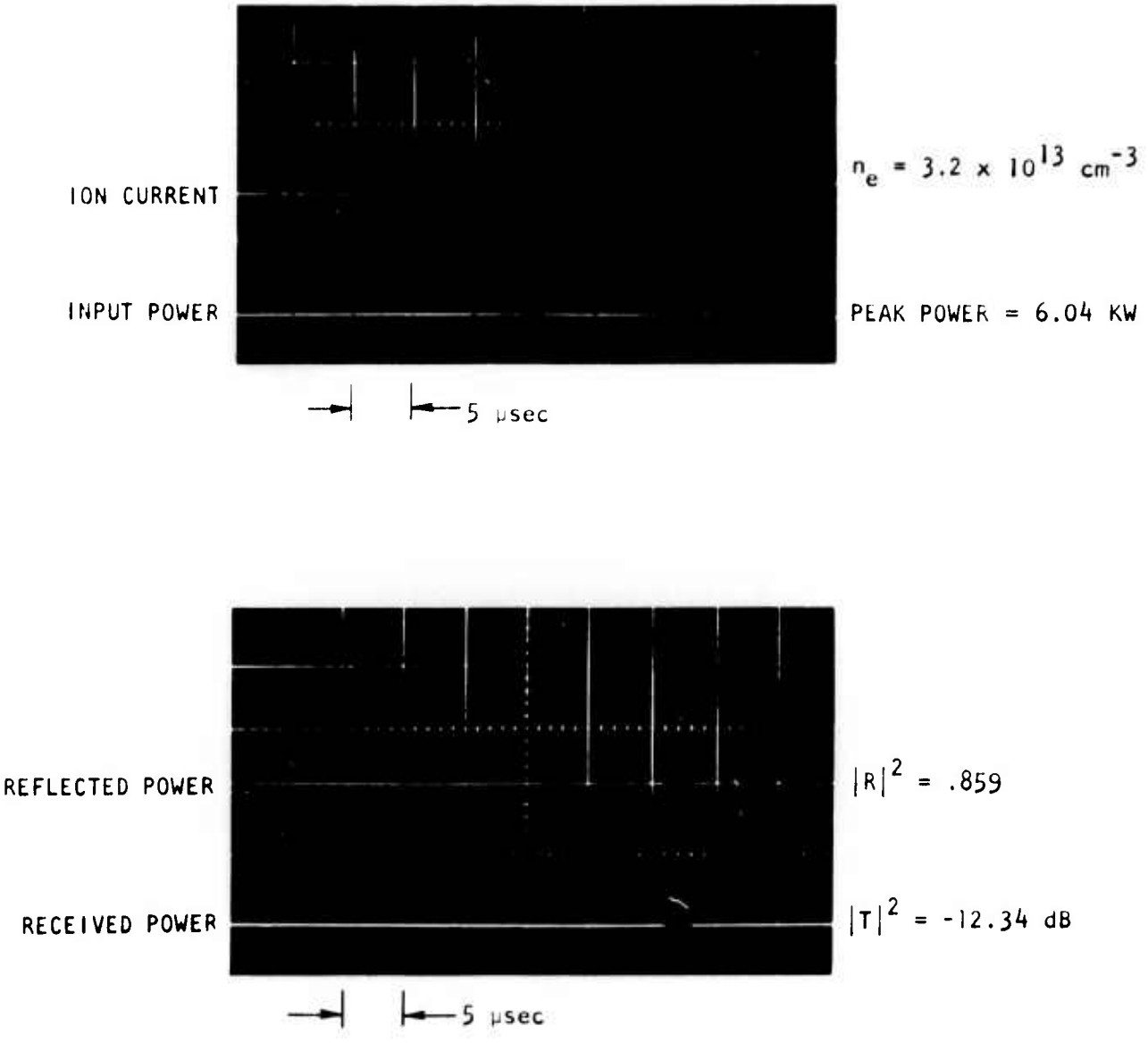

FIGURE 36. TRANSIENT RESPONSE 6.04 kW

gas covered the ion probe removed the precursor peak. The transmission coefficient is shown in Figure 37 and the reflection coefficient in Figure 38 both as a function of plasma frequency. The strong effect of the high power pulse exists over most of the experimental test conditions.

Linear impedance sheet theory predicts a linear relationship between input and output power for a fixed value of plasma frequency. The deviation from this theory occurs when the incident electric field causes sufficient ionization to cause increased attenuation and reflection of the incident wave. Based upon Fante's theory[44] the curves of Figure 39 were constructed using three values of plasma frequency. Data points based upon the faired data curve of each of the incident power attenuation curves at the selected values of plasma frequency were then used to establish the high power data curve of Figure 39. The received power is shown to deviate from the linear relationship at a few hundred watts and the received power curve continues to flatten with increased incident power. For the prescribed experimental conditions, there is a limited increase in received power beyond an incident peak power of 2 kW.

Horn Antenna Measurements - Measurements with the horn antennas were also conducted for two values of nominal peak pulse power. The plasma conditions were established over the same range of initial conditions as in the high power waveguide aperture antenna measurements. The ion current collected by two flush mounted electrostatic probes located immediately upstream and downstream of the antenna were also measured for each run. The reflected phase was also determined for each run by measuring the output of a probe installed in a slotted line in the microwave circuit and utilizing the technique described by Parzen[47]. The transient response of the microwave detectors and the electrostatic probes is shown in Figure 40 for a peak pulse power of 1.77 kW. The transient response is quite similar to the response of the detectors used with the waveguide antenna. The electron density profile is different for the two sets of measurements due to the relative thickness of the boundary layer covering the antennas. For the horn antenna measurements, the location

---

[47] Parzen, B., Proc. IRE 37 1208 (1949).

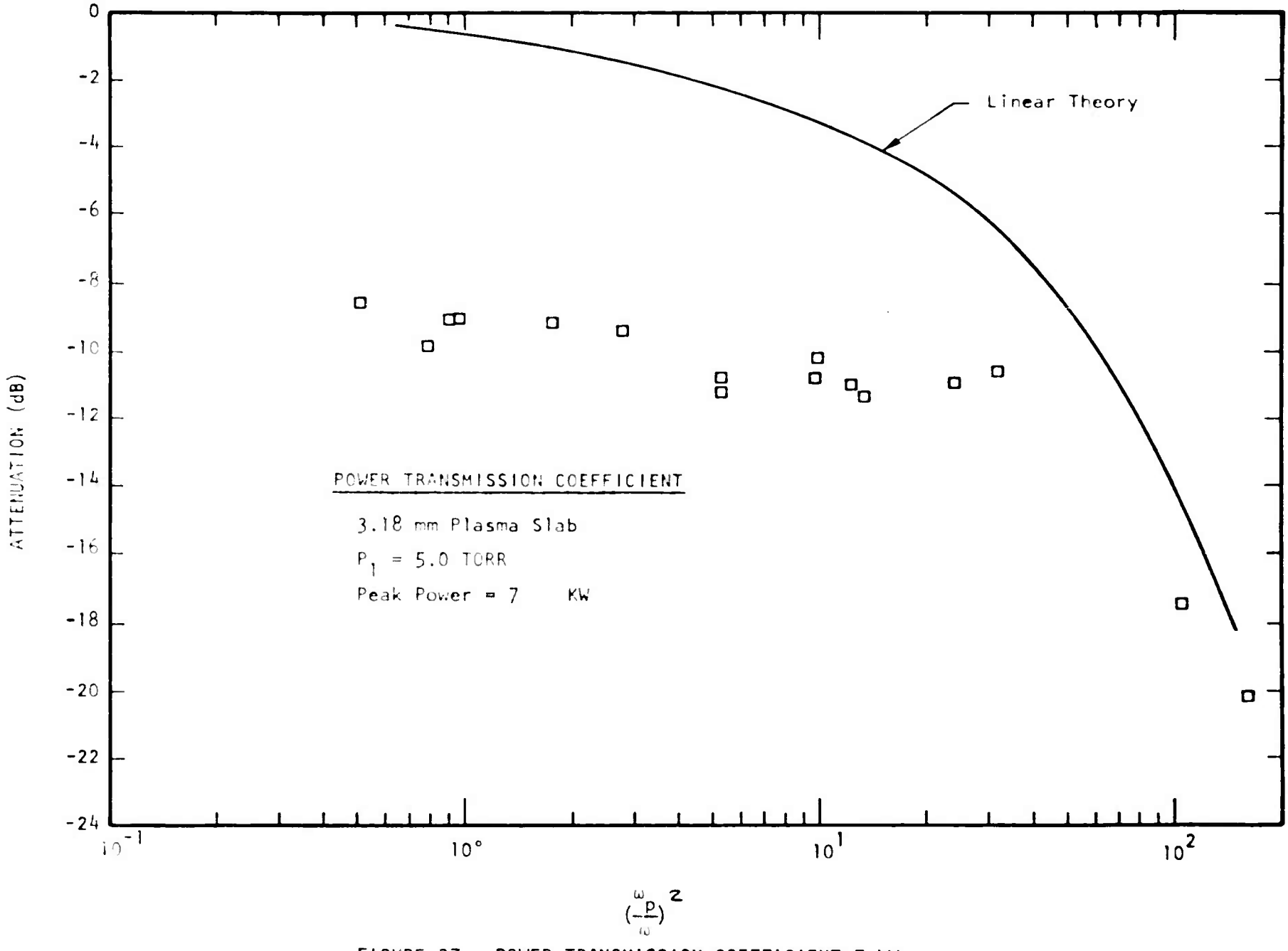

FIGURE 37. POWER TRANSMISSION COEFFICIENT 7 kW

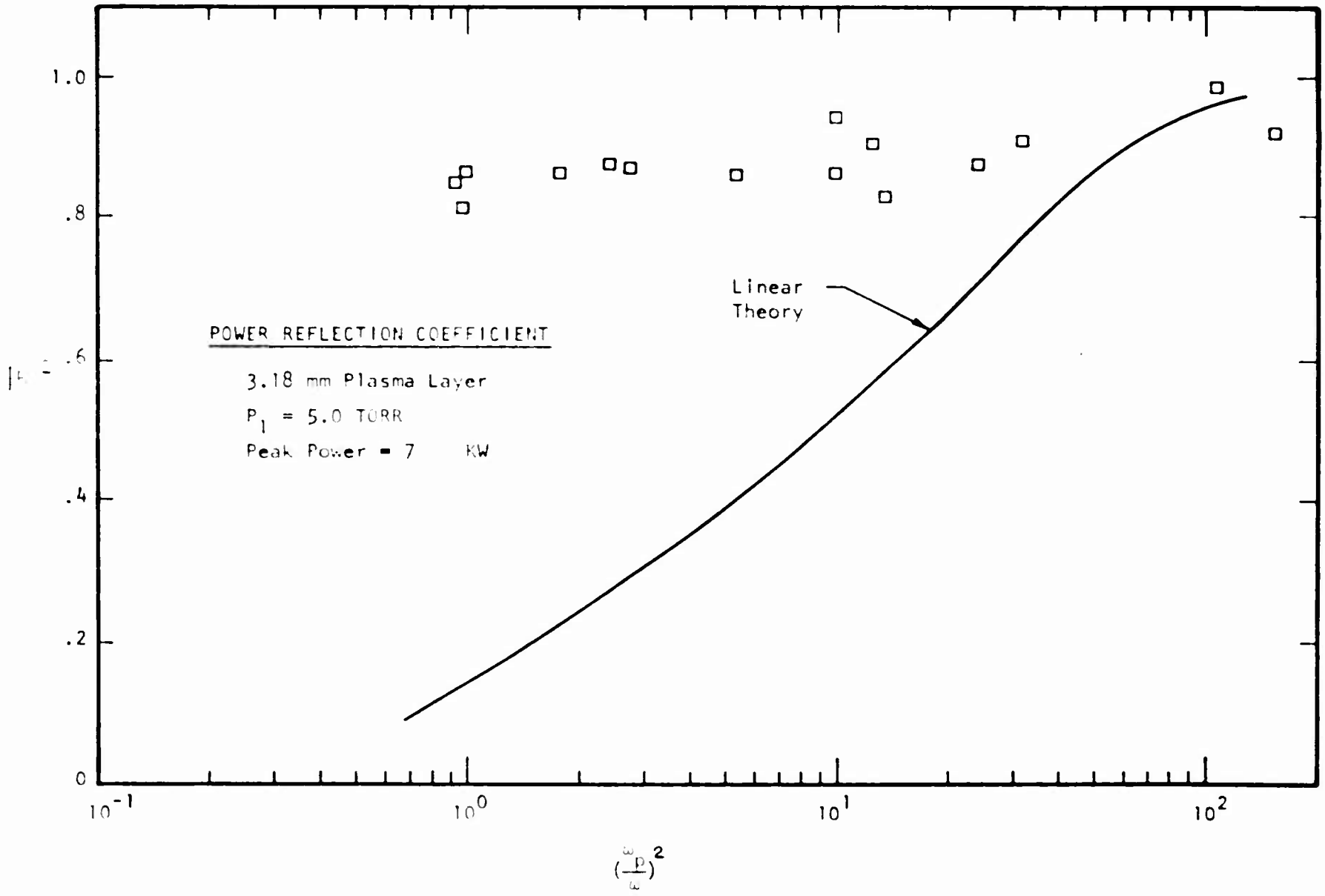

FIGURE 38. POWER REFLECTION COEFFICIENT 7kW

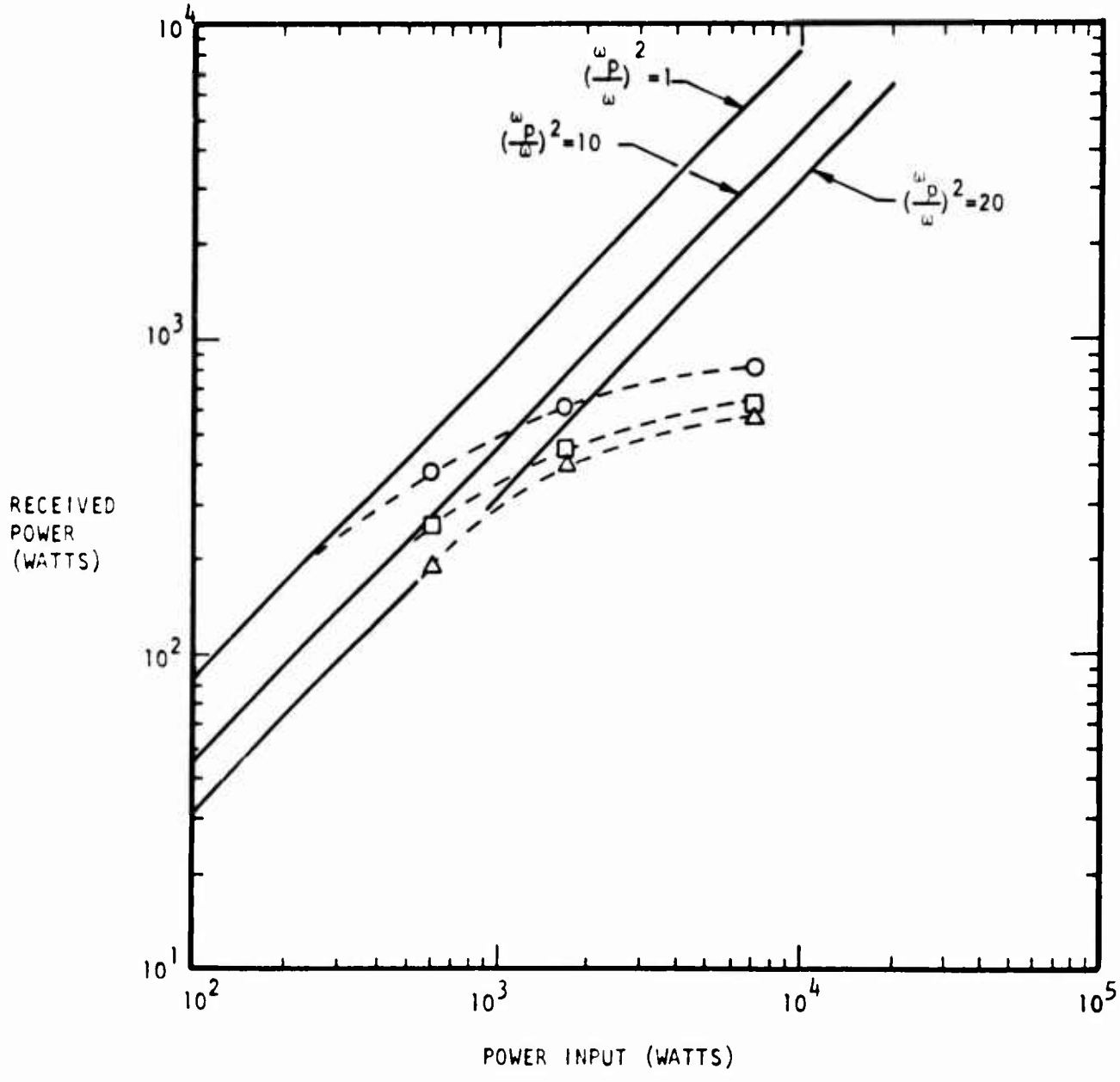

FIGURE 39. INCIDENT POWER EFFECTS

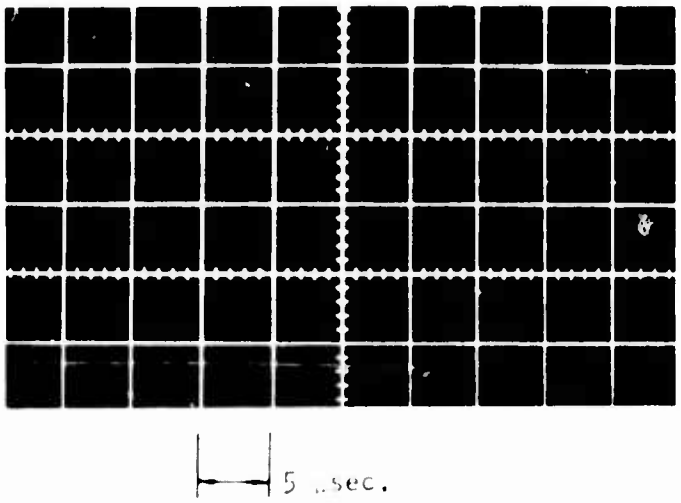

FIGURE 40. HORN ANTENNA TRANSIENT RESPONSE 1.77kW

of both the transmitting and receiving horns is not affected by the shock tube wall boundary layer. However, there is a relatively thin boundary layer covering the ground planes of both antennas which will affect the profile.

The variation of power transmission coefficient is shown as a function of plasma frequency in Figure 41. The linear theory is based upon Fante's theory[44] assuming a uniform electron density profile. The data were again measured at the trailing edge of the 2.0 microsecond pulse. The voltage reflection coefficient is shown in Figure 42 and the phase angle is shown in Figure 43 all as a function of plasma frequency. The electron density for these measurements was deduced from the ion current measurements of the upstream electrostatic probe using Chung's theory[18]. The local electron density could be determined prior to the onset of the incident pulse, and the free stream plasma frequency could be determined more accurately than from measurements of the shock velocity alone. Measurements of the shock velocity were also determined for each run to determine all other flow conditions.

Figure 44 illustrates the transient response of a 7 kW pulse. The rapid attenuation of the received pulse and the increased electron density flowing past the downstream probe is again exhibited. The power transmission coefficient is shown in Figure 45, and the voltage reflection coefficient is shown in Figure 46. The reflected phase is shown in Figure 47. The plasma frequency was calculated from the ion current measurements as in the previous incident power levels. All curves indicate a significant deviation from the linear approximations.

A tabulation of all the data collected during the horn antenna experiments is presented in Tables 1 and 2. The calculated plasma properties behind the shock wave are all deduced from the measured shock velocity using the tables of Menard and Horton[3].

ELECTROPHILIC MEASUREMENTS

The effect of the addition of an electrophilic agent to a plasma is a reduction in the electron density. Research to evaluate the effectiveness

TABLE 1

1.7 kW NOMINAL PEAK INPUT POWER

RUN	U_s (MEASURED) mm/μsec	U_2 mm/μsec	T_2 °K	P_2/P_o CALCULATED	P_2/P_o	n_e cm^{-3}	n_+ (MEASURED) cm^{-3}	$\|T\|^2$	$\|R\|^2$	$\|R\|$	ϕ DEG
1	3.70	3.33	3840	.0599	.955	3.5×10^{12}	4.6×10^{12}	.0228	.606	.78	165.65
2	4.25	3.84	4650	.0620	1.255	3.5×10^{13}	1.0×10^{13}	.00975	.665	.816	149.63
3	3.71	3.34	3840	.0600	.960	3.6×10^{12}	6.7×10^{12}	.0187	.640	.799	150.6
4	3.81	3.43	3960	.0608	1.010	5.3×10^{12}	8.0×10^{12}	--	.614	.784	163.99
5	4.03	3.64	4260	.0618	1.130	1.06×10^{13}	1.4×10^{13}	--	.739	.860	163.65
6	--	--	--	--	--	--	1.4×10^{13}	--	.720	.849	180
7	--	--	--	--	--	--	1.4×10^{13}	--	.724	.851	--
8	3.615	3.24	3740	.0591	.910	2.5×10^{12}	3.2×10^{12}	--	.513	.751	146.87
9	3.91	3.53	4200	.0614	1.062	7.6×10^{12}	1.12×10^{13}	.00884	.621	.786	152.57
10	3.65	3.28	3780	.0595	.930	2.8×10^{12}	9.5×10^{12}	.00889	.666	.818	154.58
11	3.85	3.47	4000	.0610	1.030	6.2×10^{12}	1.15×10^{13}	.00222	.716	.846	156.34
12	3.63	3.26	3760	.0593	.920	2.7×10^{12}	7.5×10^{12}	.0198	.635	.796	151.77
13	3.195	2.84	3350	.0531	.708	3.5×10^{11}	2.4×10^{12}	.215	.348	.590	138.46
14	3.60	3.23	3730	.0590	.905	2.4×10^{12}	1.705×10^{12}	.46	.136	.37	126.87
15	3.19	2.83	3350	.0532	.708	3.5×10^{11}	2.3×10^{12}	.225	.264	.51	141.69
16	3.14	2.78	3300	.0524	.684	2.7×10^{11}	2.4×10^{12}	.242	.267	.516	139.60
17	3.275	2.91	3420	.0545	.748	5.2×10^{11}	4.0×10^{12}	.1299	.429	.655	143.11

TABLE 2

7.0 kW NOMINAL PEAK INPUT POWER

RUN	U_s (MEASURED) mm/μsec	U_2 mm/μsec	T_2 °K	ρ_2/ρ_o Calculated	P_2/P_o	n_e cm^{-3}	n_+ (MEASURED) cm^{-3}	$\|T\|^2$	$\|R\|^2$	$\|R\|$	ϕ DEG
1	3.205	2.84	3360	.0534	.710	3.6×10^{11}	5.8×10^{11}	.0865	.614	.783	171.69
2	3.93	3.55	4110	.0614	1.075	8.0×10^{12}	1.3×10^{12}	.0725	.621	.789	174.8
3	3.96	3.57	4160	.0616	1.090	9.8×10^{12}	1.4×10^{12}	.078	.585	.766	167.1
4	3.63	3.26	3750	.0593	.920	2.7×10^{12}	1.8×10^{12}	.0634	.664	.814	173.3
5	3.345	2.98	3480	.0556	.780	7.4×10^{11}	1.19×10^{12}	.0925	.618	.785	170.4
6	3.36	3.0	3500	.0560	.77	8.2×10^{11}	9.4×10^{11}	.1097	.575	.758	175.7
7	3.425	3.06	3550	.0569	.815	1.05×10^{12}	1.1×10^{12}	.0814	.636	.798	175.5
8	3.38	3.02	3520	.0562	.795	9.0×10^{11}	8.0×10^{11}	.0959	.631	.794	174.09
9	3.425	3.06	3550	.0569	.815	1.05×10^{12}	1.15×10^{12}	.0743	.703	.838	175.84
10	3.90	3.52	4060	.0613	.865	7.4×10^{12}	6.5×10^{12}	.0156	.770	.878	179.0
11	3.685	3.31	3820	.0597	.945	3.3×10^{12}	8.0×10^{12}	--	.794	.891	180.0
12	3.75	3.37	3890	.0603	.980	4.4×10^{12}	1.6×10^{12}	.0875	.555	.745	176.6
13	4.14	3.74	4440	.0620	1.190	2.2×10^{13}	1.6×10^{13}	.0125	.826	.908	180.0
14	3.985	3.60	4180	.0617	1.100	1.05×10^{13}	8.2×10^{12}	.0143	.771	.878	179.1

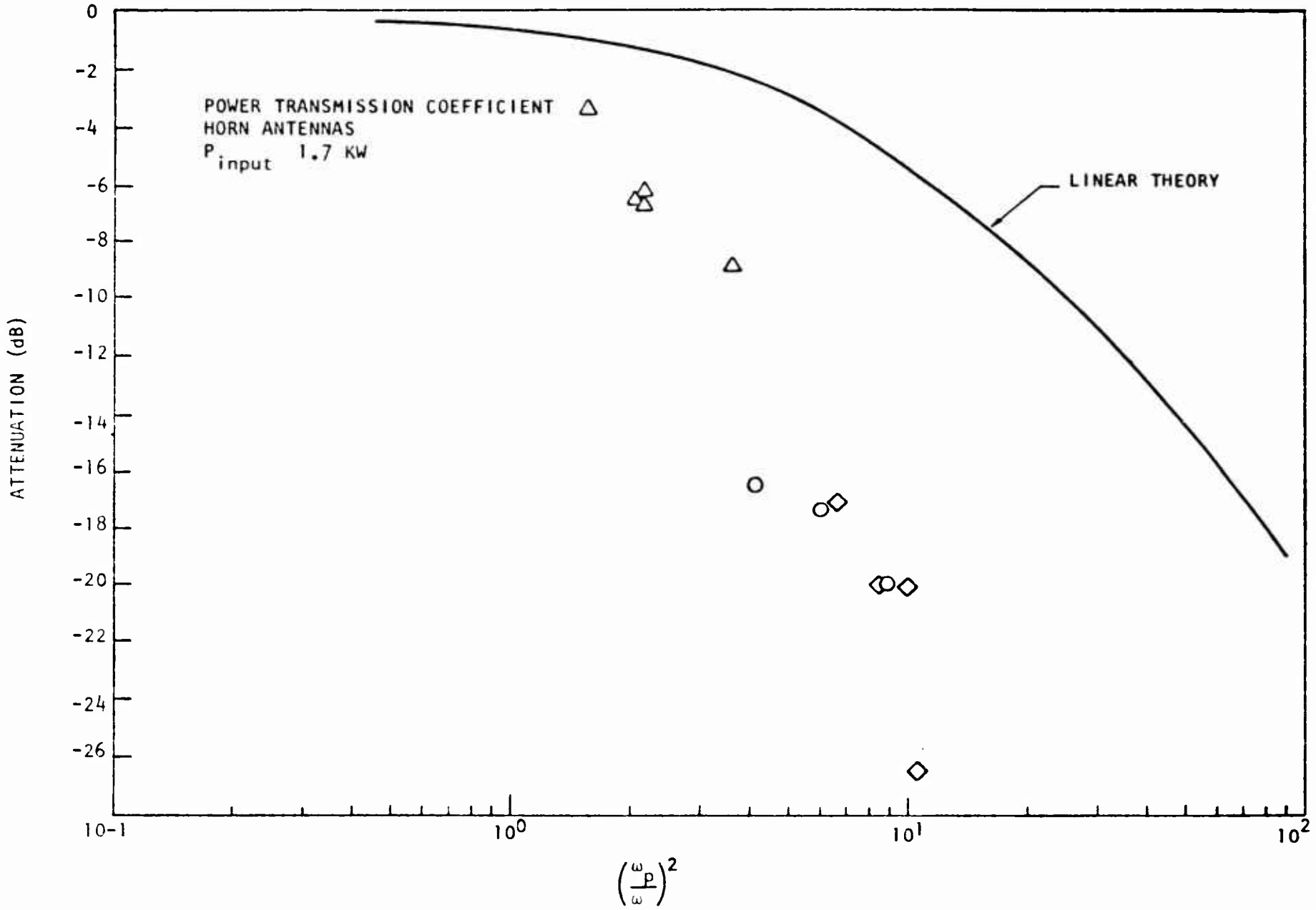

FIGURE 41. HORN ANTENNA TRANSMISSION COEFFICIENT 1.7 kW

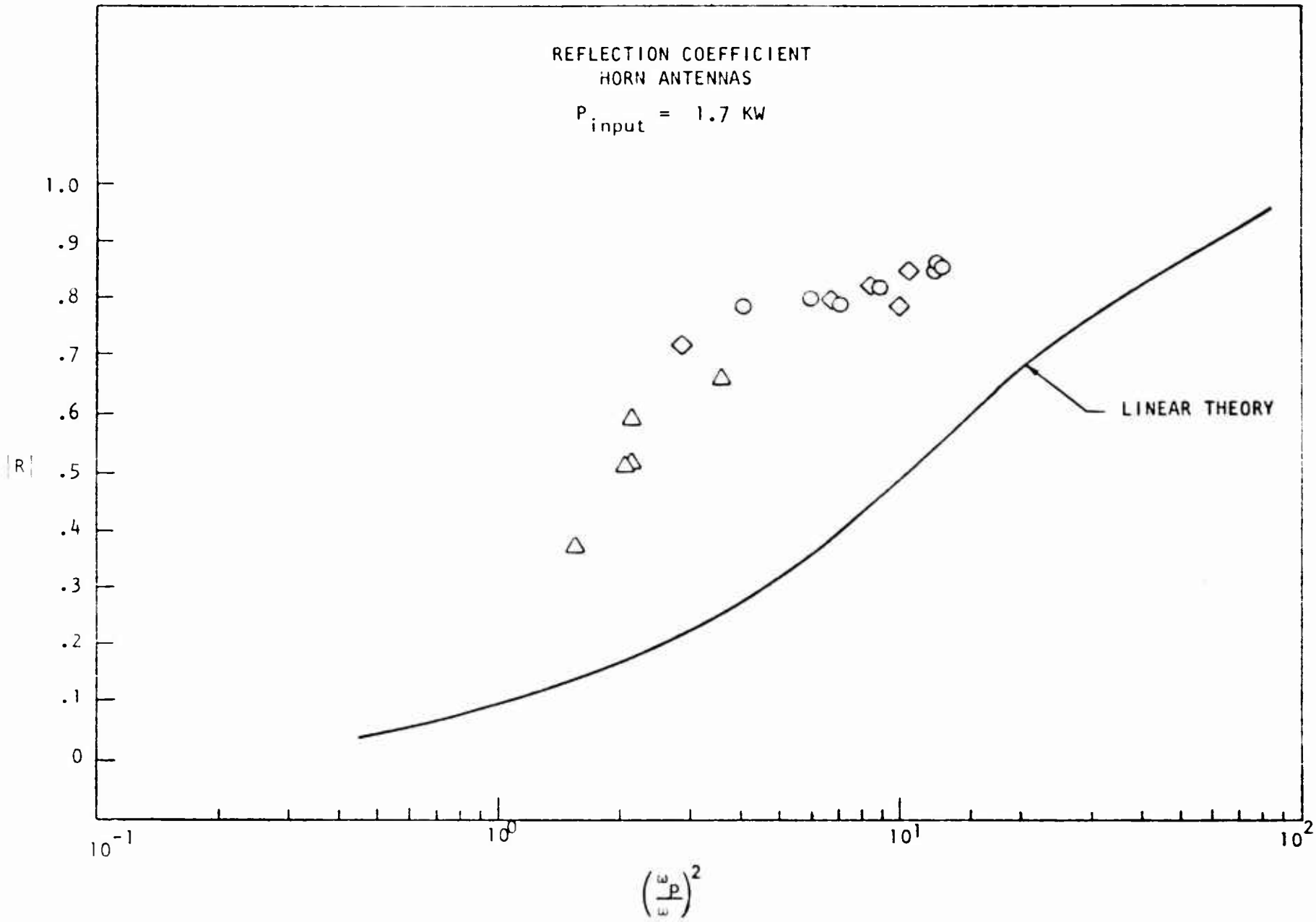

FIGURE 42. HORN ANTENNA REFLECTION COEFFICIENT 1.7 kW

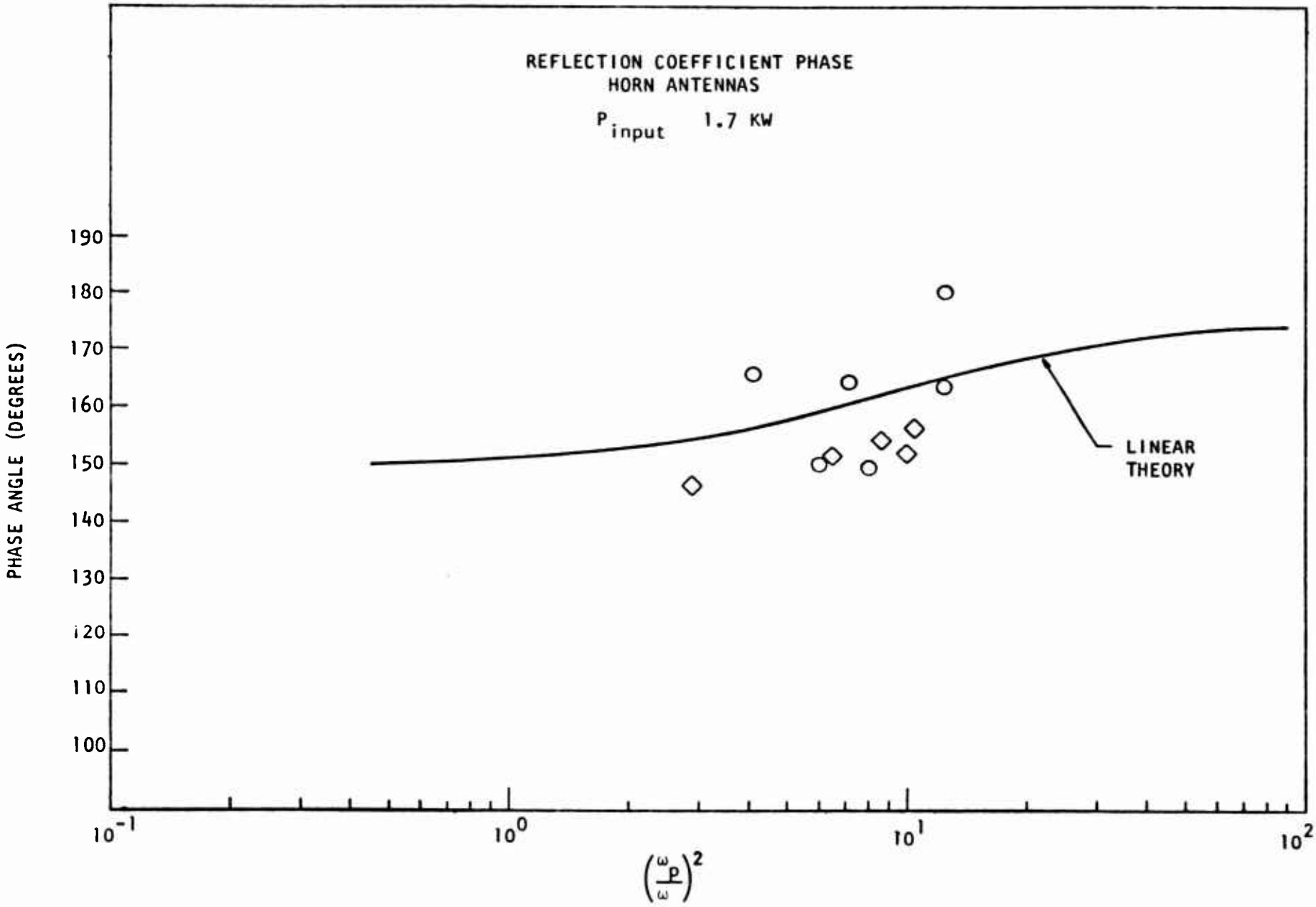

FIGURE 43. HORN ANTENNA REFLECTED PHASE 1.7 kW

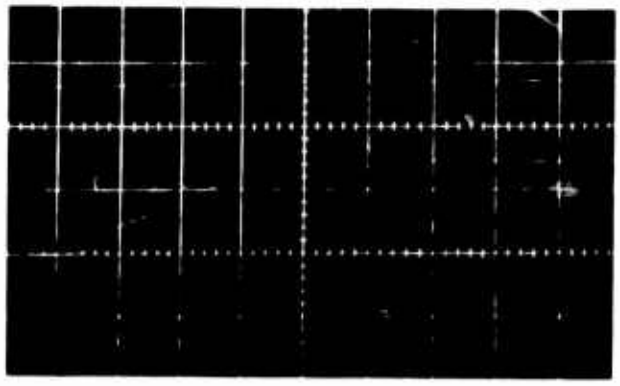

VOLTAGE PROBE

175.5°

ION CURRENT

UPSTREAM PROBE

5 μsec.

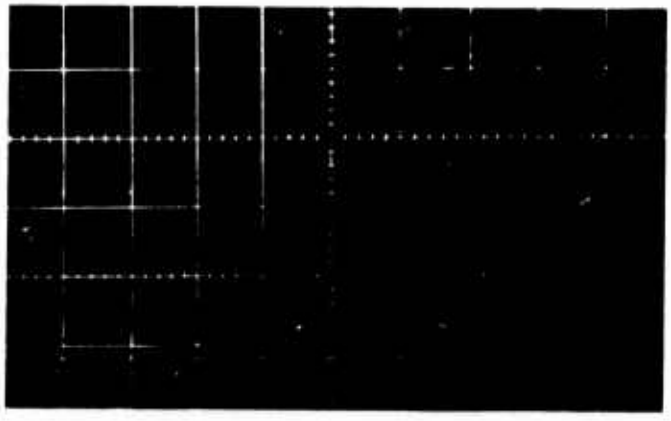

ION CURRENT

DOWNSTREAM PROBE

INCIDENT POWER

5 μsec

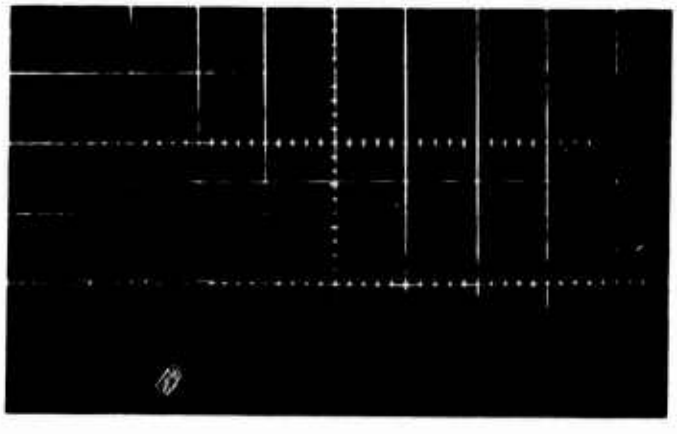

RECEIVED POWER

$|T|^2$ = - 10.89 dB

REFLECTED POWER

$|R|^2$ = .636

5 μsec

FIGURE 44. HORN ANTENNA TRANSIENT RESPONSE 7.0 kW

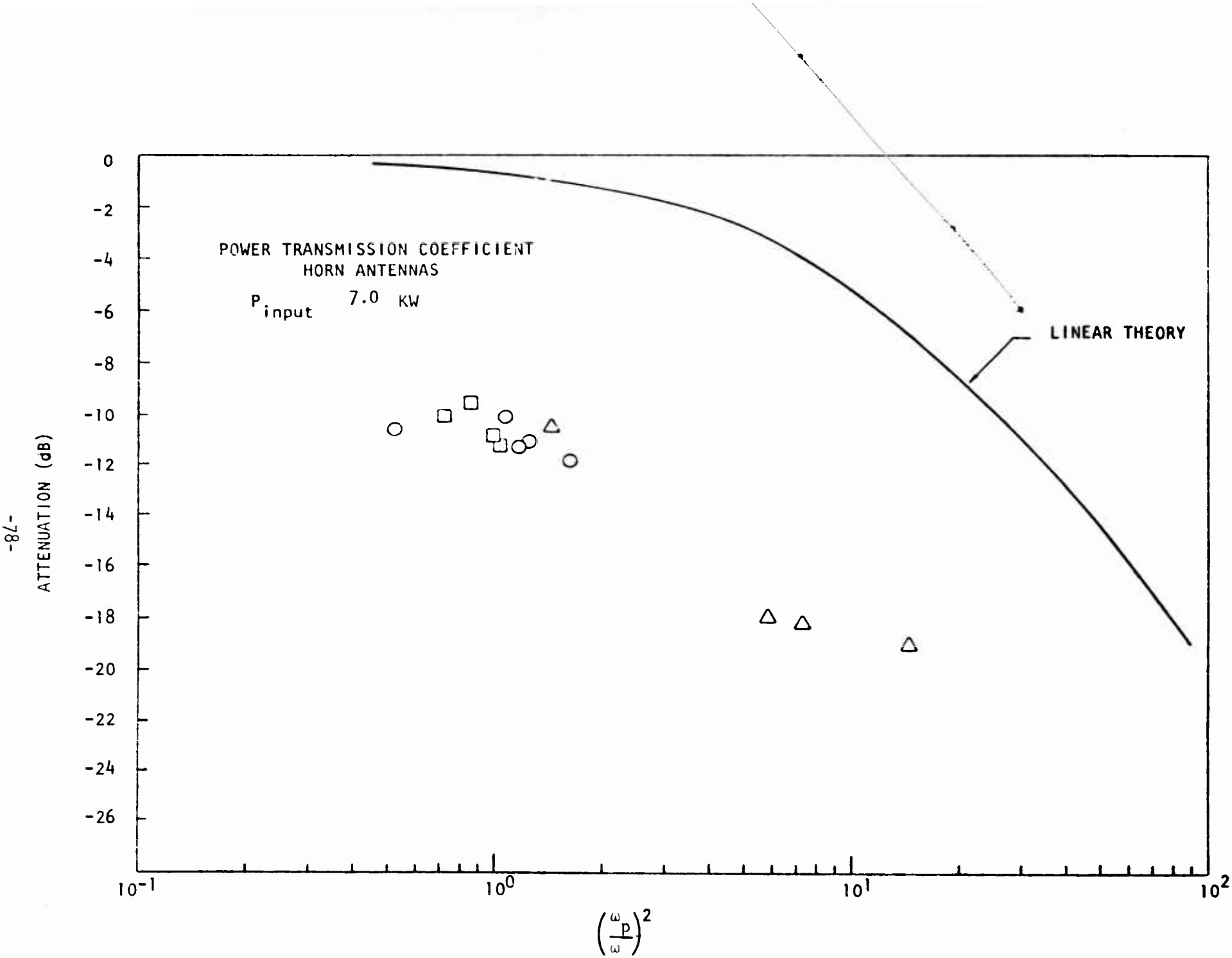

FIGURE 45. HORN ANTENNA TRANSMISSION COEFFICIENT 7.0 kW

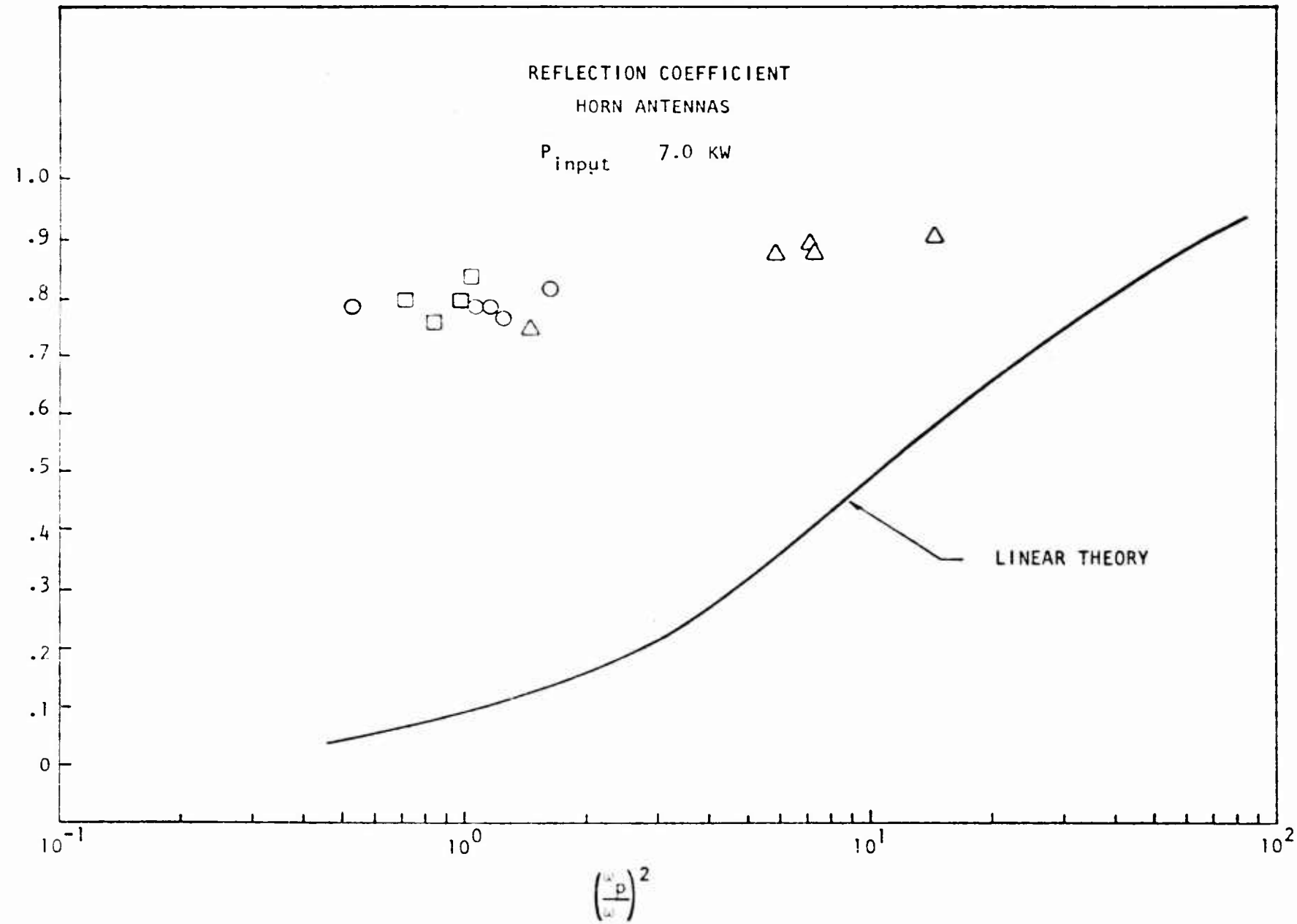

FIGURE 46. HORN ANTENNA REFLECTION COEFFICIENT 7.0 kW

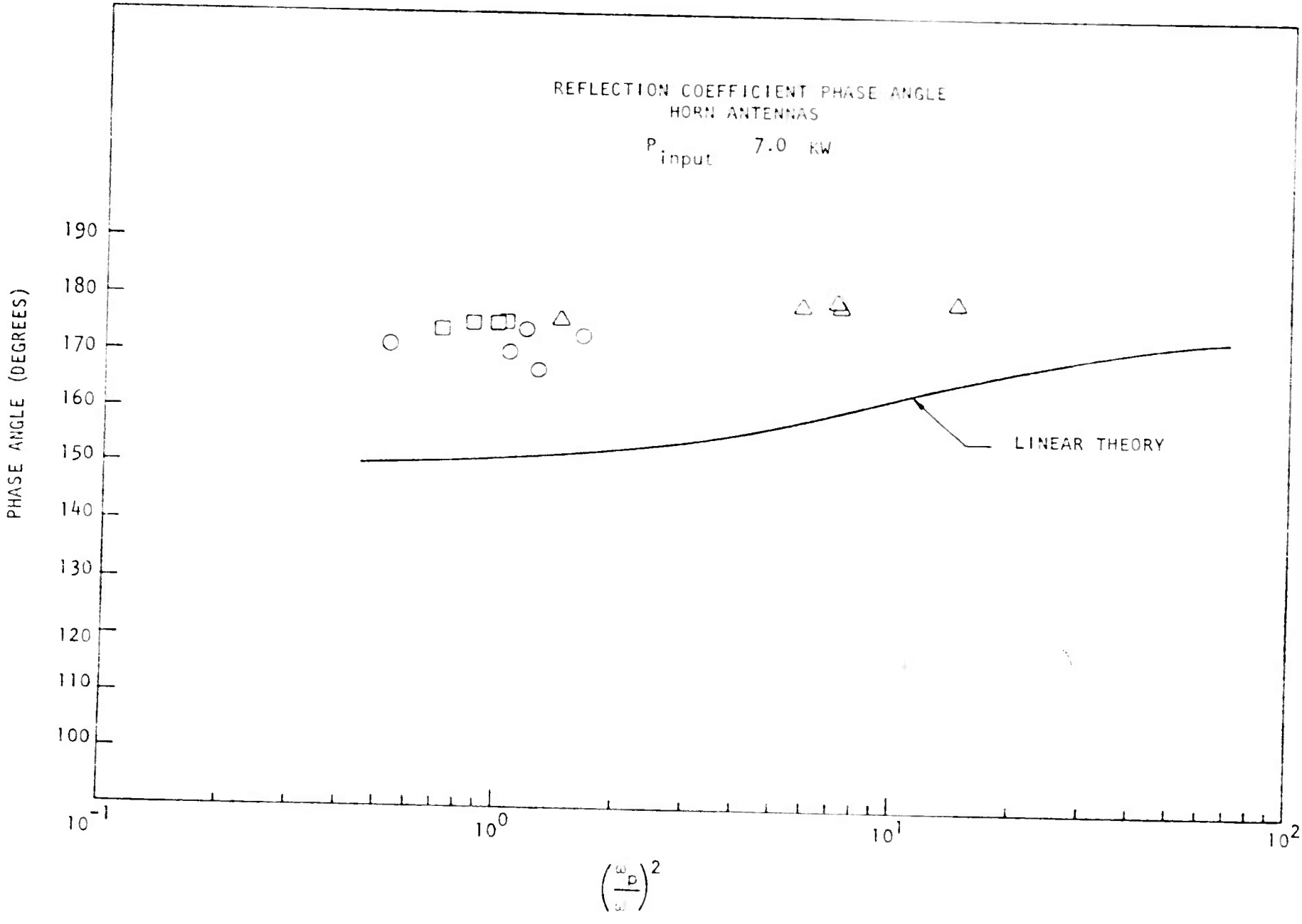

FIGURE 47. HORN ANTENNA REFLECTED PHASE 7.0 kW

of electrophilic addition upon the performance of reentry microwave systems has been conducted for a number of years[48-51]. The theoretical work of Papa[48,49] provides the most detailed analysis of the interaction of a high power electromagnetic wave with an electrophilic seeded plasma. Research to select an additive which will produce the required reduction in electron density in the required time period has resulted in the selection of the fluorocarbon compound Freon 114B2[50]. Detailed laboratory studies indicated that this particular additive meets most of the desired properties for reentry vehicle application. Full scale flight test measurements of the electrophilic injection upon a microwave system were conducted under the Trailblazer program where the results indicated significant improvement in system performance at high power levels and relatively high altitudes[51]. In order to study the effect of the electrophilic addition upon high power microwave transmission at conditions of high electron density and high neutral particle density, a series of laboratory experiments were performed using the additive Freon 114B2.

The laboratory experiments were conducted using the horn antenna configuration used in previously described experiments. The antenna ground plane spacing was maintained at 3.18 mm and the shock tube initial pressure was fixed at 5.0 torr. Since a few changes in the microwave hardware were made, additional clean air measurements were obtained in order to evaluate the effect of electrophilic addition upon antenna performance. One high power magnetron (f = 9.382 GHz) was used for all measurements which required the addition of suitable attenuators in order to obtain the low power measurements.

---

[48] Papa, R. J., and Taylor, R., "High Power Electromagnetic Transmission Characteristics of a Diffusing Reentry Plasma," J. of App. Phys. 45, 684, 1974. Also AFCRL-TR-73-0754, December 1973.

[49] Papa, R. J., "Chemical Injection into a Reentry Plasma to Improve High Power EM Wave Transmission," AFCRL-72-0556, September 1972.

[50] Lennon, J. F., and Herskovitz, S. B., "Design and Testing of a Chemical Injection System for Reentry Plasma Alleviation," AFCRL-TR-74-0113, February 1974.

[51] Hayes, D. T., Herskovitz, S. B., Lennon, J. F., and Porrer, J. L., "Inflight Electrostatic Probe Measurements of the Effect of Chemical Injection on the Properties of the Reentry Flow Field," AIAA Paper No. 73-692, AIAA 6th Fluid and Plasma Dynamics Conference, Palm Springs, Calif., July 1973. Also AFCRL-72-0640, October 1972.

The electrophilic agent Freon 114B2 is a liquid at standard temperatures and pressures. The vapor pressure of the Freon is relatively high (285 torr at 20°C) which indicates that Freon will be in the vapor phase when added to the room air at the shock tube initial static pressure of 5 torr. The short run time of the shock tube prevented the injection of the liquid Freon 114B2 directly into the shock heated plasma, therefore only the chemical electron attachment process could be simulated. The true effect of the liquid electrophilic would include mechanisms such as phase changes and droplet catalytic effects upon total electron depletion rates. The liquid Freon was placed in a small vacuum chamber and coupled to the driver section of the shock tube through a vacuum line which contained a precision needle valve for flow adjustment. The driver section was pumped to the required pressure level where the pressure was measured with the use of a digital capacitance manometer. Freon 114B2 vapor was then added to the dry air to bring the static pressure to the desired initial pressure level of 5.0 torr. The mole fraction of the Freon added to the air was then determined from measurements of the initial air pressure and the final mixture pressure. The major portion of the experiments were performed with a 1% addition of Freon 114B2 to dry air; however, a few experiments were performed to evaluate the effect of variable mole fraction of additive upon the transmission properties of the microwave signal. Microwave measurements of the incident power, reflected power, and received power were performed for all experiments. The free stream electron density was determined from the ion current collected by an upstream electrostatic probe located on the transmitting antenna ground plane. The probe was biased to -3 volts relative to the ground plane as used in previous measurements. The electron density was then determined from the calibration curve for the probe as determined from previous diagnostic measurements. An electrostatic probe immediately downstream of the transmitting antenna was biased at +18 volts relative to the ground plane in order to collect electron current. The electron current probe will give a direct comparison of the reduction in electron density due to the attachment process of the electrophilic additive. The ion current will remain unchanged during the attachment process if recombination mechanisms are negligible. In addition to the

electrostatic probe measurements, the shock velocity was measured with wall static pressure probes along the test section. Experiments were performed using a single, 2 microsecond duration pulse at a peak incident power of 18 W, 1.5 kW and 5.0 kW. A comparison of the transient behavior of some of the measured variables is shown in Figure 48 for clean air and air seeded with 1% Freon. In this comparison the peak incident power is 1.5 kW and the free stream electron density is approximately equal. Since shot to shot reproducibility is very difficult to maintain, a series of measurements fixing all initial conditions while varying shock velocity were performed.

Measurement of the attenuation of a single 18 W pulse is shown in Figure 49. Good agreement with impedance sheet theory[44] is observed for the low incident power levels where breakdown is not expected. The effect of a 1% addition of Freon to the air prior to shock heating reveals a reduction in the attenuation of approximately 2 dB up to $(\omega_p/\omega)^2 = 8$. The effect of the electrophilic upon the reflection coefficient is shown in Figure 50. Considerable reduction in the reflection coefficient over the entire range of free stream electron density is observed. The reduction in the electron density due to the addition of the electrophilic is shown in Figure 51. The upstream ion probe current, which has reached an equilibrium value prior to the onset of the incident pulse, was used as a reference current. The effect of the small concentration of electrophilic upon the upstream ion current was observed to be negligible over the entire range of incident power. The electron current collected by a probe located downstream of the transmitting antenna will be sensitive to electron production effects due to the incident wave electric field and any electron depletion effects due to seeding. The downstream probe electron current is shown as a function of upstream equilibrium ion current for a clean and seeded flow in Figure 51. Significant reduction in the electron current is observed for increasing free stream electron density levels.

Similar measurements were performed for a peak incident power of 1.5 kW. The effect of the additive upon the transmission coefficient is shown in

CLEAN AIR

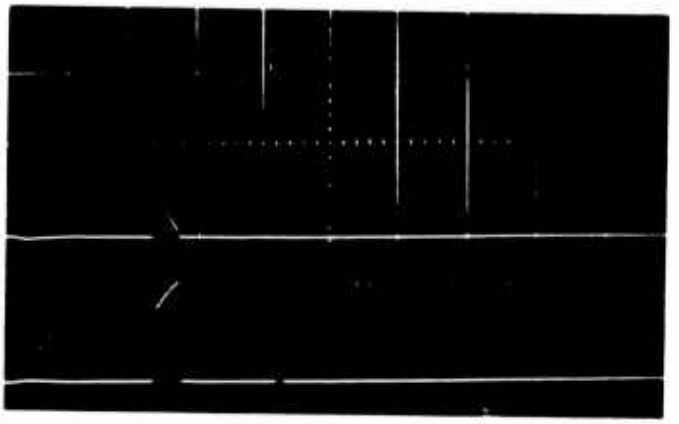

UPPER TRACE: RECEIVED POWER T^2 = -14.5 dB
LOWER TRACE: REFLECTED POWER

1% FREON 114B2

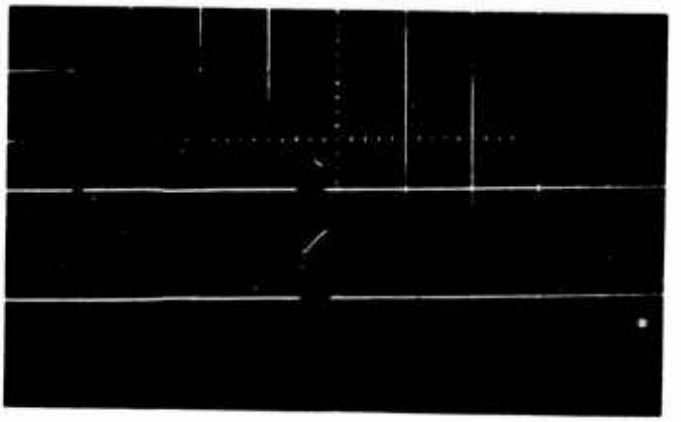

UPPER TRACE: RECEIVED POWER T^2 = -8.3 dB
LOWER TRACE: REFLECTED POWER

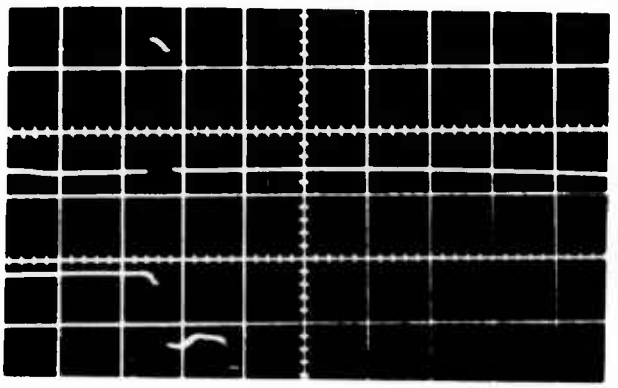

UPPER TRACE: VOLTAGE PROBE
LOWER TRACE: ELECTRON CURRENT
$j_- = 1.06 \times 10^4$ A/M^2

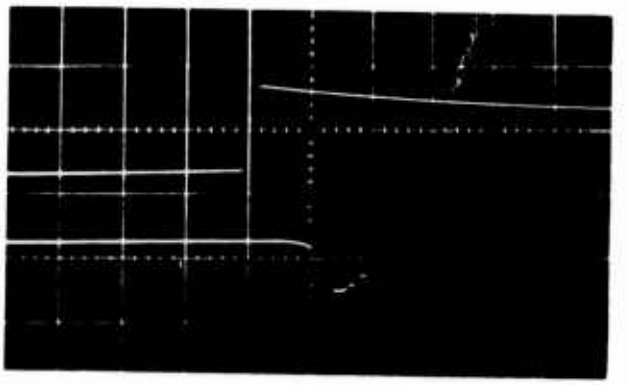

UPPER TRACE: UPSTREAM WALL STATIC PRESSURE
LOWER TRACE: ELECTRON CURRENT
$j_- = 6.19 \times 10^3$ A/M^2

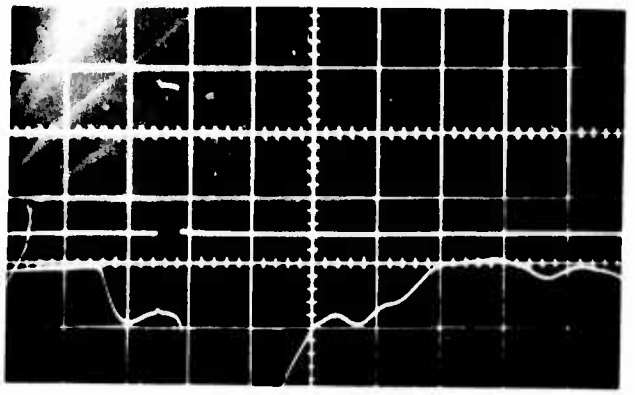

UPPER TRACE: INCIDENT POWER
LOWER TRACE: ION CURRENT, $(\omega_p/\omega)^2 = 13.3$

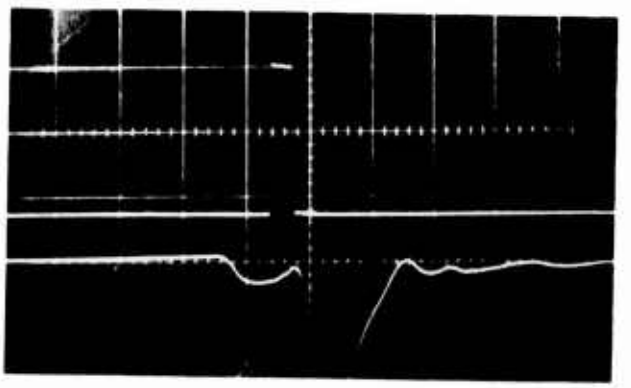

UPPER TRACE: INCIDENT POWER
LOWER TRACE: ION CURRENT, $(\omega_p/\omega)^2 = 14.9$

ALL SWEEP RATES 5 μsec/DIV

FIGURE 48. TRANSIENT RESPONSE COMPARISON 1.5 kW

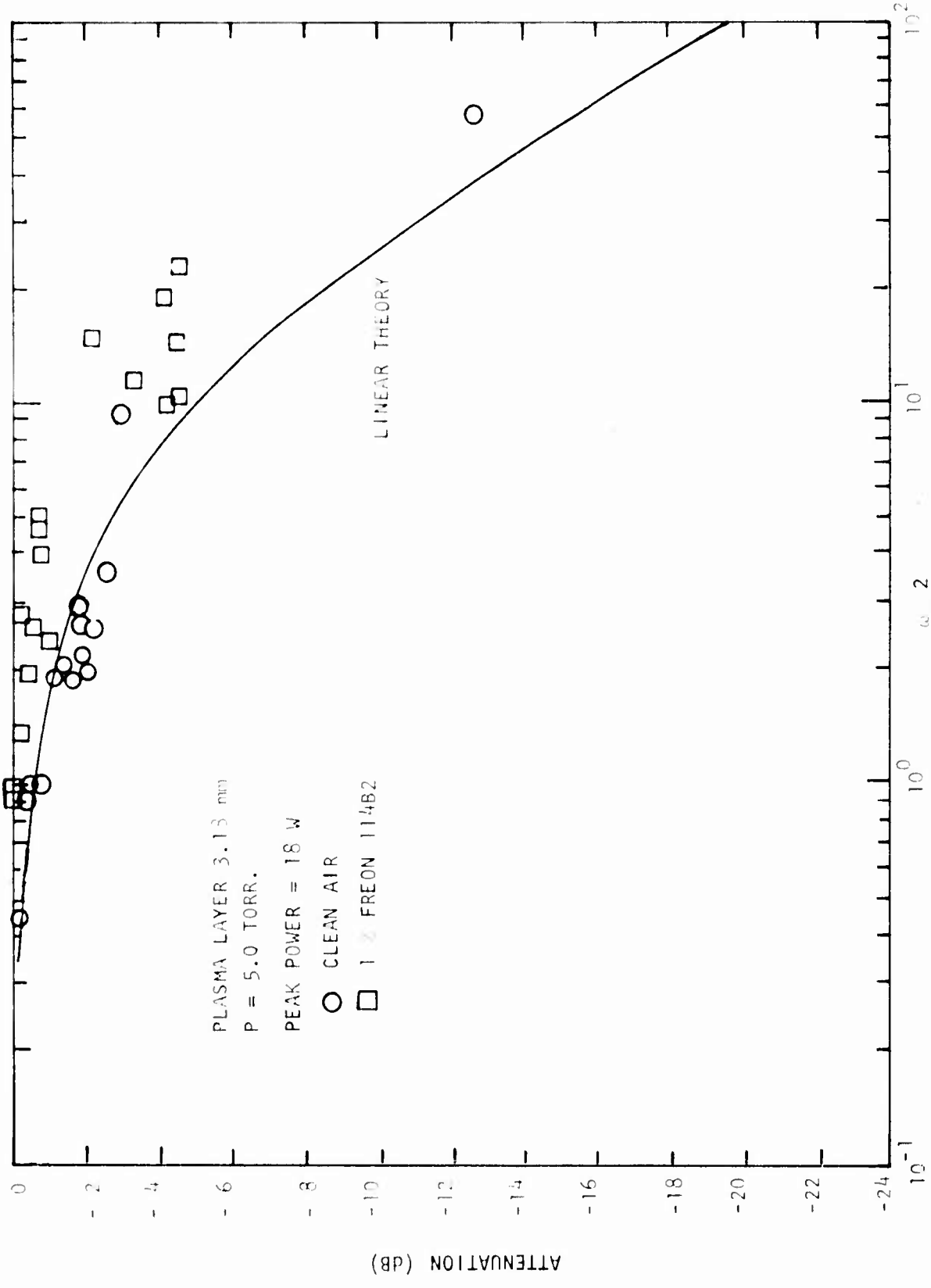

FIGURE 49. POWER TRANSMISSION COEFFICIENT, SEEDED FLOW, 18W

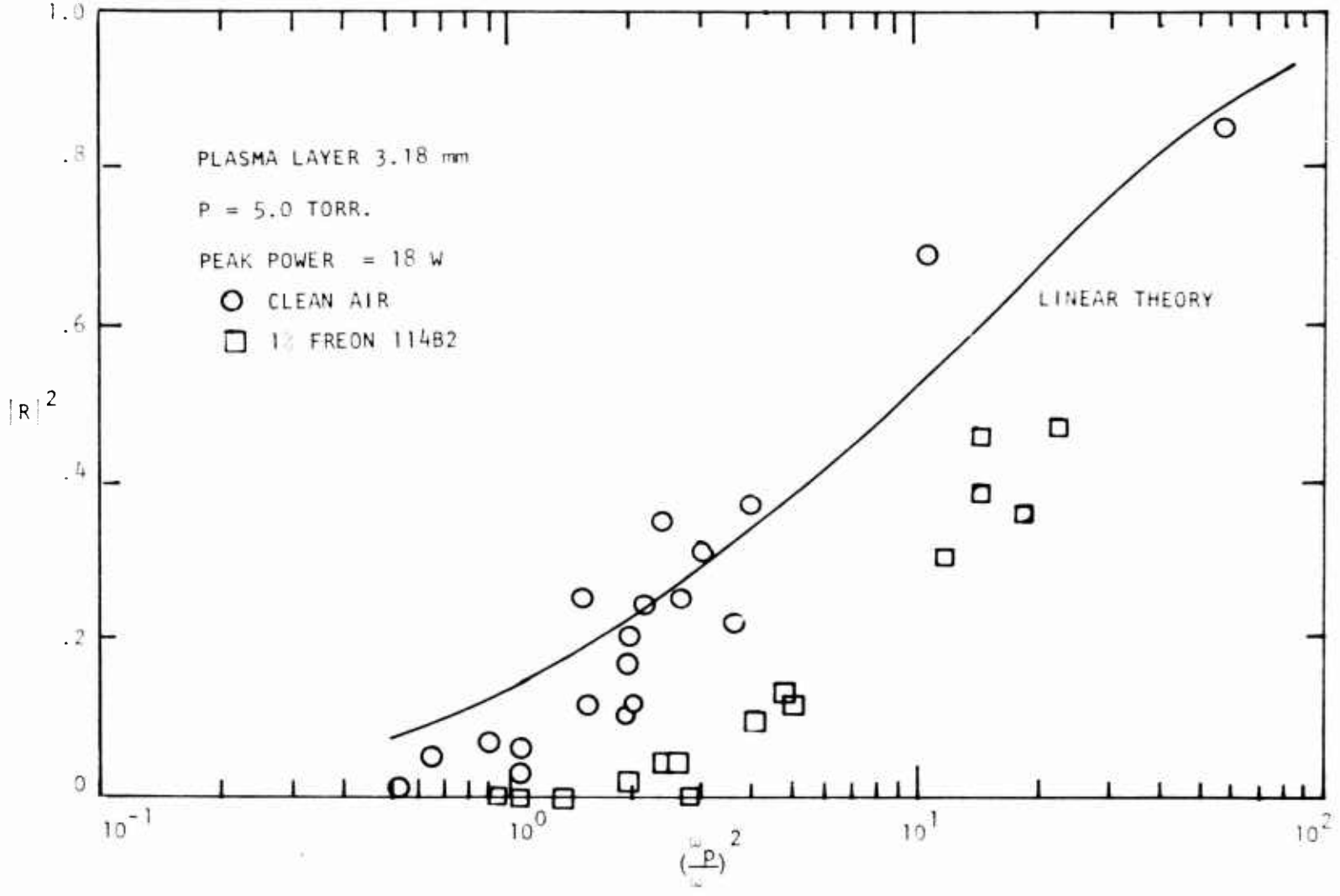

FIGURE 50. POWER REFLECTION COEFFICIENT, SEEDED FLOW, 18W

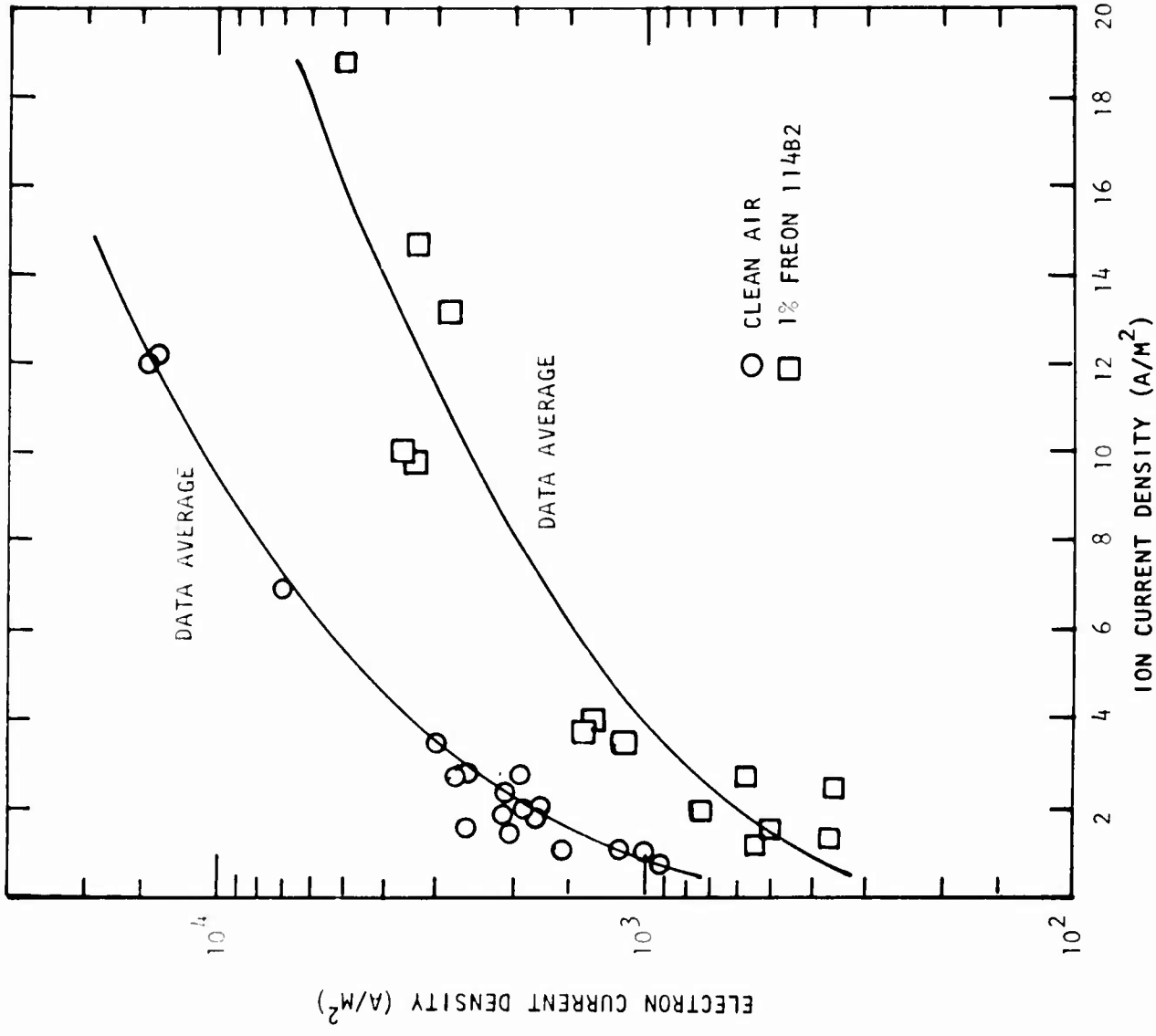

FIGURE 51. PROBE CURRENT, 18W

Figure 52. For these measurements the transmission coefficient was measured at the trailing edge of the pulse. An improvement of approximately 3 dB in transmission coefficient is observed up to an electron density where $(\omega_p/\omega)^2 = 10$. The effect upon the reflection coefficient is shown in Figure 53 where improvement is seen over the entire range of experimental plasma frequencies. Figure 54 presents a comparison of the probe current for the clean and seeded flow. The effect of the high power pulse upon the electron density is shown by comparison with the low power measurements. The addition of the electrophilic is much more effective at the lower values of free stream electron density (and corresponding lower temperatures) than at the higher values of free stream electron density. This effect is probably the result of thermal decomposition of the additive at the higher temperatures with the resulting reduction of electron attachment cross sections of the daughter products and competing electron production mechanisms.

A series of measurements were also performed for a nominal peak power of 5.0 kW. The transmission coefficient for the clean and seeded flow is shown in Figure 55, where again the measurements correspond to the trailing edge of the 2 microsecond pulse. At this incident power level an improvement of approximately 7 dB is observed up to $(\omega_p/\omega)^2 = 10$. The reduction in the amount of reflected power is shown in Figure 56. The reflection coefficient is reduced by approximately 0.2 over the value of the high power, clean air reflection coefficient. The collected electron current is shown in Figure 57 where the effect of the increased electron density due to the high power pulse is an order of magnitude greater than the low power results for clean air at the lower free stream electron densities. The result of the additive upon electron depletion is still significant at the lower electron densities and temperatures becoming less effective as the free stream electron density increases.

A few measurements were performed to examine the effect of the initial concentration of Freon 114B2 upon the transmission coefficient at an incident power of 1.5 kW. Measurements indicated that only a slight change in transmission coefficient was observed when the initial mole fraction of Freon was

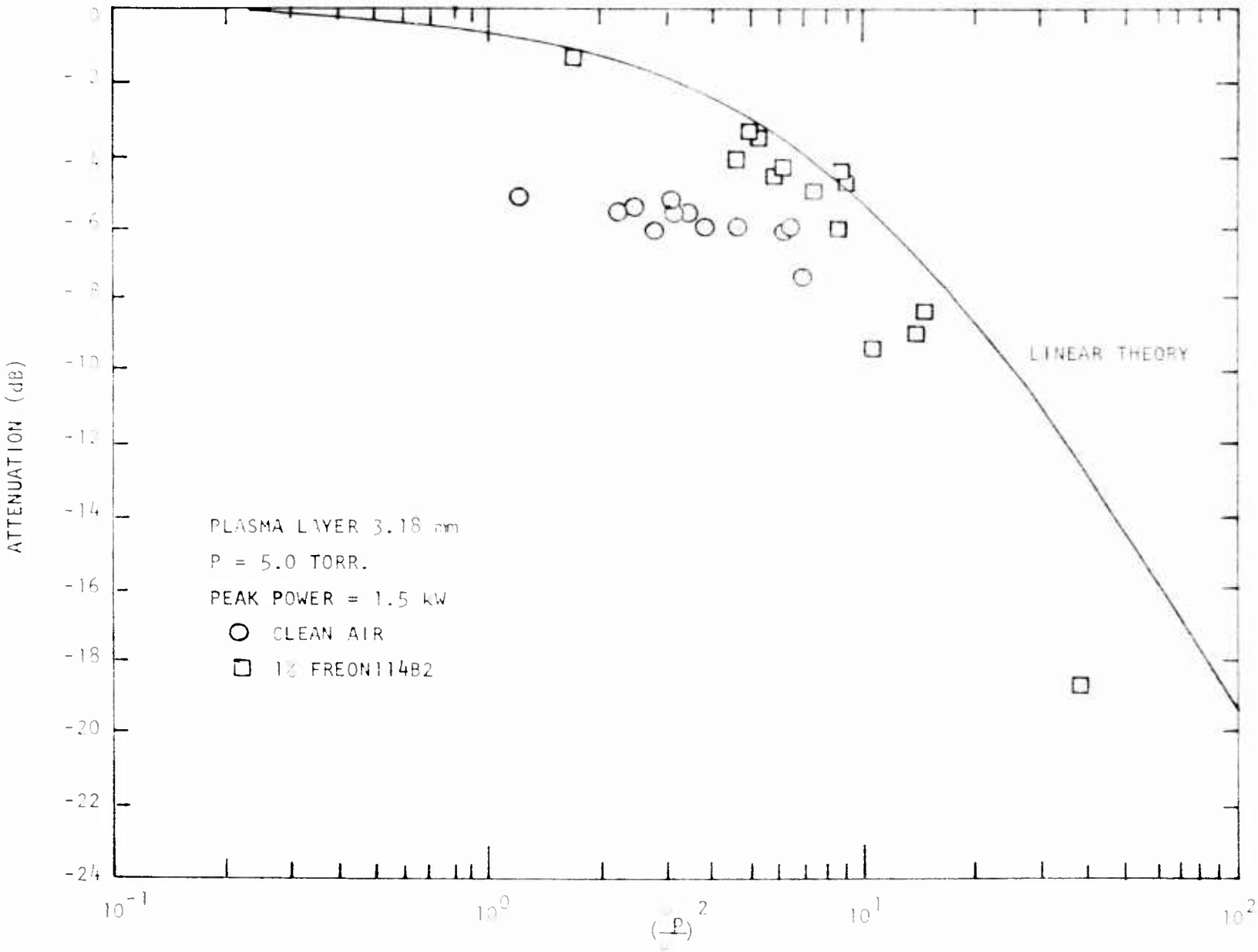

FIGURE 52. POWER TRANSMISSION COEFFICIENT, SEEDED FLOW, 1.5 kW

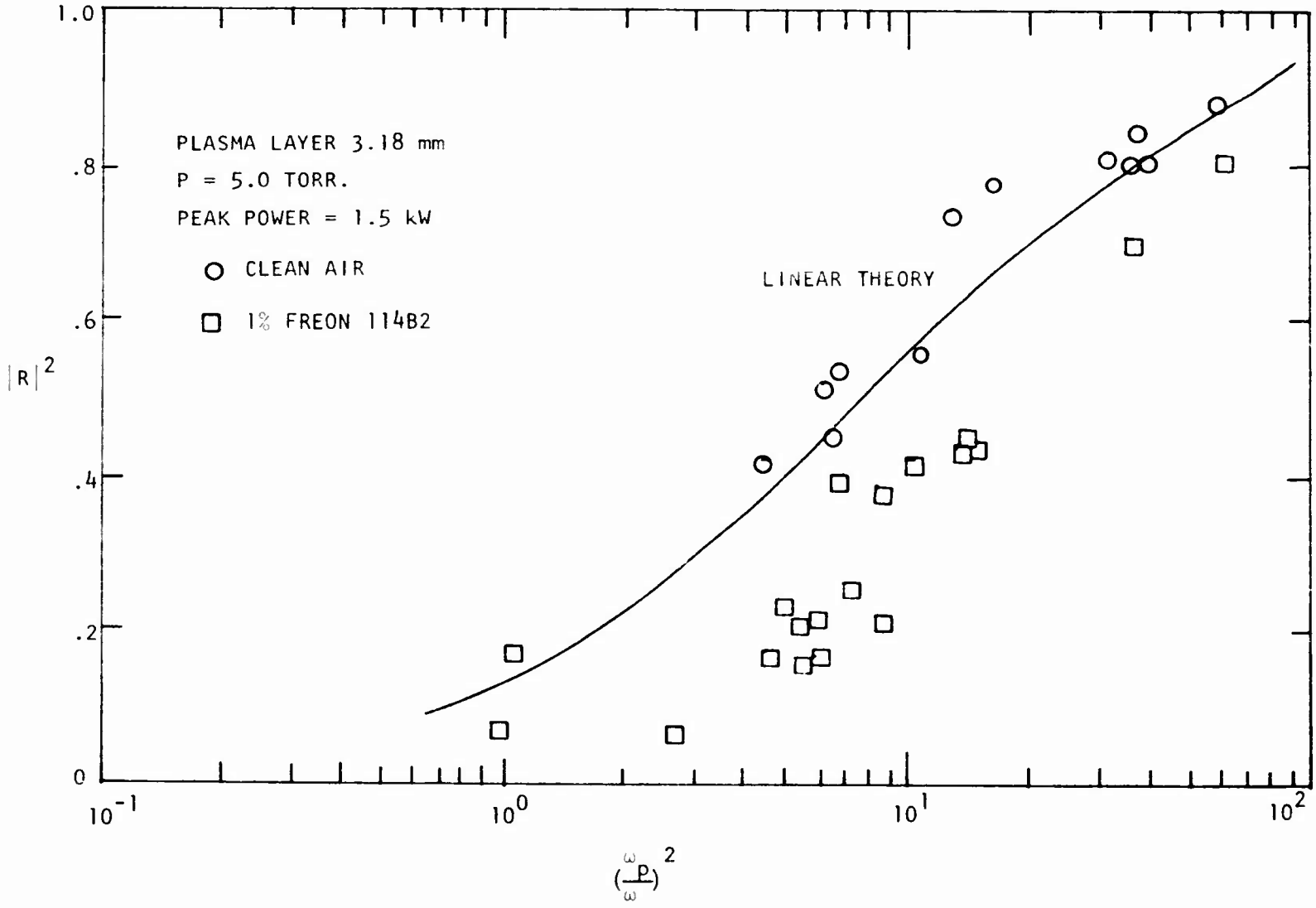

FIGURE 53. POWER REFLECTION COEFFICIENT, SEEDED FLOW, 1.5 kW

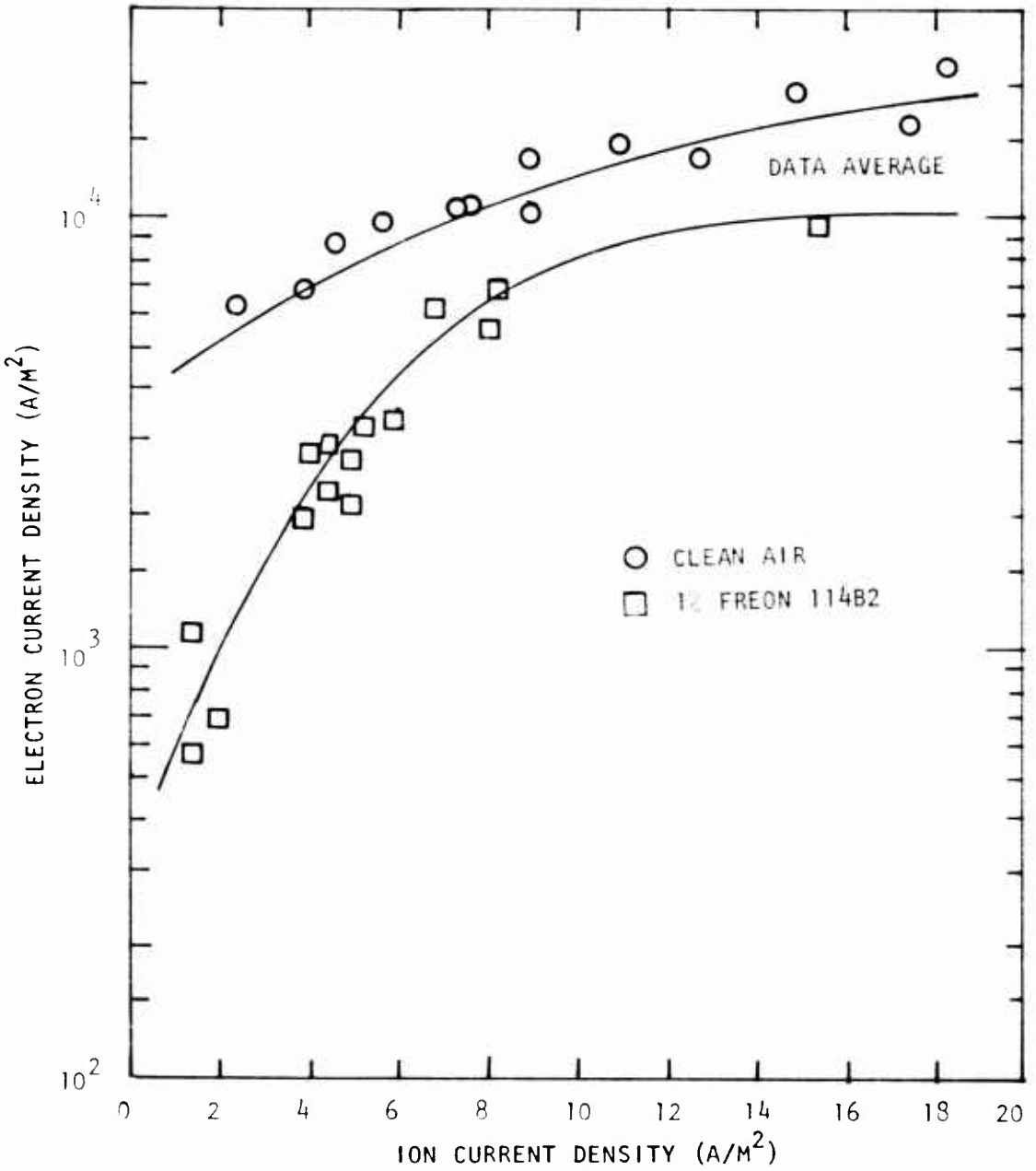

FIGURE 54. PROBE CURRENT, 1.5 kW

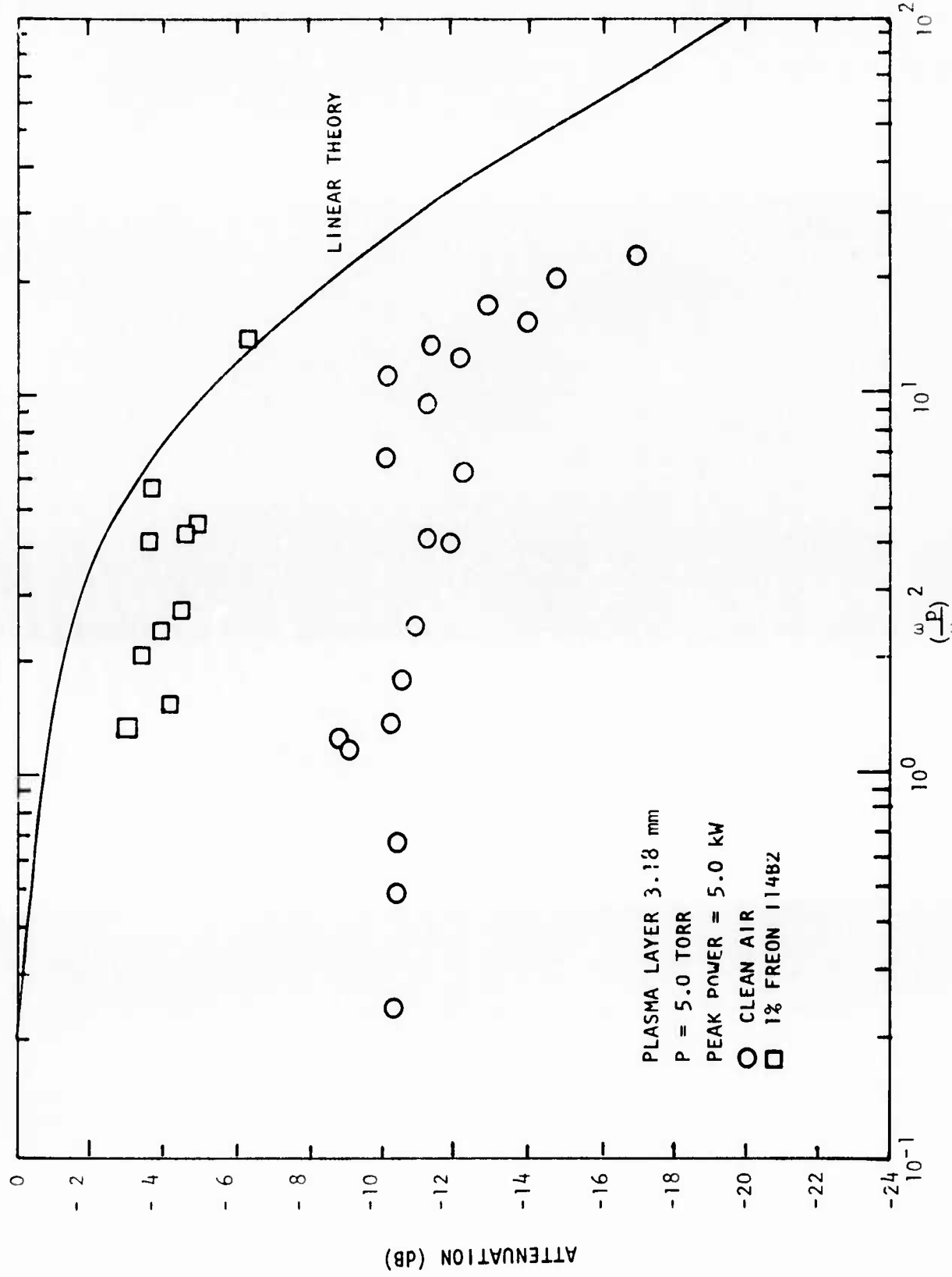

FIGURE 55. POWER TRANSMISSION COEFFICIENT, SEEDED FLOW, 5.0 kW

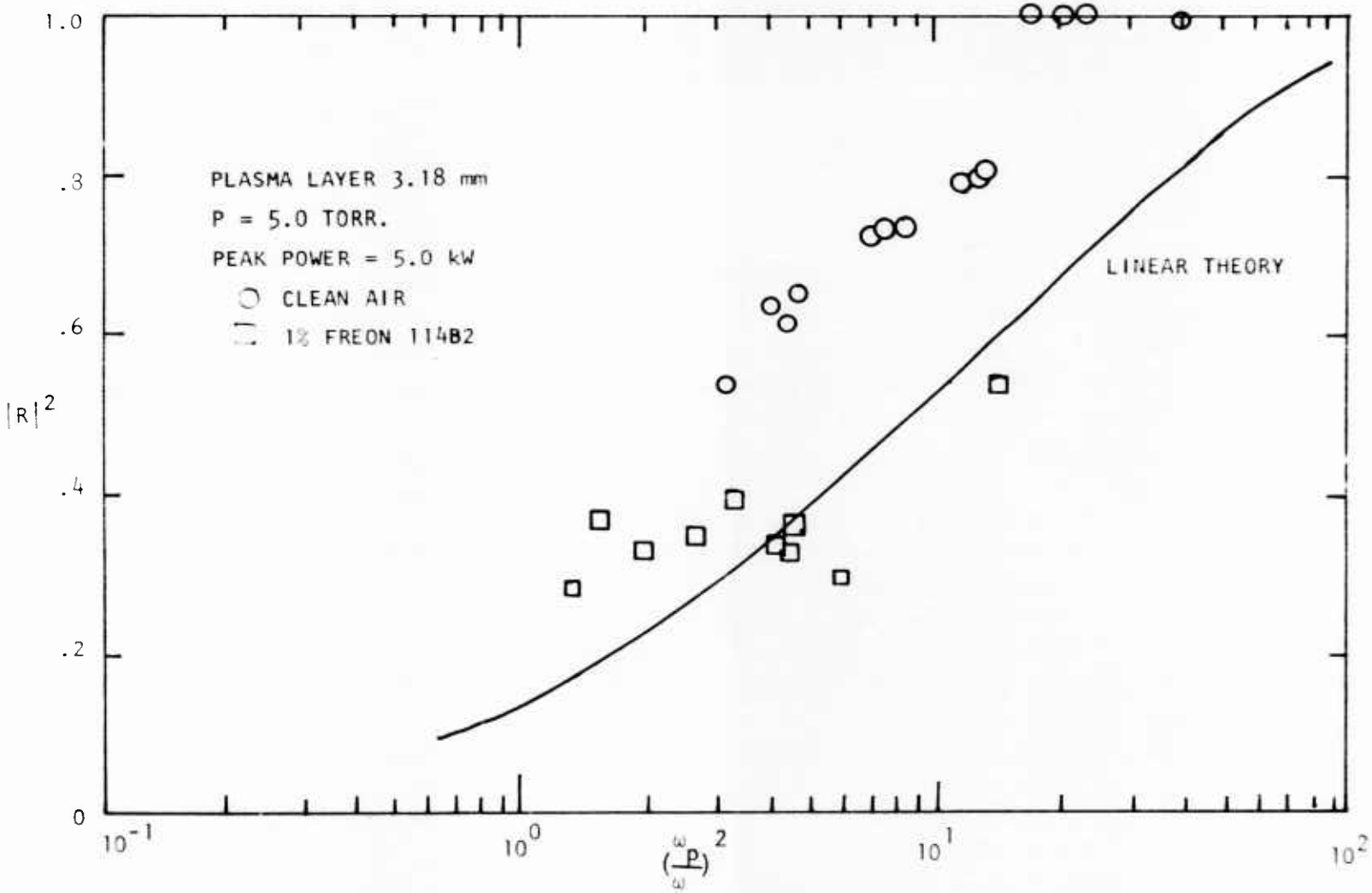

FIGURE 56. POWER REFLECTION COEFFICIENT, SEEDED FLOW 5.0 kW

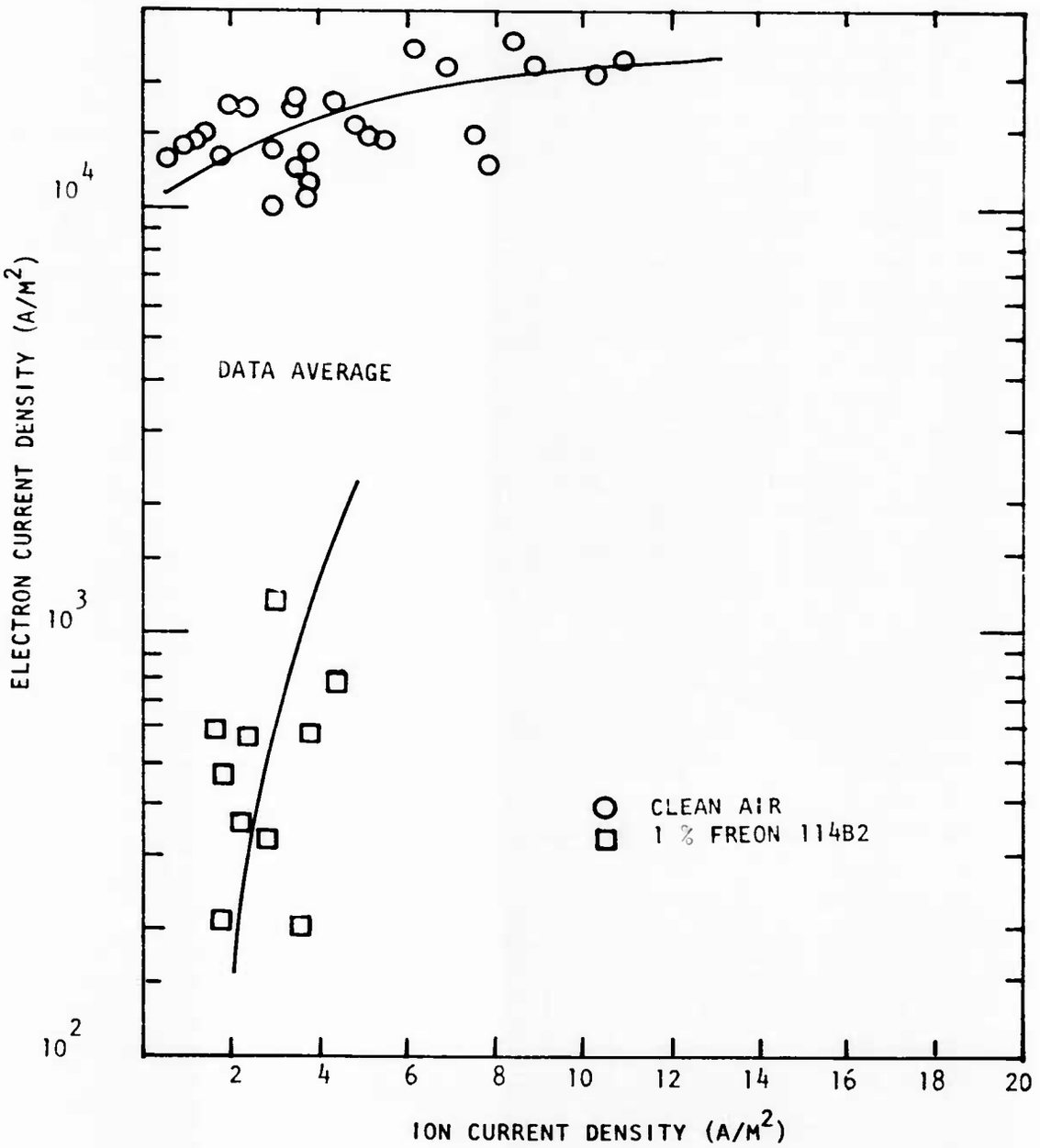

FIGURE 57. PROBE CURRENT 5.0 kW

reduced to 0.5%. Increasing the initial mole fraction to 3% caused a noticeable reduction in shock velocity indicating significant changes in the speed of sound and other thermophysical properties of the test gas were taking place. In general, insufficient data were obtained to evaluate the effect of initial concentration of the electrophilic upon the microwave performance of the plasma covered antennas.

CONCLUSIONS

A detailed experimental program has been performed to study the effect of the interaction of intense microwave fields with plasmas which are typical to those encountered during high speed, low altitude reentry conditions. A diagnostic study of the plasma produced in a high performance shock tube indicated the usefulness of the electrostatic probe under conditions of high neutral particle density and high electron density. Diagnostic studies of the shock produced plasma using different experimental techniques produced similar results giving confidence to the determination of the plasma properties. Measurements of the effect of a plasma layer upon the performance of an aperture antenna at low incident power levels under cw and pulsed operation were performed. The experimental results agree with impedance sheet theory for thin plasma layers, while thick layers require a more detailed analysis. High power transmission experiments were also performed for several power levels over a range of free stream electron density levels. High power pulsed microwave interactions with thin plasma layers produce an apparent plateau for maximum power transmission. The plateau will also be a function of the free stream electron density.

The effect of the electrophilic agent Freon 114B2 upon high power transmission was also investigated for high density conditions. Experimental results indicate that the additive is still effective in reducing the electron density level and can provide improvement in transmission up to 7 dB at a peak power of 5 kW.

REFERENCES

1. Rudderow, W. H., J. Appl. Phys. 43, 373 (1972).
2. Rudderow, W. H., J. Appl. Phys. 43, 380 (1972).
3. Menard, W. A. and Horton, T. E., NASA CR 10660 (1969).
4. Rudderow, W. H., J. Appl. Phys. 39, 1 (1968).
5. Mirels, H., AIAA J. 2, 84 (1964).
6. Bredfeldt, H. R., Scharfman, W. E., Guthart, A., and Morita, T., AIAA J. 5, 91 (1967).
7. Lederman, S., and Avidor, J., Israel J. of Tech. 9, 19 (1971).
8. Burke, A. F., AIAA Paper No. 68-166, 1968.
9. Chung, P. M., and Blankenship, V. D., AIAA J. 4, 442 (1966).
10. Boyer, D. W., and Touryan, AIAA J. 10, 1667 (1972).
11. Russo, A. J., and Touryan, K. J., AIAA J. 10, 1675 (1972).
12. Hayes, D. T., and Rotman, W., AIAA J. 2, 675 (1973).
13. Hayes, D. T., AIAA Paper No. 72-694, 1972.
14. Cobine, J. D., Gaseous Conductors, p. 36, Dover, New York, 1958.
15. Jacobs, H. R., "Engineering Approximations of the Effects of Blunting on Cones in Laminar and Turbulent Flow," Aerospace Report No. TR-0158 (S3816-41)-1, 1967.
16. "Thermodynamic Properties of High Temperature Air," Chance Vought Research Center Report RE-IR-14, 1961.
17. Logan, J. G. and Treanor, C. E., Tables of Thermodynamic Properties of Air from 300°K to 10,000°K at Intervals of 100°K, Cornell Aero. Lab. Report BE-1007-A-3, 1957.
18. Chung, P. M., Talbot, L. and Touryan, AIAA J. 12, 144 (1974).
19. W. E. Scharfman, and H. R. Bredfeldt, SRI Final Report Subcontract 601603 under Contract DA 30-069 AMC-333(Y), 1967 (unpublished).

20. Talbot, L., Phys. Fluids 3, 289 (1960).

21. Pollin, I., Phys. Fluids 7, 1433 (1964).

22. Fay. J. A. and Riddell, F. R., AIAA J. 25, 73 (1958).

23. Schlichting, H., Boundary Layer Theory, McGraw-Hill, 1960.

24. Aisenberg, S., and Chang, K. W., "An RF Coil System for the Measurement of Plasma Electrical Conductivity," AFCRL-70-0033, October 1969.

25. Aisenberg, S., and Hu, P. N., "A Theoretical and Experimental Study of Plasmas," AFCRL-71-0018, November 1970.

26. Churchill, R. J., Chan, P. W., and Wilhelm, H. E., "Environmental Effects on Aerospace Sensor Systems," AFCRL-TR-74-0535, October 1974.

27. Rotman, W. and Maloney, L. E., Air Force Cambridge Research Laboratories Report No. AFCRL-TR-73-0072, 1973.

28. Gould, L. and Roberts, L., J. Appl. Phys. 27, 1162 (1956).

29. Taylor, W. C., Chown, J. B., and Morita, T., J. Appl. Phys. 39, 191 (1968).

30. Epstein, M., Phys. Fluids, 11, 896 (1968).

31. Light, G. C. and Taylor, E. C., J. Appl. Phys. 39, 1591 (1968).

32. Light, G. C., J. Appl. Phys. 40, 1715 (1969).

33. Fante, R., J. Appl. Phys. 42, 4202 (1971).

34. Mayhan, J. T., Fante, R., O'Keefe, R., Elkin, R., Klugerman, J., and Yos, J., J. Appl. Phys. 42, 5362 (1971).

35. Mayhan, J., IEEE Trans. Antennas Prop., 251 March (1969).

36. Mayhan, J. and Fante, R., J. Appl. Phys. 40, 449 (1969).

37. Mayhan, J. and DeVore, R. V., J. Appl. Phys. 39, 5746 (1968).

38. Mayhan, J. and Fante, R., J. Appl. Phys. 40, 5207 (1969).

39. Mayhan, J. T., Air Force Avionics Laboratory Technical Report 2151-6, December 1967.

40. Mayhan, J. T., Stockum, L., and DeVore, Air Force Avionics Laboratory Technical Report 2151-5, August 1967.

41. Papa, R. J. and Taylor, R. L., J. Appl. Phys. 45, 684 (1974).

42. Papa, R. J. and Taylor, R. L., Air Force Cambridge Research Laboratories Report No. AFCRL-TR-73-0754, 1973.

43. Papa, R. J. and Taylor, R. L., Air Force Cambridge Research Laboratories Report No. AFCRL-TR-73-0362, 1973.

44. Fante, R. L., Radio Sci. 2, 87 (1967).

45. Poverlein, H., J. Atmospheric and Terres. Phys. 12, 126 (1958).

46. Baños, A. and Golden, K. E., Aerospace Report No. TR-1001 (2220-10)-2, February (1967).

47. Parzen, B., Proc. IRE 37 1208 (1949).

48. Papa, R. J., and Taylor, R., "High Power Electromagnetic Transmission Characteristics of a Diffusing Reentry Plasma," J. of App. Phys. 45, 684, 1974. Also AFCRL-TR-73-0754, December 1973.

49. Papa, R. J., "Chemical Injection into a Reentry Plasma to Improve High Power EM Wave Transmission," AFCRL-72-0556, September 1972.

50. Lennon, J. F., and Herskovitz, S. B., "Design and Testing of a Chemical Injection System for Reentry Plasma Alleviation," AFCRL-TR-74-0113, February 1974.

51. Hayes, D. T., Herskovitz, S. B., Lennon, J. F. and Porrer, J. L., "Inflight Electrostatic Probe Measurements of the Effect of Chemical Injection on the Properties of the Reentry Flow Field," AIAA Paper No. 73-692, AIAA 6th Fluid and Plasma Dynamics Conference, Palm Springs, Calif., July 1973. Also AFCRL-72-0640, October 1972.